NATIONAL ENERGY TECHNOLOGY LABORATORY

Study of the Use of Saline Formations for Combined Thermoelectric Power Plant Water Needs and Carbon Sequestration at a Regional Scale: Phase II Report

June 2010

U.S. DEPARTMENT OF ENERGY

Disclaimer

Study of the Use of Saline Formations for Combined Thermoelectric Power Plant Water Needs and Carbon Sequestration at a Regional Scale: Phase II Report

---

DOE/NETL-FWP 08-014050

June 2010

NETL Contact:

Andrea McNemar
Project Manager

National Energy Technology Laboratory
www.netl.doe.gov

This Page Intentionally Left Blank

SAND2010-8073P
Unlimited Release
Printed June 2010

Study of the Use of Deep Saline Formations for Combined Thermoelectric Power Plant Water Needs and Carbon Sequestration at a Regional-Scale: Phase II Report

Peter H. Kobos, Jim L. Krumhansl, Thomas A. Dewers, Malynda A. Cappelle, Jason E. Heath, Brian P. Dwyer, and David J. Borns

Sandia National Laboratories
P.O. Box 5800
Albuquerque, New Mexico 87185

Andrea McNemar
National Energy Technology Laboratory

Abstract

The National Energy Technology Laboratory and Sandia National Laboratories are developing a geochemical and desalination assessment tool to examine changes in water quality in brackish water formations, CO_2 plume migration during injection, and water extraction and treatment options for new uses. The initial assessment focused on the San Juan Basin of northwestern New Mexico. An extended analysis examines other regions of the country such as the southeastern US. The regional assessment framework modeled changes in San Juan Basin groundwater chemistry using REACT software and also modeled flux and trapping of supercritical CO_2 in saline formations using TOUGH2. Initial water-CO_2-formation reactions include dissolution of carbonate minerals as expected and suggest that very little CO_2 will be sequestered in mineral form within the first few centuries. CO_2 plumes within target formations migrate from a given injection well at rates commensurate with the specified well spacing, design, and other constraints. Water treatment options vary depending upon site-specific water characteristics. The high-efficiency reverse osmosis system shows promise for economical desalination at the volumes of recovered water under consideration. The extended analysis examines feasibility for combined water extraction, treatment, and beneficial use with CO_2 storage in the southeastern US. This includes examining salinity levels of regional saline formations, evaluating water usage for select power plant profiles, and determining cost and systems management requirements in an effort to develop a decision support analysis for potential CO_2 storage and extracted water use at the power plant level.

Table of Contents

Figures

Tables

Acknowledgements

Sandia National Laboratories and the authors would like to thank the National Energy Technology Laboratory, and Andrea McNemar and the Existing Plants, Emissions & Capture (EPEC) program in particular, for funding the research in the areas of Energy-Water Program Management and Research. Thanks also go to Geoff Klise who provided several key Geographic Information Systems capabilities and results, as well as Mike Hightower and Tom Feeley for their guidance during the initial phases of this project and Lynn Brickett and Jared Ciferno for their support in the latter phases. Substantial portions of this study were first presented at the 2008 Carbonsq conference in Pittsburgh (May 2008), the December 2008 conference of the US/International Association for Energy Economics (USAEE/IAEE) in New Orleans, and the 2009 Carbonsq conference in Pittsburgh (May 2009). This report contains format updates as of December 2010.

Sandia National Laboratories is a multi-program laboratory managed and operated by Sandia Corporation, a wholly owned subsidiary of Lockheed Martin Corporation, for the U.S. Department of Energy's National Nuclear Security Administration under contract DE-AC04-94AL85000.

Acronyms and Abbreviations

3-D	three-dimensional
$	dollars (United States)
°C	degrees Celsius
°F	degrees Fahrenheit
BC	brine concentrator
BTU	British Thermal Unit
BWRO	brackish water reverse osmosis
Ca	calcium
CCS	carbon capture and storage
CCW	circulating condenser water
CCW/FG	circulating condenser water/flue gas
CF	capacity factor
cfs	cubic feet per second
Cl	chlorine
cm^3	cubic centimeters
CO_2	carbon dioxide
EDR	electrodialysis reversal
eGRID	Emissions & Generation Resource Integrated Database
EPA	Environmental Protection Agency
F1	Fruitland Formation 1
F2	Fruitland Formation 2
Fm	formation
ft	feet
ft^3	cubic feet
g	grams
g/cm^3	grams per cubic centimeter
gpm	gallons per minute
H_2O	water
HCO_3	bicarbonate
HERO™	high-efficiency reverse osmosis
hp	horsepower
K	potassium
kg/s	kilograms per second
km	kilometers
kWh	kilowatt-hours
lb_f	pounds (force)
lb_m	pounds (mass)
LE	low-energy
m	meters
M1	Morrison Formation 1
M2	Morrison Formation 2
m^2	square meters
m^3	cubic meters

Mg	magnesium
mg/L	milligrams per liter
MGD	millions of gallons per day
MGY	millions of gallons per year
mi	miles
MMBTU	a thousand thousand BTUs
mmt	million metric tonnes
MPa	megapascals
MSL	mean sea level
MVS	Mining Visualization System
MW	megawatts
MWh	megawatt-hours
Na	sodium
NatCarb	Distributed National Carbon Sequestration Database and Geographical Information System
NETL	National Energy Technology Laboratory
NM	New Mexico
OCD	Oil Conservation Division
P	pressure
Pa	pascals
pH	acidity/alkalinity
ppm	parts per million
psi	pounds per square inch
RO	reverse osmosis
s	seconds
SG	specific gravity
SJGS	San Juan Generating Station
SNL	Sandia National Laboratories
SO_4	sulfate
Std	standard
TDH	total developed head
TDS	total dissolved solids
UF	ultrafiltration
U.S.	United States
USBR	United States Bureau of Reclamation
WECS	Water, Energy, and Carbon Sequestration
yr	years

This page is intentionally blank.

1. An Introduction to the Energy, Water, and Carbon Sequestration Systems Analysis

The National Energy Technology Laboratory (NETL) and Sandia National Laboratories (SNL) have been developing an analysis for a potential combined system that includes a coal-fired power plant, a geologic carbon storage system, water extraction from a saline formation, and the treatment of the extracted water for use as cooling water in the coal-fired power plant. The key areas addressed in this analysis are the geochemical effects of potential carbon dioxide (CO_2) injection into a series of candidate geological formations, geomodeling of the CO_2 plume in a formation, and the scale-up of a water extraction and treatment system for potential use in a power plant to supplement cooling water demands. Figure 1-1 illustrates the overarching conceptual analytical framework used in the analysis.

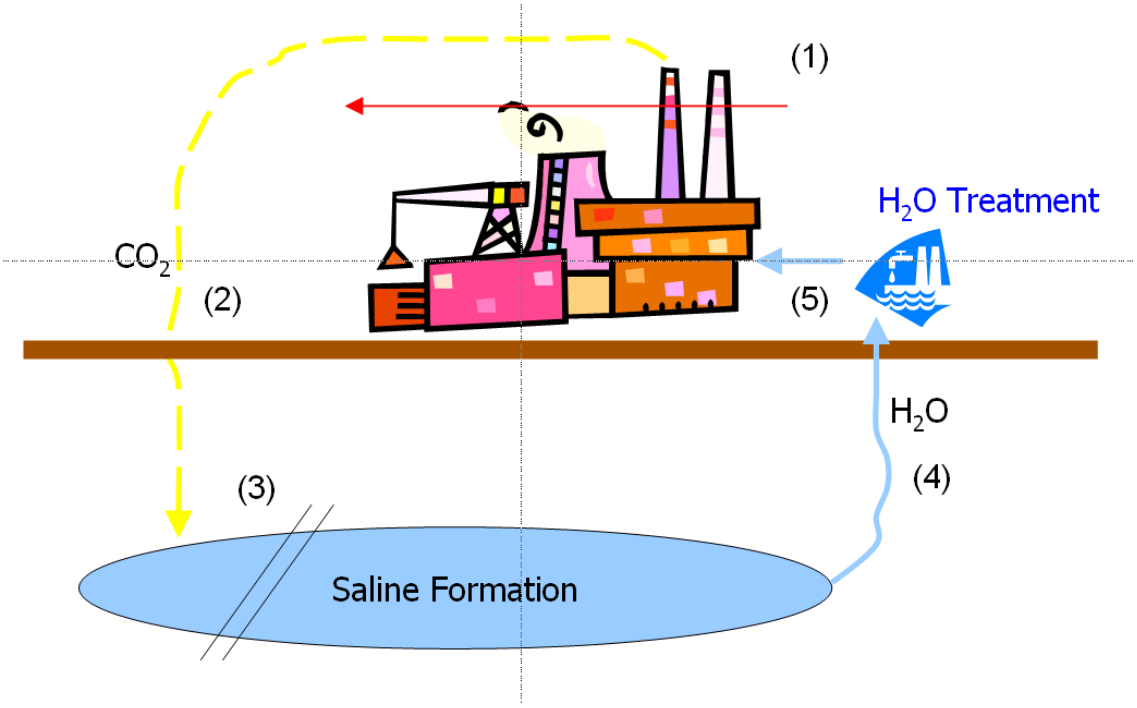

Figure 1-1. Assessment Methodology and Model Framework. (1) Power Plant Metrics, (2) Carbon Capture and Storage System, (3) Saline Formation Geochemical and Geomodeling Assessment, (4) Water Extraction Analysis, (5) Water Treatment Analysis for Power Plant Cooling

The analysis builds from the framework outlined in Figure 1-1 by using the San Juan Generating Station (SJGS) in northwestern New Mexico, along with the Morrison and Fruitland geological saline formations as representative candidates for this combined CO_2 storage, water extraction, and water treatment system. The analysis presents the respective multidisciplinary components by first selecting geological saline formations in the region that appear to meet the potential

coupled-use criteria (i.e., size, depth, chemistry, and location criteria). The analysis investigates how the down-hole CO_2 plumes may evolve over time (geomodeling with TOUGH2), what engineering and other resources would be required to develop a water extraction and treatment system, and finally develops a working analytical economic-engineering dynamic model. It is assumed that water extraction for treatment and use would occur ahead of the CO_2 plume. This brings together and evaluates all of the system components in an integrated model building on the activities developed in Phase I of this analysis (see Kobos et al. [2008] for an introduction).

2. Identification of Potential Host Formations and the Geochemical Assessment

2.1. Identification of Potential Host Formations

The San Juan Basin shown (in green) in Figure 2-1 is a bowl-shaped structural depression situated in northwest New Mexico. The basin formed in the early-late Cretaceous and Tertiary during which time it filled with several thousand feet of brine-bearing shallow marine and near-shore deposits. These clastic sediments, as well as older sediments in the basin, may be attractive locations for the geological storage of CO_2. Allis et al. (2003) offers a good characterization of the region. Figure 2-1 shows the locations of three potential storage sites (green hatched squares) as well as two coal-fired power plants (red squares) in the region.

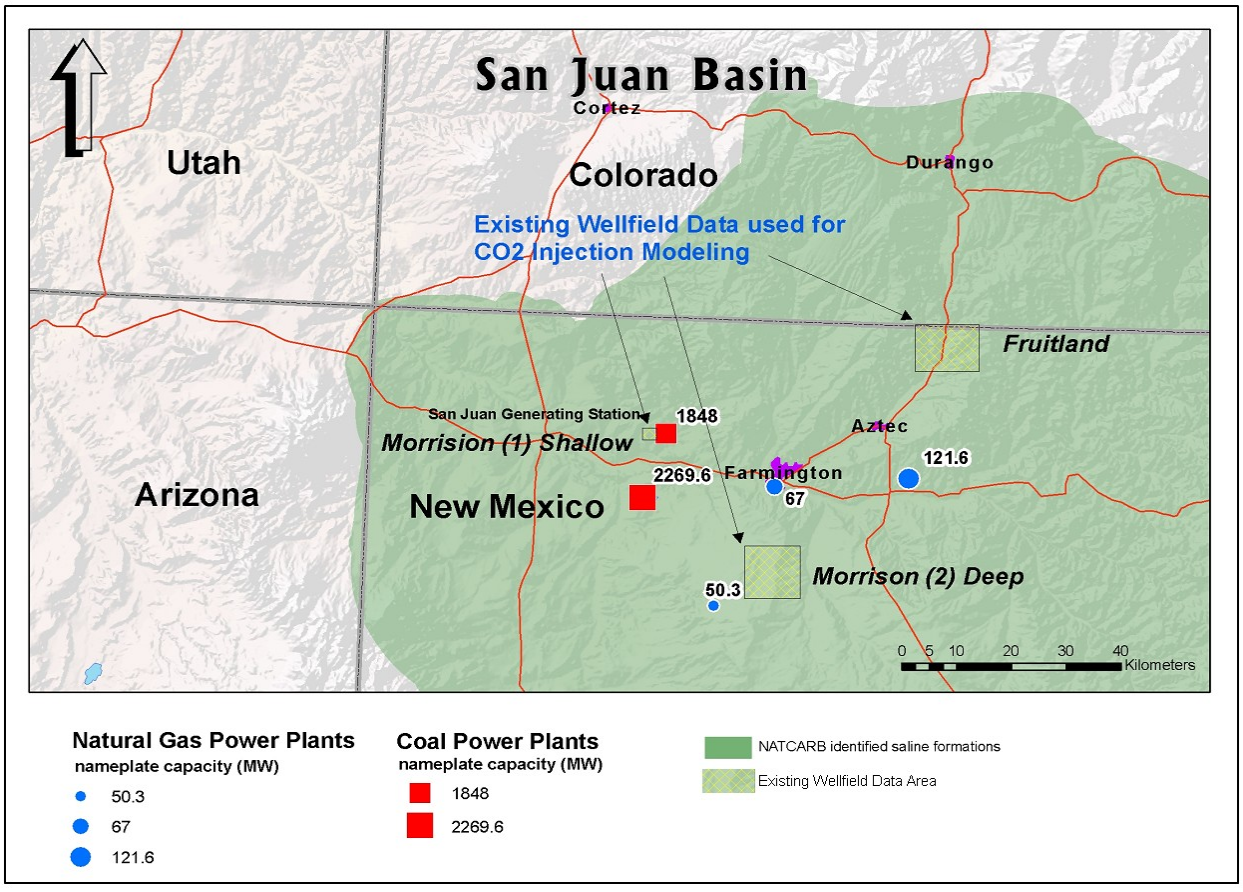

Figure 2-1. Region and Power Plant Used in the Coupled CO_2 Storage and Water Extraction and Treatment Study. (Kobos et al. [2009]; select data from the NatCarb database, NETL [2007a])

The last deposits laid down prior to the formation of the San Juan Basin were a thick sequence of Cretaceous shallow marine shales interbedded with occasional sandy layers, which themselves are interbeded as former beach deposits. Figure 2-2 illustrates the stratigraphic detail of the northern San Juan Basin and includes the formation (Fm.) names.

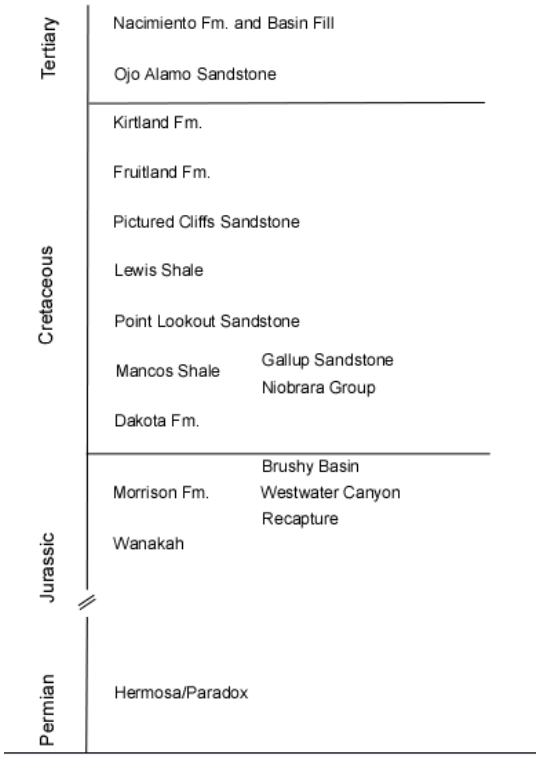

Figure 2-2. Generalized Stratigraphic Column of the Northern San Juan Basin

The Cretaceous sand units have a relatively high permeability in some regions. At the base of this sequence lies the Dakota formation sandstone, below which lies the Jurassic Morrison formation, a mix of lake-bed, riverbed, and deltaic deposits. Beneath this formation are still more alternating layers of sandstones, conglomerates, shales, and limestones, including the Permian Hermosa limestone. The whole stack of sediments ultimately rests on a basement of very low permeability crystalline Precambrian material (granite, gneiss, schist, etc.) similar to the rocks exposed in the deepest parts of the Grand Canyon. The power plants providing the focus for this study are located on the western edge of the basin. Therefore, east of this site, wells several thousand feet deep may just penetrate into the top portion of the Tertiary basin fills or late Cretaceous strata, while west of the site a similar well could penetrate all the way into the Permian Hermosa limestone.

Two key criteria were used to evaluate the region's potential for coupled CO_2 sequestration. First, saline formation water must be both available and treatable economically. Between the first and second phases of this analysis, it became evident that common regulatory considerations

dictate that formations with waters with less than 10,000 parts per million (ppm) of total dissolved solids (TDS) (e.g., 10,000 grams of salt per 1,000,000 grams of brine) would likely not be considered for CO_2 storage. Alternately, if the brackish water is to be desalinated economically, it cannot contain more than approximately 20,000–30,000 ppm TDS. Second, the economics of pumping CO_2 between site locations and the injection process itself are also included in the systems study. To drive the system economically, the CO_2 must be compressed until it has a density of about 0.6 grams per cubic centimeter (g/cm^3). The depth of the host formations into which CO_2 is to be injected must be at least 2,500 feet (800 meters [m]) to achieve requisite pressure and temperature conditions to confine CO_2 as a dense supercritical phase.

With these two criteria (salinity and formation depth) in mind, the NatCarb database (NETL [2007a]) was queried for wells within about thirty miles (initially) of the target power plant that were both of sufficient depth and had a record of producing waters with the desired salinity range. Table 2-1 summarizes the results of this search for both the early and later phases of the study.

Table 2-1. Water Chemistries Used in Geochemical Models

Formation	Depth[1] (ft)	pH	Element/Compound						TDS[2] (ppm)
			Na (ppm)	Ca (ppm)	Mg (ppm)	Cl (ppm)	SO_4 (ppm)	HCO_3 (ppm)	
Fruitland (initial, F1)	2,402	8.4	4,050	44	27	1,460	5.6	8,015	13,620
Fruitland (second, F2)	2,795	8.6	5,798	48	12	922	6.8	11,800	18,587
Point Lookout, Mesa Verde	—	7.9	1,572	87	28	2,500	4.2	256	4,447
Gallup Sandstone in Mancos	—	8.4	3,378	8	7	4,060	7.7	1,684	9,145
Dakota	—	8.6	741	16	10	356	1.4	959	2,083
Morrison (initial, M1)	4,725	7.9	1,491	313	49	58	3,764	272	5,947
Morrison (second, M2)	6,359	7.2	5,372	286	34	2,529	7,915	882	17,018
Hermosa/Paradox	—	8.0	2,654	368	49	425	5,500	708	9,704

Notes

1. NETL (2007a) (NatCarb database).
2. Included in the initial geochemical modeling for additional perspective, but not included in the subsequence formation and systems analysis.

2.2. Selection of the Morrison and Fruitland Formations

There are two geochemical objectives of this study: first, to evaluate whether underground CO_2 storage might affect geochemical properties of the host formations sufficiently to prevent them from being considered as candidate formations, and second, to identify a single formation of regional extent to serve as an initial resource for the overall coupled system model being developed by the broader study. The former objective dictated identifying the widest possible range of rock types and water chemistries (Table 2-1), while the latter required performing a down-select on the range of possibilities initially identified.

Eliminating the Hermosa/Paradox as a potential candidate formation was relatively straightforward because it lies below the other formations, thus, at least to the east of the power plants shown in Figure 2-1, drilling a well to access this formation would hit all the other possibilities first. Also, because the formation actually consists of a limestone-shale mix, it may not contain a sufficient amount of saline water. Next, the Gallup, Point Lookout, and Dakota formation sandstones all are substantially thinner than that of the Morrison formation, so from the standpoint of selecting the largest volumetric resource, the Morrison formation was the obvious choice. For perspective, the Dakota formation sits right on top of the Morrison formation, so by selecting the Morrison formation, one is also able to access the Dakota formation, in which case the CO_2 storage capacity of the total reservoir increases by roughly 20% (based on relative formation thicknesses).

The second phase of the study broadened our perspective on potential saline formations. Early runs of the overall coupled-use model indicated that the expense of the pipelines to bring in water to the power plant (and take CO_2 out) did not contribute much relative to the cost of the CO_2 capture system and to the overall cost of the process. Thus considering sites somewhat beyond the initial thirty mile radius limit (where the balance of the Fruitland resource is located) was explored in the second phase of the study.

2.3. Geochemical Modeling

The reaction path code REACT (from The Geochemist's Workbench® commercially available package; Bethke [1998]) was used to assess what chemical changes might occur if CO_2 was injected into various formations. This report presents results for the three well sites, and the reader is referred to Kobos et al. (2008) for a parallel discussion of Phase I results, as well as more details on how the models were constructed. Briefly, the REACT models considered mixtures of the appropriate formation minerals and brines together with an excess of CO_2 (i.e.; CO_2 gas remained at the end of the computation). Reaction rates for the minerals were values typically found in the literature (Xu, Apps, and Pruess [2003, 2004, and 2005]; Xu et al. [2007]; Pruess, Oldenburg, and Moridis [1999]; Pruess et al. [2003]; and White et al. [2005]), and the proportions of different minerals put into the models were based on formation descriptions in the geologic literature. Consideration was given to (1) how the fluid and rock would interact in the absence of CO_2 (the result of which should compare favorably with the actual assemblage of minerals found in a formation that had equilibrated with that brine), (2) the interaction of the brine and CO_2 in the absence of any rock (essentially a baseline for assessing how the brine chemistry changes when the brine-CO_2 mix comes in contact with the rock), (3) the state of the

system after 100 years (somewhat longer than the probable lifetime of an injection operation), (4) the state of the system after 350 years, and (5) when the CO_2-rock-brine mix had fully equilibrated (presumably many thousands of years into the future).

Results of calculations on the Morrison and Fruitland formations (Appendix A, Tables A-1 and A-2, respectively) are arranged with the evolving fluid chemistries shown at the top and the amounts of the various minerals consumed (or produced) at the bottom. Additionally, the mineralogical data is subdivided so that upper entries reflect what happens to minerals that were added as inputs to the models, while lower entries chronicle the precipitation (and occasionally subsequent dissolution) of new minerals as the systems react.

2.3.1. Comparisons with Earlier Study Results

In general, the second Morrison site (**Morrison (2) Deep** in Figure 2-1) brine is saltier than the first Morrison (**Morrison (1) Shallow**, Figure 2-1) site, and now chloride has been added to sulfate as a significant anion (sodium was, and remains, the dominant cation). In all, the greater salinity causes the CO_2-charged brine to be more reactive than was observed with the "initial" (Table A-1) Morrison brine. In particular, the higher sulfate level in this brine allowed for the transient early appearance of gypsum. However, this mineral disappears when the rock and fluid fully equilibrate because the calcium is consumed in producing (disordered) dolomite [$(CaMg)(CO_3)_2$]. This reflects the fact that calcite dissolution (and production of dissolved calcium) is rapid, so the relatively soluble-phase gypsum ($CaSO_4 \cdot 2H_2O$) precipitates early on because of the high initial sulfate concentration in the brine. Over time, though, silicate minerals slowly dissolve, releasing magnesium, which then reacts with the gypsum (solid) and bicarbonate (dissolved) to produce relatively insoluble dolomite.

More interesting is the early appearance of dawsonite and clinoptilolite (a calcium-aluminum-silicate-zeolite mineral), though the amounts are small (equivalent to 0.7% and 0.8% of the weight of the non-quartz constituents in the rock, respectively, in the first century, and 2.1% and 2.4%, respectively, after 350 years). Thus in this venue, one could anticipate some minor mineralization of the injected CO_2 but still not nearly enough to be beneficial from the standpoint of guaranteeing solid-phase storage of the injected gas. Components for the new minerals actually came from degradation of all the primary silicates given in the initial recipe, though the bulk of the material came from clay minerals: kaolinite > rapidolite > smectite.

The second Fruitland (F2) brine is also somewhat more saline than the first brine chosen to represent this formation ("initial," Table A-2). Sodium remains the dominant cation, but now chloride is somewhat diminished (relative to the first brine chosen), while bicarbonate is much elevated. The impact of this is, again, somewhat greater reactivity, which produces marginally more dawsonite and clinoptilolite than the first Fruitland model. However, as before, in the first 350 years, the reactions only involve just a few percent of the rock, so they are quantitatively insignificant from the perspective of fixing carbon dioxide underground in a mineral form. Finally, because this brine starts out essentially free of sulfate, the mineral gypsum ($CaSO_4 \cdot 2H_2O$) is not precipitated although, again, early rapid calcite dissolution is likely to occur.

In summary, consideration of two new brine chemistries did not change the overall geochemical picture regarding potential benefits and shortcomings of applying a coupled-use strategy to brackish water-bearing formations in the San Juan Basin. However, the additional studies did broaden the applicability of conclusions reached previously by expanding the evaluation criteria. In particular, the brines evaluated in this installment represent conditions associated with higher salinity fluids at greater depths, and thus, allow us to increase the geographic extent over which our multiple-use models could be applied. The main geochemical considerations relative to using the waters produced from these formations are as follows:

1. Water users will (still) need to accommodate levels (parts per million) of both silica and iron, and possibly bisulfide (HS^-).

2. In time frames relevant to CO_2 storage, the overall salinity levels of CO_2-charged brines will not change much from that characteristic of the indigenous brines. However, levels of minor constituents such as Mg, Ca, K, and $SO_4^=$ may have changed.

3. Clays and other Al-Si-containing minerals only react very slowly with the mildly acidic CO_2-charged brines that will be injected underground. Hence mineralization of the injected CO_2 is not going to be a quantitatively-significant process until many thousands of years have elapsed.

4. Precipitation of calcium sulfate has been identified as a mineralogical change that could occur in the short term and possibly impact CO_2 injection activities.

2.4. Regional Comparisons

Choosing the San Juan Basin initially was a fortunate choice because it was possible to identify several promising formations. Additionally, this region in particular may have multiple-use potential with many centuries of CO_2 storage capacity (Kobos et al. [2008]). It is also, however, a fact that national surveys find much larger potential CO_2 storage formations (and higher densities of CO_2-producing power plants) in other parts of the country, particularly along the Gulf Coast (Hovorka et al. [2000]).

3. Reservoir Modeling of CO2 Injection into San Juan Basin Saline Formations

Building upon the down-selection of formations and regions with a potential for coupled use (e.g., CO_2 storage and water extraction and treatment), the analysis refined its focus on the formations within the San Juan Basin from a geomodeling perspective. The feasibility of carbon dioxide injection and storage in two saline formations in the San Juan Basin was assessed by combining information on formation and caprock geometry and properties with fate and transport modeling using TOUGH2 (Pruess, Oldenburg, and Moridis [1999]). Three sites were examined in detail based on geochemical criteria. These are the initial "shallow Morrison" site (as seen earlier in Figure 2-1), located within the Jurassic Morrison formation (Dam et al. [1990a]) about 1.4 kilometers (km) deep and 24 km north and west of Farmington, NM; the second "deep Morrison" site, located approximately 1.9 km deep and 16 km south of Farmington, NM; and a third site within the Fruitland formation, a little less than 1 km deep and 24 km east of Farmington, NM. Simulations of injection of supercritical carbon dioxide were done using the TOUGH2 software (Pruess, Oldenburg, and Moridis [1999]) with the recently developed ECO2N equation of state for CO_2-brine-salt multiphase system (Pruess [2005]). In order to constrain saline formation geometries and flow properties, geologic framework models, also known as *earth models*, of both sites were developed using information from the State of New Mexico (NM) Oil Conservation Division (OCD) online database on petroleum wells in the region, combined with data on hydraulic conductivities from calibrated U.S. Geological Survey flow models and other recent results from the Southwest Partnership on Carbon Sequestration (SWP), a project managed by NETL.

3.1. Geologic Framework Earth Models

A first step in the development of a numerical CO_2 storage simulator for the SJGS is to create a geologic earth model to represent the relevant rock strata in the subsurface. Using data from the NM OCD database and data from the literature (e.g., Stone and Mizell [1978]), this study compiled petroleum well log data for the San Juan Basin sites. Formation boundary locations from well log data are combined in a three-dimensional earth model using C Tech Development Corporation's Mining Visualization System (MVS) software. Point data are *kriged* to create boundary surfaces that constrain formation geometries. Figure 3-1 illustrates one location for the Morrison (deep) and the Fruitland site as first depicted in Figure 2-1. The shallow Morrison case has the same stratigraphy and depositional characteristics as the deep case. In all three cases, the layered sequences are discretized into grids of adjoining cells for use with the TOUGH2 reservoir simulator. For purposes of the feasibility study presented here, all three cases examine a two-dimensional, north-south oriented simulation domain because it follows the regional structural trend of extension fractures in this portion of the San Juan Basin (Lorentz and Cooper [2003]), and thus, the trend of highest hydraulic conductivity.

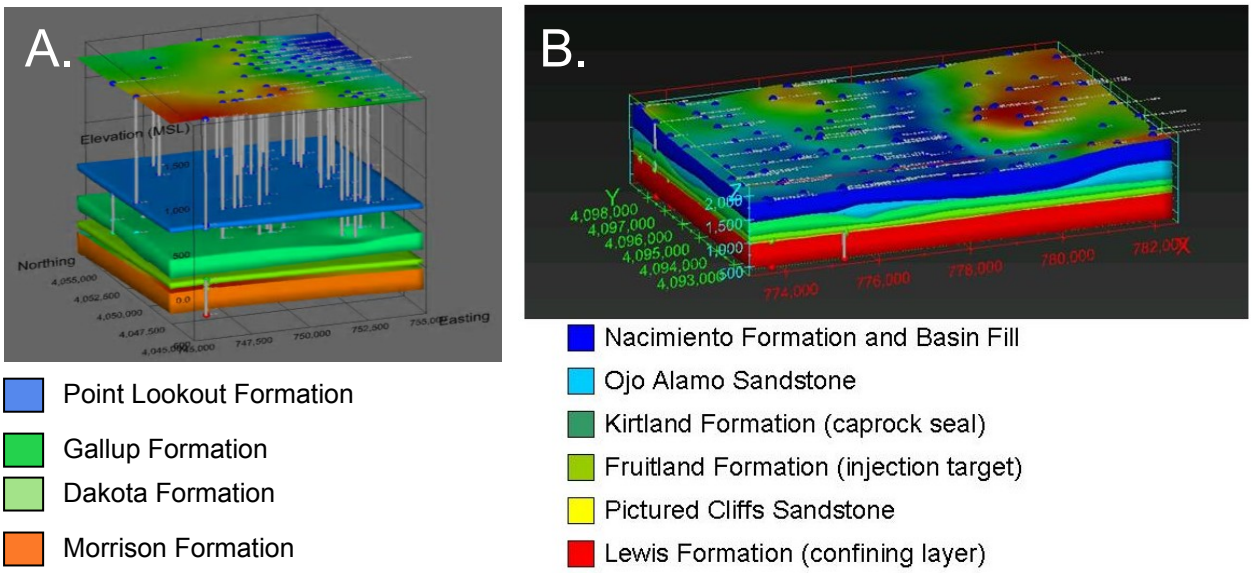

Figure 3-1. Geologic 3-D Framework Model for (A.) Deep Morrison Site and (B.) Fruitland Site Developed Using the MVS Software (C Tech) and Formation Tops Found in the NM OCD Database. (Wells shown as vertical pipes in A).

As shown in Figure 3-1, the dominantly clastic sections consist of sandstone formations, which potentially could serve as reservoirs for CO_2 injection, separated by finer-grained shales and mudstones, which are proposed as seals or caprocks. This is discussed further in section 3.2 in the context of hydrogeological units. Referencing Figure 3-1 (A.), the volumes of sandstone bodies were determined from well data, using a kriging algorithm to derive tops and bottoms of formations. Referencing Figure 3-1 (B.), the Cretaceous marine formations (Lewis Formation, Pictured Cliffs Sandstone, and Fruitland Formation) are roughly flat lying tabular bodies. The top of the Kirtland Formation (dark green) is part of a regional unconformity and shows large paleo-topography comparable to modern river channel in the present-day surface topography.

3.2. Hydrogeological Models

In assessing hydrogeologic properties of the three sites (i.e., two Morrison and one Fruitland) for the purposes of modeling injection and storage, hydrostratigraphic units are defined and permeabilities determined using calibrated groundwater models. As shown earlier, Figure 2-2 illustrates the stratigraphic layout of the San Juan Basin. For the Morrison cases modeled for the hydrogeologic models, the units introduced by Thomas (1989) are used; while for the Fruitland case, the analysis used hydrostratigraphy proposed by Kernodle (1996), Kernodle et al. (1989), and Frenzel and Lyford (1982). These are shown in the **Permeability (m^2)** column of Table 3-1 for both cases. The permeability values listed in Table 3-1 and used in the reservoir simulations were determined by the cited authors by calibrating groundwater models against available well and recharge data. Hydrostratigraphic units for the Morrison

cases include the lower Jurassic Wanakah confining layer (or seal), members of the Jurassic Morrison formation and injection horizon (Recapture and Westwater Canyon members), the Jurassic Brushy Basin confining unit (upper member of the Morrison formation, the overlying Cretaceous Dakota formation, and the Cretaceous lower Mancos confining unit, also known regionally as the Niobrara Group). Units for the Fruitland site (all Cretaceous) include the Lewis Formation confining unit, the Pictured Cliffs formation, the Fruitland formation (and injection horizon), the overlying Kirtland Formation confining unit, and the Ojo Alamo Sandstone. Lithologically, the injection and storage horizons are interbedded sands, muds, and shales, while the confining units are mostly mudstones and shales.

Table 3-1. Hydrostatigraphic Units and Absolute Permeabilities Used for TOUGH2 Modeling

Hydro-stratigraphic Unit	Permeability (m^2)[1]	
	Horizontal	Vertical
Lower Mancos Confining Unit[2]	7.5E-16	7.5E-20
Dakota Formation[3]	3.3E-13	2.9E-17
Brushy Basin Confining Unit[3]	7.5E-15	7.1E-18
Lower Morrison Formation[3]	4.1E-13	2.9E-17
Wanaka Confining Unit[3,4]	7.5E-15	3.1E-17
Ojo Alamo Formation[5,6]	2.5E-13	5.1E-15
Kirtland Confining Unit[4,6]	2.9E-18	8.2E-20
Fruitland Formation[7]	5.8E-15	5.8E-17
Pictured Cliffs Formation[8]	2.0E-15	2.0E-17
Lewis Shale Confining Unit	7.5E-16	7.5E-20

Notes:

[1] assumes temperature of 30°C and brine density of 1100 kg/m^3

[2] Frenzel, 1983

[3] Thomas, 1989

[4] Kernodle, 1996

[5] Thorn et al., 1990

[6] Unpublished values of K_z from Heath et al., personal communication, 2009

[7] Stone et al., 1983

[8] Dam et al., 1990a

[9] values taken to be equivalent to those for Mancos Shale

3.3. Injection and Storage of CO_2

To model CO_2 injection, migration, and phase partitioning with the TOUGH2 reservoir simulator, we require parameters for the multiphase flow properties, porosities, and densities for the hydrogeologic layers, most of which are largely unknown. We have used porosities of 13% and 15% for the Morrison formation and Fruitland formation injection horizons, respectively, based on best estimates from the literature (Dam et al. [1990a and 1990b] and Kernodle et al. [1990]); other parameters to describe multiphase flow in clastic sands, mudstones, and shales were taken from Pruess (2005). Grids constructed in all cases consist of a coarse horizontal 500-m-spaced grid with a finer grid (progressively, down to 1-m spacing) surrounding an injection well centered within the simulation domains. Vertical grid resolution was taken to be a coarse grid of 50- to 100-m depending on formation thickness, fining at caprock reservoir boundaries and near injection zones to 1 m.

Examples of CO_2 injection and storage are shown in Figures 3-2 through 3-4. Figure 3-2 shows a two-dimensional example of injection at modest rates of 0.1 kg/s into a 1-m-thick (dimension into the page) horizon for the deep Morrison case as is applicable to injection from a horizontal well. In this case, vertical permeabilities were assumed equal to horizontal permeabilities. This shows the classic "gravity override" buoyancy-driven plume migration up against the Brushy Basin caprock.

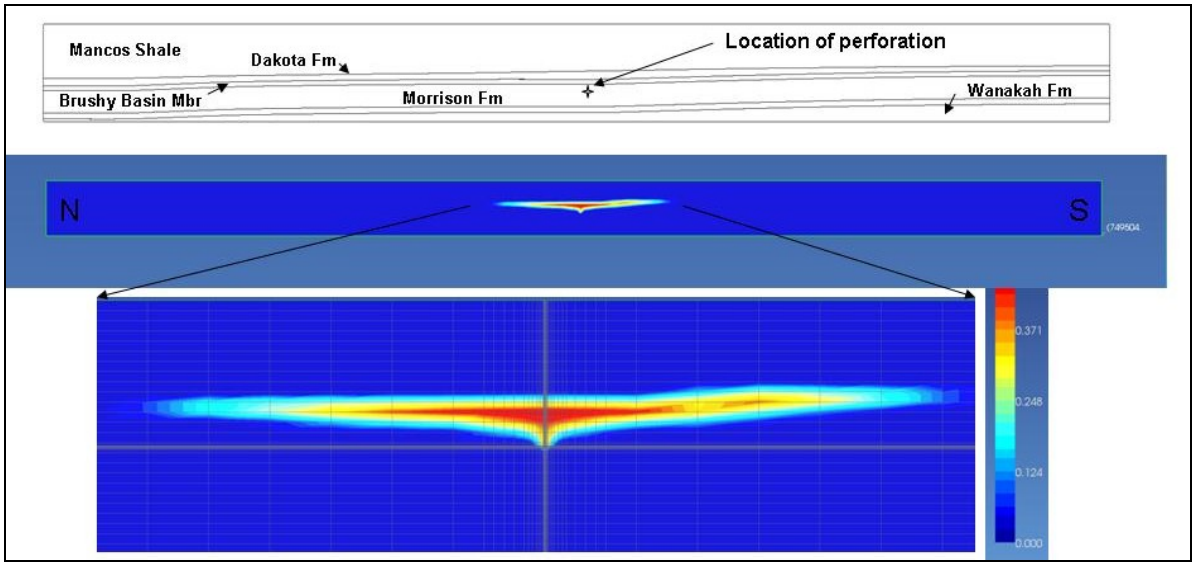

Figure 3-2. TOUGH2 Simulation Showing Injection (0.1 kg/s) into the Morrison Formation Assuming Isotropic Hydraulic Conductivities

Note that in Figure 3-2, the CO_2 plume migrates upward and against the Brushy Basin caprock after 30 years of injection. (The horizontal axis is 12 km; vertical axis is 1 km.)

Figure 3-3 shows a case using anisotropic permeabilities; in this case, the large anisotropy yields a more "pancake" shaped plume. This is likely a more realistic scenario, with large lateral plume migration given the layered nature (i.e., with finer and coarser layers) of these sandstone reservoirs. A small "mound" of overpressure produced by the injection is evident in Figure 3-3.

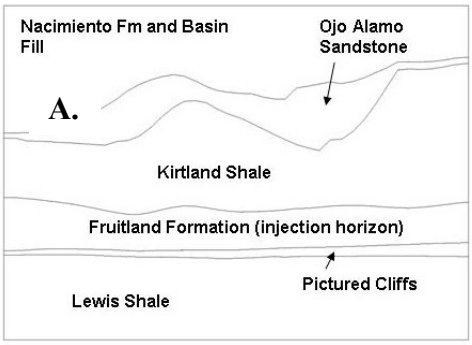

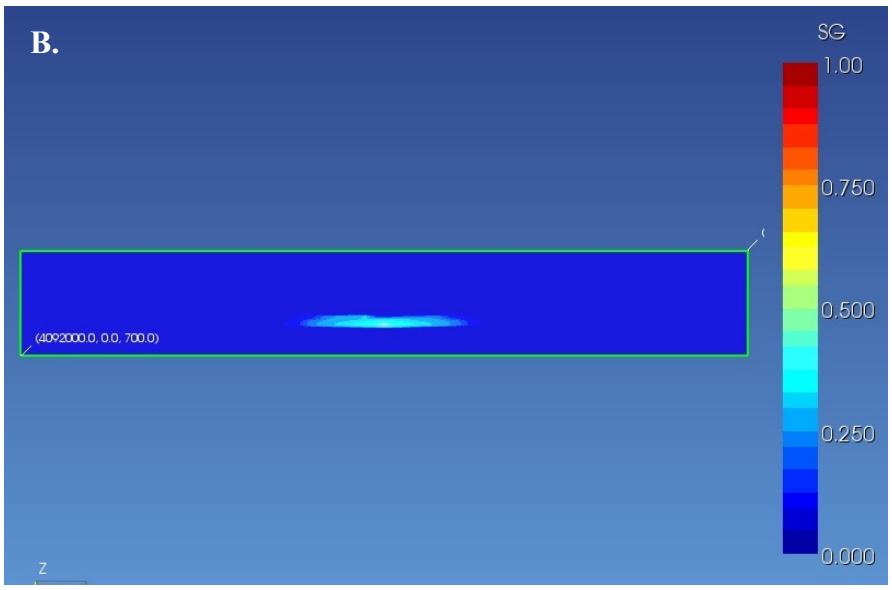

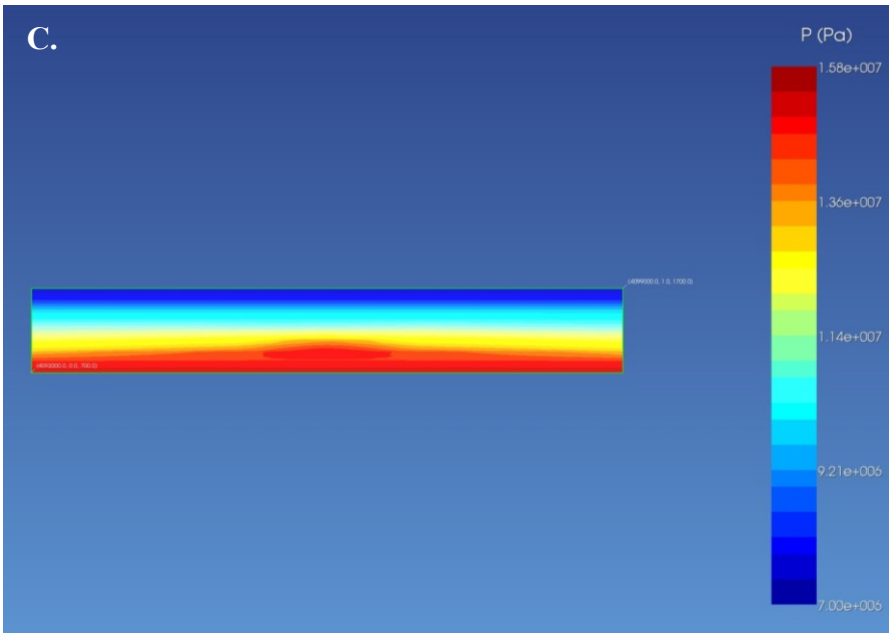

Figure 3-3. TOUGH2 Model of Injection within the Fruitland Formation

In Figure 3-3, the Fruitland formation is shown in (A). Assuming anisotropic permeabilities, the CO_2 plume spreads laterally and up against the Kirtland Shale caprock (Figure 3-3 [B].) and induces a "mound" of overpressure (Figure 3-3 [C]) after 30 years of injection. In Figure 3-3 (B) and (C), the horizontal axis is 7 km, and the vertical axis is 1 km.

Figure 3-4 shows the effect of simultaneous water withdrawal from a well positioned 6 km away from the injection well on the induced overpressure. Even at this great distance, overpressure can be mitigated by water withdrawal and treatment for beneficial use prior to the arrival of the CO_2 plume at the withdrawal well.

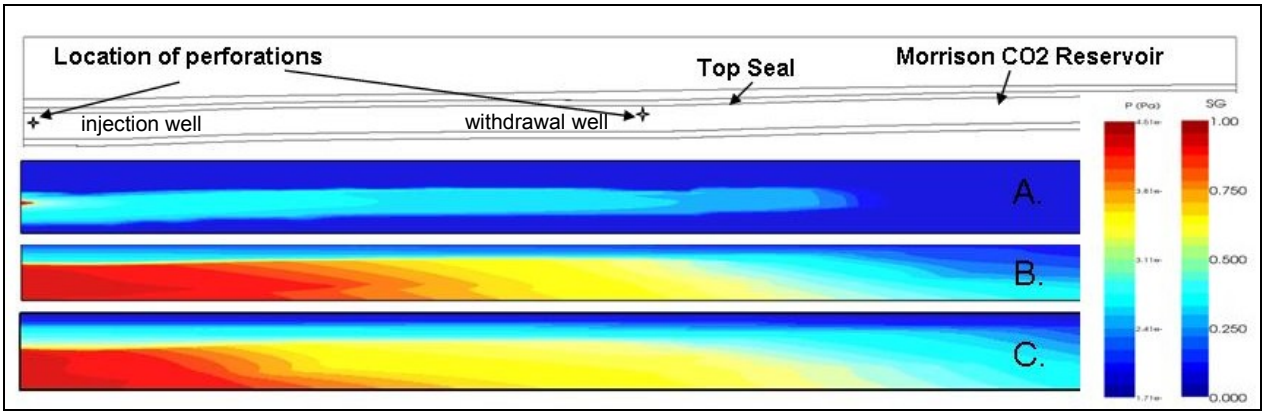

Figure 3-4. Example of CO_2 Injection in the Morrison, Both with and without Water Withdrawal

Figure 3-4 (A) shows the saturation of supercritical CO_2 after 30 years of injection. Figure 3-4 (B) shows pressure without water withdrawal. Figure 3-4 (C) shows pressure after equi-volume withdrawal of the formation. In some cases, water extraction from injection horizons may be necessary to offset potentially damaging fluid pressure increases accompanying CO_2 injection. (In Figure 3-4, the horizontal axis is 12 km, and the vertical axis is 1 km.)

3.4. Plume Migration and Mass Conservation

TOUGH2 modeling similar to that portrayed in the previous sections can be used to bound plume migration extents and to determine the partitioning of CO_2 among phases on time scales relevant to power plant operation. To do this, TOUGH2 models were constructed using two-dimensional radial grids but based on formation hydrostratigraphic properties as in the above models. This allows a proper assessment of three-dimensional migration of CO_2 as the radial coordinate system used in these simulations accounts for radial flow centered on the injection well location. Plume migration distances, correlating to breakthrough times in water production wells, can be determined from sets of numerical experiments discussed above, by varying injection rates and measuring plume extent with time.

Figure 3-5 shows results of plume migration distances as a function of time (up to several decades of migration) for the Morrison case. At small injection rates, distances increase roughly linearly with time, but as injection rates increase, plumes increase approximately with the square root of time in accord with analytical models (i.e., Bickle et al. [2007]). When expressed as a power law, our results show a departure from the square root of time ideal, which can be attributed to the combined effects of anisotropy, dissolution of CO_2 into brine, and gas/brine leakage into bounding formations that have contrasting hydrogeologic properties. In the Morrison case, the radius of an effectively pancake-shaped CO_2 plume increases as a power law function of both injection rate and time, such that

$$L = 6.35 I^{0.49} t^{0.40} \quad (1)$$

where L is the plume radius (km), I is injection rate (tonnes/day) and t is time in years. The solid lines in Figure 3-5 are plotted using Equation (1), and R^2 from a linear regression analysis is found to be 0.98, showing excellent agreement between Equation (1) and the simulation results.

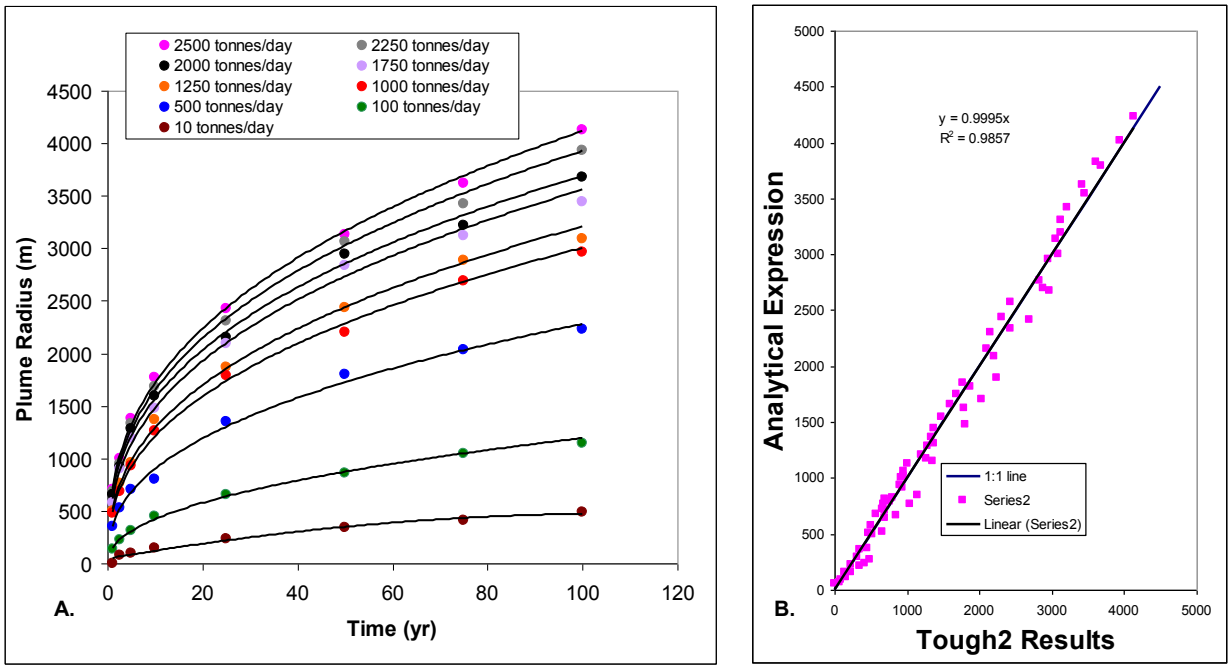

Figure 3-5. Plume Migration Distance for Morrison Example

Figure 3-5 (A) shows the plume migration distance plotted as a function of time and injection rate. Figure 3-5 (B) shows the comparison of the TOUGH2 numerical experiments with a power law expression for migration distance as a function of injection rate and time.

Figure 3-6 shows the distribution of CO_2 between supercritical and aqueous phases for the Morrison and underlying Wanakah formations. A small amount of CO_2 enters the Wanakah, but a negligible amount was seen to enter the Brushy Basin caprock overlying the Morrison sandstone members, and any substantial amount leaking from the Morrison would be contained by the extensive Mancos shale and other overlying mudrocks. Most CO_2 is present as a (supercritical) separate phase, but roughly a third is present as dissolved CO_2. In fact (and this is not shown), most of the CO_2 entering the Wanakah during Morrison injection is as a dense CO_2-laden brine phase.

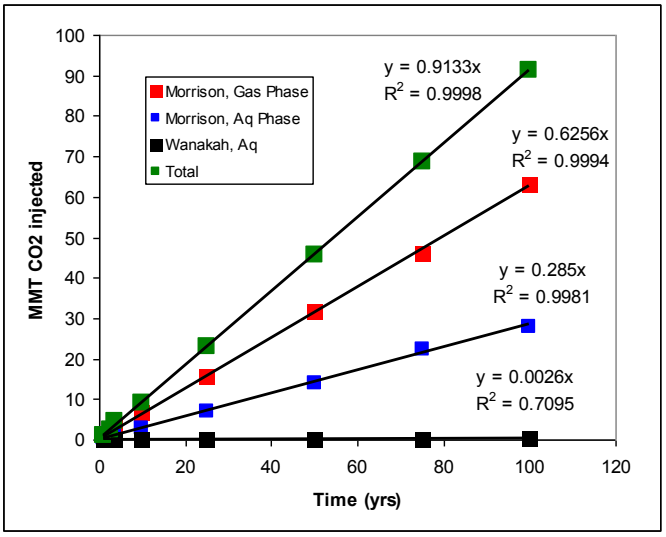

Figure 3-6. CO_2 Mass Distribution in the Morrison Case for a 100-Year Injection Time

A similar treatment for the Fruitland case is shown in Figures 3-7 and 3-8. In the case of the Fruitland, a different power law relation is given by

$$L =).019 I^{0.34} t^{0.44} \tag{2}$$

with a similar R^2 coefficient of 0.98 between predicted results using Equation (2) and TOUGH2 results.

The differences between the Morrison and Fruitland models are attributable to differences in formation geometries, hydrogeologic properties, and those of surrounding lithologies, including caprocks. For example, more CO_2 is seen to leak into the bounding formations in the Fruitland case (Figure 3-8) than in the Morrison case. A small amount of supercritical CO_2 enters the underlying Pictured Cliffs sandstone, for example, and aqueous CO_2 is pushed into the overlying Kirtland formation. The latter is important to consider because the Ojo Alamo, which overlies the Kirtland, is a source of drinking water in some parts of the San Juan Basin. Less carbon dioxide is stored in the aqueous phase in the Fruitland situation, which is likely because of the lesser gas solubility in brine at shallower depths in the Fruitland case. The power law expressions shown in Equation (1) and Equation (2) are in an ideal form for direct application in systems dynamics models.

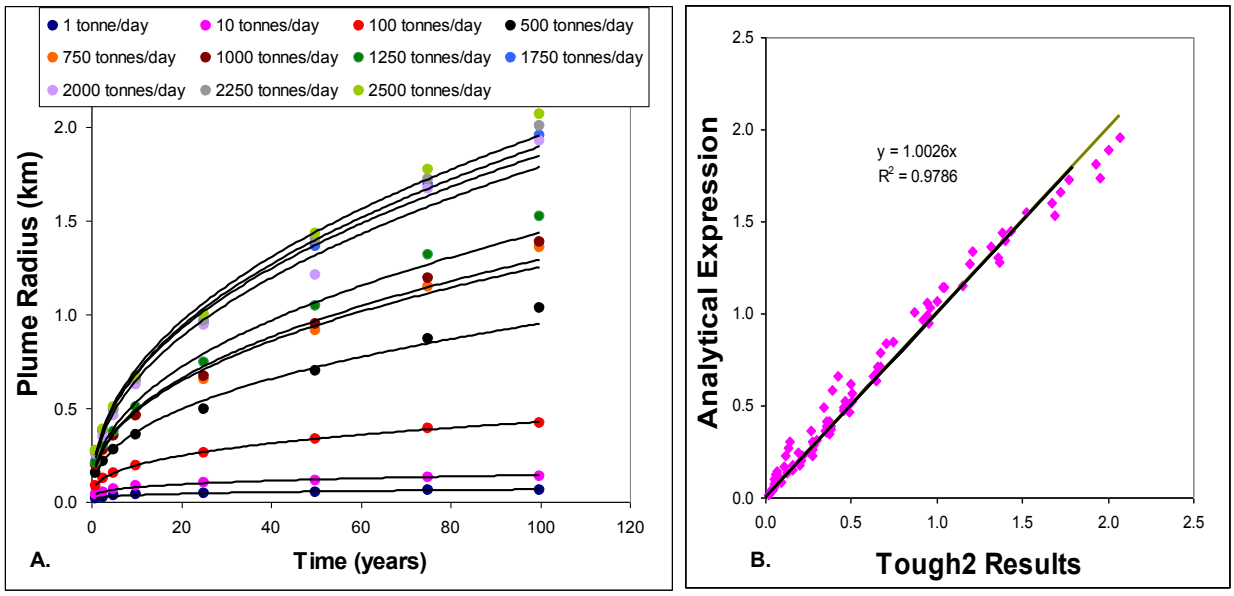

Figure 3-7. Plume Migration Distance for Fruitland Example

Figure 3-7 (A) shows the plume migration distance plotted as a function of time and injection rate. Figure 3-7 (B) shows the comparison of the TOUGH2 numerical experiments with a power law expression for migration distance as a function of injection rate and time.

The simulation results shown in Figure 3-8 suggest that minimal overpressure might result from CO_2 injection at reasonable rates. Figure 3-8 (A) shows carbon stored as gas and aqueous phase in the Fruitland formation. Figure 3-8 (B) shows an increase in aqueous phase in the overlying Kirtland Shale caprock and the underlying Pictured Cliffs Sandstone, as well as the increase in gas (supercritical) phase CO_2 in the Pictured Cliffs.

To explore the bounds on injection rates with regard to geomechanical and other considerations, numerical experiments designed to examine near wellbore pressure as a function of injection rates were run using a three-dimensional radial injection scenario taken from an example in Pruess (2005) using Morrison-constrained parameters. Although not shown here, the simulations suggest that an injection rate of approximately 200 kg/s (~17,280 tonnes/day) should be used as a cap on the injection rate in order to not cause near wellbore damage from induced shear fracturing.

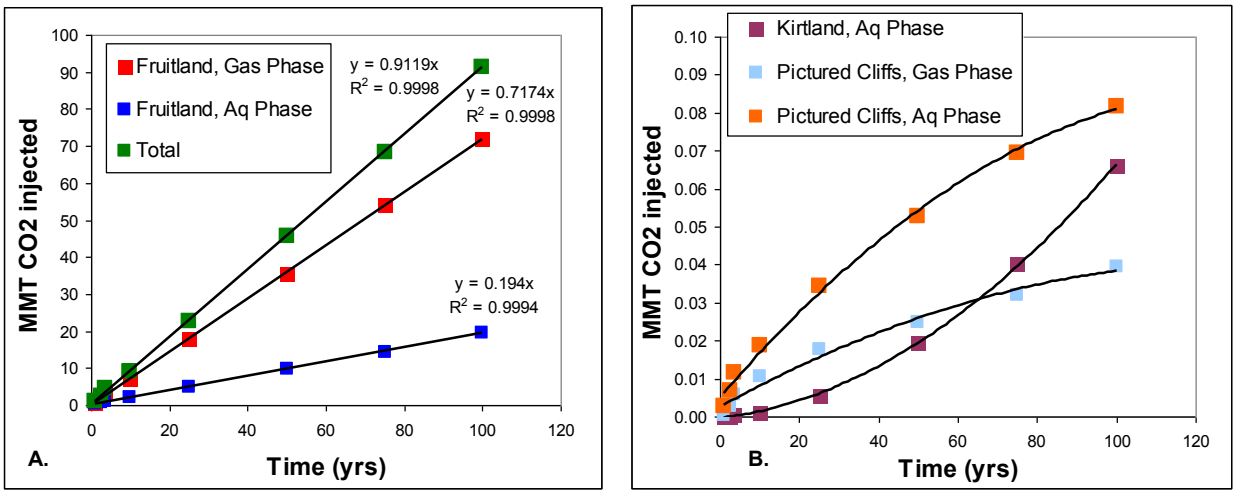

Figure 3-8. Mass Distribution for the Fruitland Case over a 100-Year Injection Period

Considerations of wellbore integrity and stability are an issue with safe injection pressures. Ogden (2002) gives a practical upper limit on safe injection rates per well as 2,500 tonnes per day (~29 kg/s), limited by the friction induced by flow in the wellbore and other pipe-flow physical constraints. For a 100-m injection interval, and using Morrison formation parameters, this would translate to a bottom hole flowing pressure of at most a few MPa for virtually all depths of interest. Thus the wellbore flow physics and current wellbore design constraints limit the maximum available injection rate for CO_2 into the Morrison, not geomechanical considerations. For comparison, Sleipner-magnitude rates are approximately 32 kg/s (Bickle et al. [2007]).

3.5. Formation Volume Calculations for Carbon Dioxide Storage Capacity Calculations

Storage capacity calculations for CO_2 in the San Juan Basin require an assessment of the total volume available for storage, which includes total formation volume, available porosity, and the sweep efficiency for injection into formations of interest. At best, this is complicated by formation heterogeneity. For the Fruitland formation, CO_2 storage is further complicated by the presence of coals, which can absorb CO_2, and the presence of natural gas.

The CO_2 storage capacity of deep saline formations can be calculated in a number of ways depending on the time- and length-scale of interest (i.e., local versus basin scale) and the trapping mechanism (i.e., as residual gas saturation versus in aqueous solution). We will adopt an approach related to that used by petroleum engineers for CO_2 flooding in Enhanced Oil Recovery (EOR). The approach, using an injection well and recovery well at some spacing, is to simply determine the mass of CO_2 stored (not recovered at the recovery well) by the reservoir as (ignoring oil shrinkage) follows:

$$M_{CO_2} = \rho_{CO_2 res} \bullet R \bullet OOIP \tag{3}$$

In Equation (3), M_{CO2} is the total mass of CO_2 stored in the formation (Mass Storage Capacity), ρ is the density of CO_2 at reservoir conditions, R is a recovery/retention factor, and $OOIP$ is the total volume of original oil in place (Gozalapour, Ren, and Tohidi [2005]). For our purposes, we modify this slightly using the mass density of CO_2 per rock volume of a representative elementary volume of rock (i.e., equivalent to a grid block in the numerical simulations) as shown in Equation (4):

$$d_{CO_2} = \phi S_g \rho_{CO_2} \tag{4}$$

where ϕ is porosity, S_g is gas saturation, and ρ is density of CO_2 at formation conditions as before. For our purposes, here, we can determine the mass storage capacity of CO_2 in the Morrison and Fruitland formations by constraining the storage period to last until the CO_2 plume has reached the nearest water extraction well (i.e., *breakthrough*). Calling this distance L, and assuming a pancake-like geometry for the plume, as roughly observed in the numerical simulations (see Figures 3-3 and 3-4), and a constant formation thickness t_f, as is a decent approximation for the Morrison and Fruitland formations in much of the San Juan Basin, we can integrate the mass density of CO_2 over the relevant formation volume to obtain the total mass of CO_2 in place at breakthrough as shown in Equation (5)

$$M_{CO_2} = \rho_{CO2} \bullet \pi \bullet S_{g,eff} \bullet r^2 t_f \tag{5}$$

where $S_{g,eff}$ is understood to be the integrated residual gas saturation across the integrated volume, and so is analogous to the recovery factor (which includes a sweep efficiency of the CO_2 flood) used in EOR operations.

To gain a gross estimation of the total mass of CO_2 that could be stored within a porous formation, the latter multiplicative term in Equation (5) can be replaced by the total volume V_t such that

$$M_{CO_2} = \rho_{CO_2} \bullet \varphi \bullet S_{g,eff} \bullet V_t \tag{6}$$

Average porosities of the Morrison and Fruitland formations have been reported in section 3.3. The integrated residual gas saturation is a poorly constrained parameter ranging between, say, 0.1 and 0.5 (Gozalapour, Ren, and Tohidi [2005]). Here we are concerned with an estimation of the V_t parameter for inclusion in Equation (6).

For the Fruitland formation, the stratigraphy of concern here includes, from the bottom up, the Cretaceous-Paleocene Ojo Alamo formation. The Pictured Cliffs and later Lewis Shale, Fruitland, Kirtland, and Cretaceous formations mark the final regression of the Cretaceous interior seaway, and the Ojo Alamo conglomerates mark the initiation of the Laramide Orogeny in the region. From results of overview computer simulations of CO_2 storage in the Fruitland, it

was observed that much storage occurred in the underlying Pictured Cliffs. In what follows we include the Pictured Cliffs along with the Fruitland volumes in estimating available volumes for CO_2 storage.

To calculate V_t, we use published structure contour maps for the tops and bottoms of the formations of interest from Kernodle (1996). Such maps are based on formation tops obtained from driller's logs from wells drilled for oil and gas exploration and development. Kernodle (1996) contains maps of the top of the Kirtland Shale and Fruitland formations (Kernodle [1996], Figure 17), top of the Lewis Shale (base of the Pictured Cliffs Sandstone, Kernodle [1996], Figure 19), top of the Morrison formation (Kernodle [1996], Figure 25), and top of the Wanakah Formation (base of the Morrison, Kernodle [1996], Figure 55). These were imported into ArcGIS®, georeferenced, and multipoint shapefiles were created from digitized points of contours from Kernodle's (1996) maps. The geographic location of the San Juan Basin in northwestern New Mexico and two examples of contour shapefiles are shown below in Figure 3-9. Only contours at and below 4,500feet mean sea level (MSL) were included to ensure formation volumes occur at sufficient depths for CO_2 to be stored as a supercritical phase. (This is approximately 2500 feet below ground surface.)

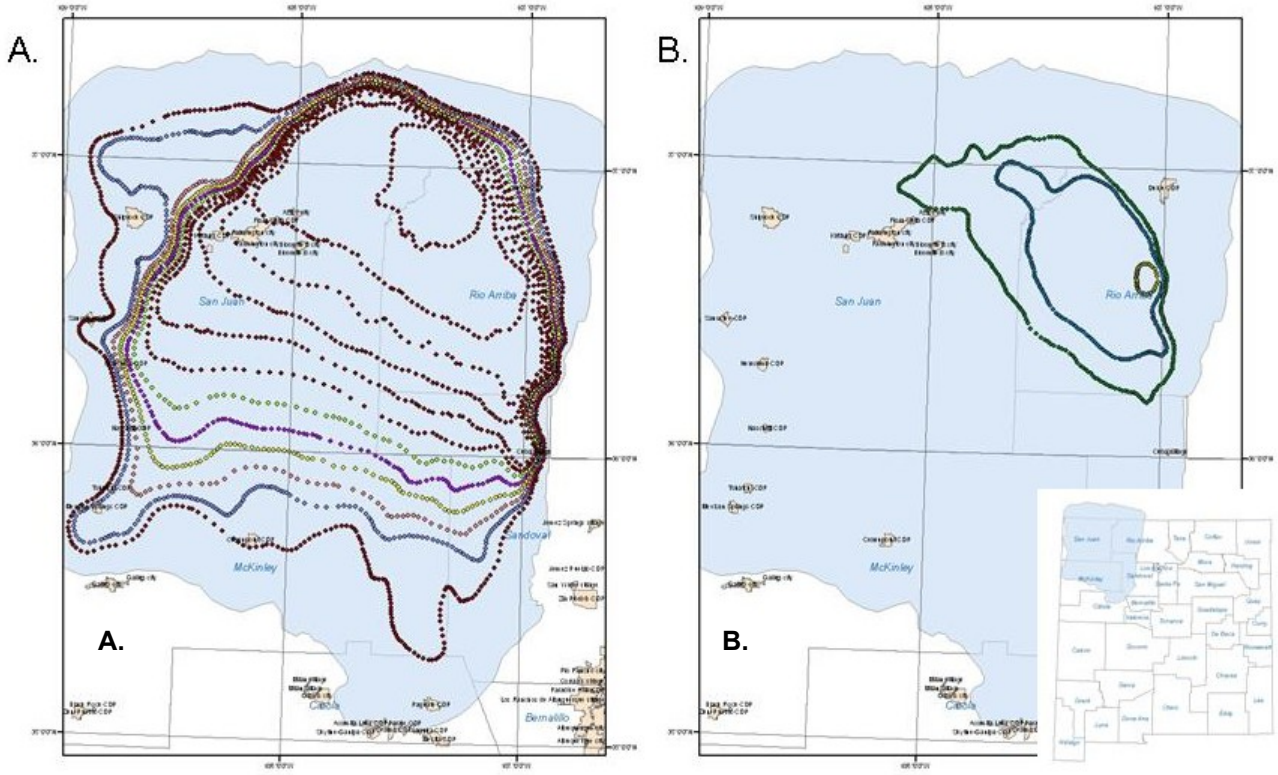

Figure 3-9. Structure Contour Maps Showing the Tops of the Morrison (A) and Kirtland/Fruitland formations (B) in the San Juan Basin (Adapted from Kernodle, 1996).

For the Morrison example (A), contours range from 4,500 feet near the basin perimeter to -1,500 feet MSL in the basin interior. For the Fruitland/Kirtland example (B), contours range from 4,500 feet to 3,500 feet MSL. Contour intervals are 500 feet in all cases. In Figure 3-9, the inset (lower right) shows the location of San Juan Basin in the upper northwest corner of New Mexico.

3.6. Basin-Scale Geologic Framework Models

The digitized contours in the form of ArcGIS® shapefiles were converted to ASCII *xyz* files and then imported into C Tech's MVS software. Locations of formation tops were then kriged to obtain smoothed surfaces bounding formation volumes. Formation volumes are shown in Figures 3-10 (for the Morrison) and 3-11 (for the Pictured Cliffs/Fruitland/Kirtland). Fence diagrams with both North-South and East-West orientation are included to enable visualization of basin cross section lines; these are shown in green in Figures 3-10 and 3-11. The large contour interval used in the kriging resulted in portions of the basins having a stair-step form, which is especially evident for the Fruitland/Kirtland volume seen in Figure 3-11.

Using the MVS software, we calculated total volumes for each formation. These findings are presented in subsections 3.6.1 and 3.6.2.

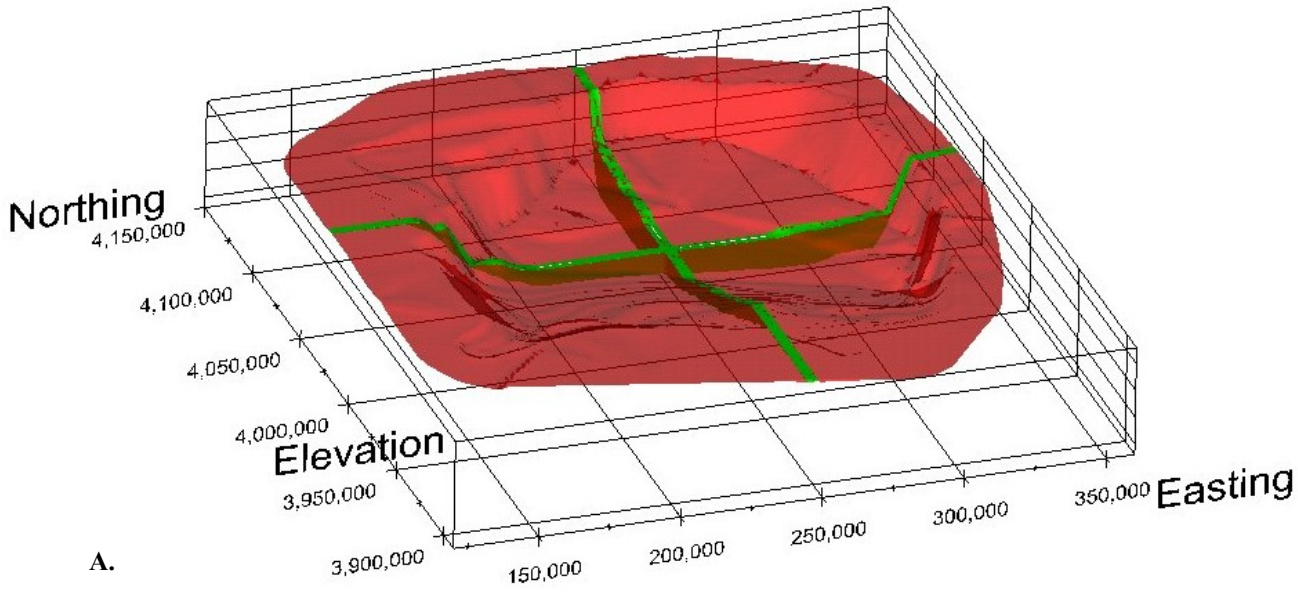

A.

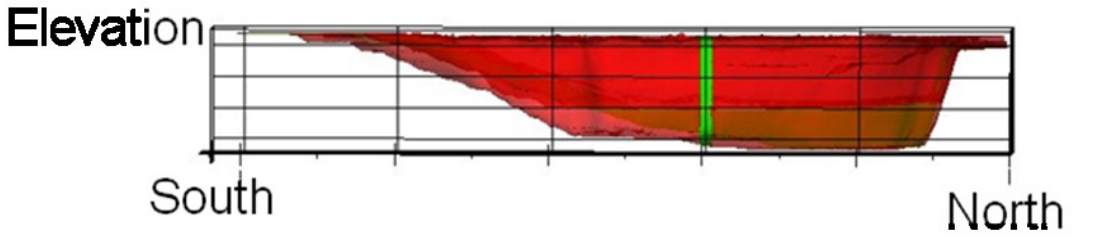

B.

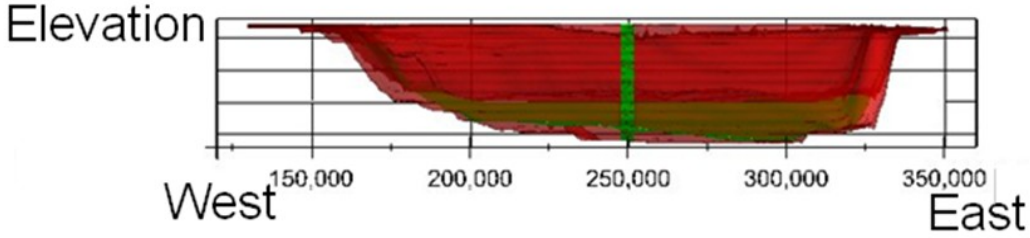

C.

Figure 3-10. Views of San Juan Basin Morrison Formation Geologic Framework Model. Grid coordinates are UTM NAD27 Zone 13. Illustration (A.) is from the top; illustration (B.) is North-South; illustration (C.) is East-West. (Note: Green EW and NS lines are for visual reference).

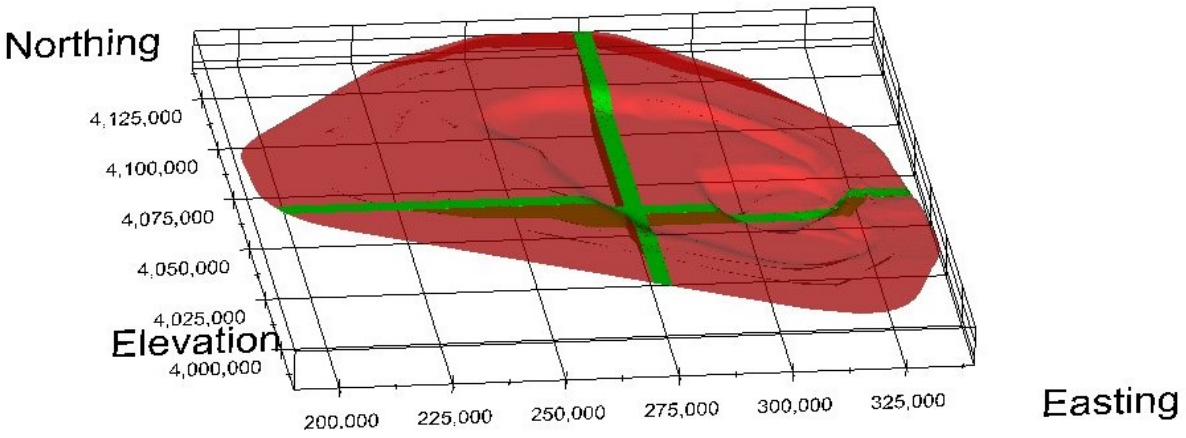

A.

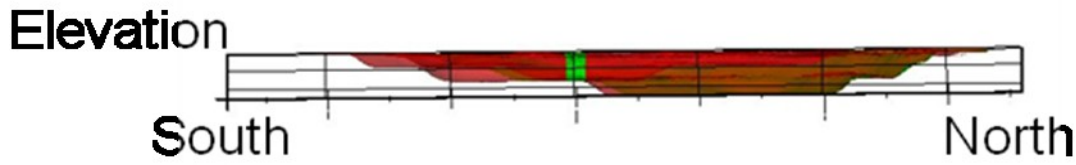

B.

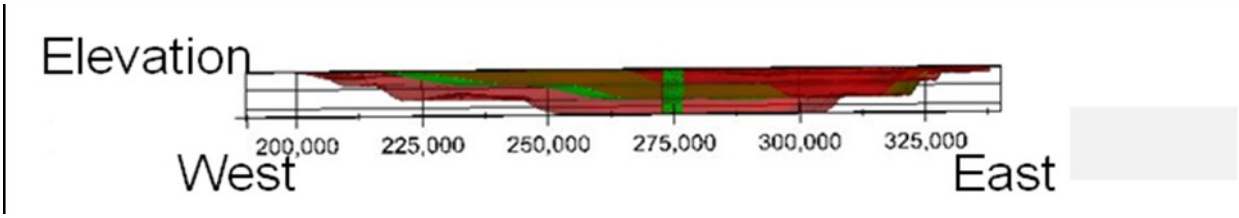

C.

Figure 3-11. Views of San Juan Basin Kirtland/Fruitland Geologic Framework Model. Grid coordinates are UTM NAD27 Zone 13. Illustration (A.) is from the top; illustration (B.) is North-South; illustration (C.) is East-West. (Note: Green EW and NS lines are for visual reference).

3.6.1. Morrison Formation

The total volume of the Morrison formation below 4,500 feet in elevation was determined to be 2.94×10^{11} cubic meters. The Morrison outcrops around the San Juan basin rim at approximately 6,000 feet, or 1,829 meters in elevation. Eight hundred meters below this depth marks a "safe' depth below which storage of CO_2 as a supercritical phase is feasible, at 1,029 meters. The portion of the estimated Morrison formation volume below this depth is found to be 2.74×10^{11} cubic meters. The resulting Morrison volume is shown in Figure 3-12, with colors referenced to formation thickness, or isopachs. The largest available volume for CO_2 storage in the Morrison occurs in the thickest northeastern portion of the Morrison formation.

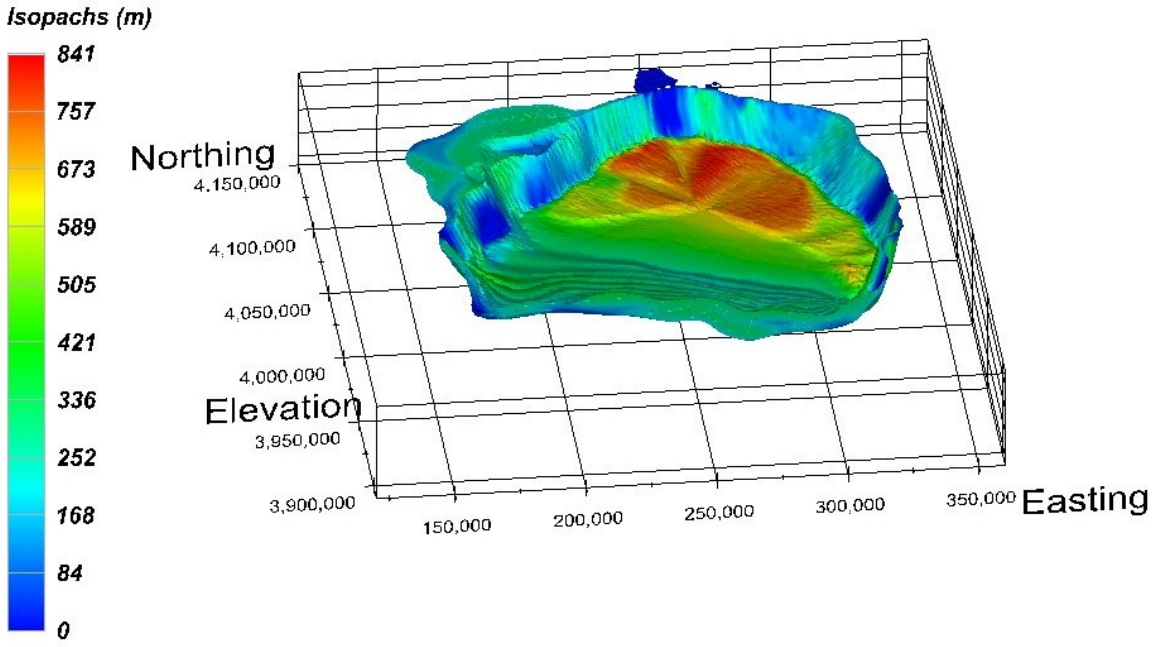

Figure 3-12. Visualization of the Thickness of the Morrison Formation Occurring below 1,029 m MSL

3.6.2. Fruitland Formation

The total Pictured Cliffs/Fruitland/Kirtland volume below 4,500 feet in elevation is found to be 5.57×10^{10} cubic meters. The lowest elevation of Kirtland outcrop is at the intersection of the "Hogback" NW of Farmington and the San Juan River at 5,040 feet MSL or 1,536 meters. Eight hundred meters below this is an elevation of 736 meters, which is well below the lowest elevation of Fruitland occurrence at 914 meters. Much of the Fruitland/Kirtland outcrop occurs at about 7,000 feet (2,133.6' MSL). Eight hundred meters below this elevation is at 1,333.6 meters MSL. The total volume of the Pictured Cliffs/Fruitland/Kirtland formations below this depth is 5.19×10^{10} cubic meters. Colors in Figure 3-13 refer to formation thickness, and it can be seen that most available volume for CO_2 storage occurs in the northern half of the basin.

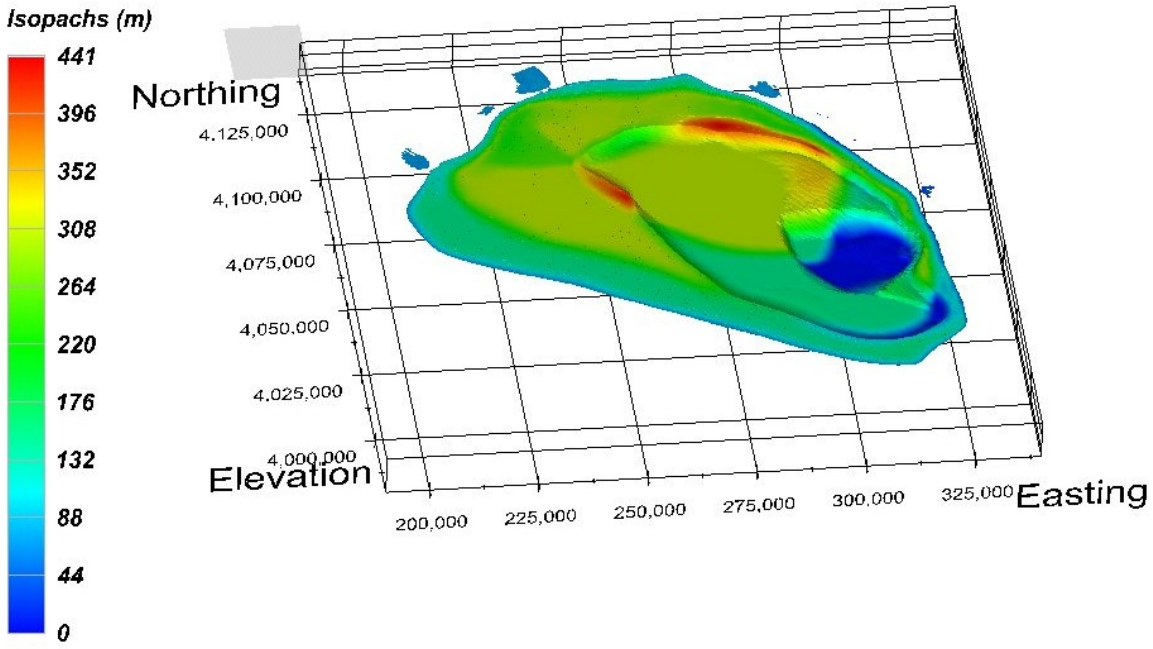

Figure 3-13. Visualization of Pictured Cliffs, Kirtland, and Fruitland Formations Occurring below 1,333.6 m MSL

3.7. Discussion and Summary

Refinement of the above volume calculations is necessary to remove the volume of relatively nonporous and permeable portions of the formations. In the case of the Morrison formations, this requires determining the percentage of total Morrison volume that exists as the Brushy Basin Member (a mudstone), which forms an upper seal in the CO_2 storage simulations shown in Figures 3-2, 3-3, and 3-4. In the case of the Pictured Cliffs/Fruitland/Kirtland formations, this requires determining the percentage of this stratigraphic package that occurs as the Kirtland Shale, which forms a potential upper seal. One complicating factor in the assessment of CO_2 storage within the Fruitland formation is the approximately 200 billion tons of coal it contains, often in thin beds 2 or more feet thick to depths of 4,500 feet (Fassett and Hinds [1971]).

Stone et al. (1983) and Frenzel (1983) provide a detailed examination of Morrison stratigraphy, wherein it can be seen that roughly 50% of the Morrison across the basin occurs as the porous Westwater Canyon Member, with the remaining Morrison occurring as the Brushy Basin and relatively nonporous Recapture and Salt Wash Members. Thus a conservative estimation for the total volume of the Morrison available for CO_2 storage is 50% of 2.74 $x10^{11}$ cubic meters, or 1.4 x 10^{11} cubic meters. Using a previously-determined porosity value of 0.13, a CO_2 density of 600 kg/m3, and an integrated gas saturation of 0.1, a conservative estimate for the CO_2 storage capacity in the San Juan Basin Morrison formation is 1.1 x 10^{12} kg, or 1.1 x 10^3 mmt (million metric tonnes).

Fassett and Hinds (1971) provide a detailed examination of Fruitland and Kirtland formation stratigraphy wherein it can be seen that roughly 65% of this stratigraphic package (which includes the Farmington Sandstone "Tongue" within the Kirtland Shale) consists of the Kirtland formation. A conservative estimation for the total available volume for CO_2 storage in the Fruitland and Pictured Cliffs formations is thus 35% of 5.19×10^{10} cubic meters, or 1.82×10^{10} cubic meters, roughly an order of magnitude less than the available volume in the Morrison formation. As above, using a porosity of 0.15 for the Fruitland/Pictured Cliffs reservoirs, a CO_2 density of 600 kg/m^3, and an integrated gas saturation of 0.1 a conservative estimate for the CO_2 storage capacity in the San Juan Basin Pictured Cliffs and Fruitland formations is 1.6×10^{11} kg, or 1.6×10^{2} mmt.

4. Water Treatment

Power plants may have the resources required to treat saline water from geological formations thereby supplementing their demands on other water resources. Population growth, drought, power generating technologies, carbon dioxide capture systems, and water desalination technologies may all be very region-specific; however, the confluence of these factors will determine the relative water stress due to water supply and demand imbalances.

Carbon capture technologies and their associated energy and water streams were analyzed in a recent DOE/NETL report (U.S. Department of Energy/National Energy Technology Laboratory 2007). For pulverized coal subcritical power plants, the CO_2 capture system is assumed to be an amine absorber, which at the current technology development stage has a substantial water demand. Along with this technology, it is important to account for water chemistry in the design of the plant's systems. There are site-specific limits based on the metallurgy of the piping system, materials of construction of the cooling tower itself, and regulations on the waste water. General recommendations from the Electric Power Research Institute (EPRI) and the Cooling Technology Institute (CTI) were described in Kobos et al. (2008). Cooling towers that utilize surface waters and/or low TDS well waters can easily meet the requirements and operate efficiently. However, many alternative sources of water (brackish, produced water, waste water) will have elevated levels of chloride and other problematic constituents such as organic constituents, calcium, and silica. Elevated levels of chloride can lead to corrosion; elevated calcium, magnesium, and/or silica can lead to scale formation and increased energy consumption by the condensers. Higher TDS waters would require different and likely more expensive operation and maintenance (O&M) costs, but they offer the possibility of expansion in an age where every drop of water counts.

The water treatment for cooling water calculations used in the model in this study are based on a 2006 NETL/EPRI cost-benefit analysis by Zammit and DiFilippo (2004), U.S. Bureau of Reclamation (USBR) desalination cost estimations (USBR [2003]), and standard engineering calculations (McCabe, Smith, and Harriott [1993]). In the 2006 report NETL/EPRI evaluated the use of produced water in the Fruitland formation for use by the SJGS cooling towers. The study found that produced water required substantial treatment before it could be used by the cooling towers. This is due primarily to the need for additional evaporation ponds, as well as existing water quality restrictions for the cooling towers and other equipment. The best treatment approach (i.e., most cost effective) for utilization of produced water was a combination of High-Efficiency Reverse Osmosis (HERO™) and refurbishing two of the existing brine concentrators (not currently used) to eliminate the potential of additional water sent to the SJGS evaporation ponds.

Several potential formations have been studied for their geochemical properties and are summarized in Table 4-1. The initial analysis focused on the Morrison formation, primarily due to its geochemical properties, as well as its closeness and ability to store significant amounts of carbon dioxide. However, this original focus was on a formation with a relatively low salt level, which is beneficial for water treatment (easier, more cost effective). However, current regulations suggest that a formation must have salinity greater than 10,000 mg/L to be

considered for alternative uses, such as storing CO_2. The current work focuses on formations with a salinity range of 10,000–30,000 mg/L. The upper bound is essentially related to a suggested maximum potential for reverse osmosis with minimal waste stream and energy expense. Future work may expand this range.

Similar to our previous work, several desalination options were studied using a straightforward spreadsheet analysis. These options all utilized reverse osmosis for desalination and varied in the mode of waste water disposal. The options studied were as follows:

Option A Desalination & Gathering - HERO™ desalination; no concentrate disposal

Option B Desalination & Gathering - HERO™ desalination; evaporation ponds for concentrate disposal

Option C Desalination & Gathering - HERO™ desalination; injection pipeline and well for concentrate disposal

Option D Desalination & Gathering - HERO™ desalination + brine concentrator retrofit (based on Zammit and DiFilippo [2004])

All formations studied are summarized in Table 4-1; abbreviations and the formations' salinities, or TDS levels, are summarized along with the results in Table 4-2. The assumptions included in this model are based on the USBR desalination handbook (USBR [2003]), standard pumping equations, and the analysis in the NETL/EPRI 2006 report (Zammit and DiFilippo [2004]), which was based on the Fruitland formation. Therefore, for any formation with a differing salinity, depth, or specific location (i.e., distance and height difference), it is assumed that the capital and operational costs may vary. Future work will attempt to evaluate this further along with other potential water sources for power plants.

Table 4-1. Summary of Formations Studied

Abbreviation	Formation	TDS (mg/L)	Depth (ft)
F1	Fruitland–initial	13,620	2,402
F2	Fruitland–second (*new*)	18,587	2,795
PL/MV	Point Lookout/Mesa Verde	4,447	4,418
GS	Gallop Sandstone in Mancos	9,145	4,476
D	Dakota	2,083	3,558
M1	Morrison–initial	5,947	4,725
M2	Morrison–new	17,018	6,359
H/P	Hermosa/Paradox	9,704	8,965

Table 4-2. Summary of Water Treatment Cost Analysis

Total Cost of Treatment (incl. concentrate disposal, GW pumping) in $/1000 gal treated capacity								
	F1	F2	PL/MV	GS	D	M1	M2	H/P
Annualized Total Capital	$2.42	$2.69	$2.51	$2.36	$2.37	$2.38	$2.54	$2.93
Annual O&M	$3.96	$4.51	$4.46	$4.52	$4.10	$4.51	$5.29	$5.94
Electrical	$2.35	$2.67	$2.66	$2.74	$2.33	$2.73	$3.49	$4.06
Membrane Replacement	$0.08	$0.08	$0.08	$0.08	$0.08	$0.08	$0.08	$0.08
Chemicals	$0.93	$0.93	$0.93	$0.93	$0.93	$0.93	$0.93	$0.93
Other	$0.60	$0.83	$0.79	$0.77	$0.77	$0.77	$0.80	$0.87
Total Cost (O&M+Cap)	**$6.37**	**$7.20**	**$6.96**	**$6.87**	**$6.47**	**$6.89**	**$7.84**	**$8.87**
Cost of Desalination only - includes only equipment & O&M for desalination (i.e. no ponds, no groundwater (GW) pumping) in $/1000 gal treated capacity								
	F1	F2	PL/MV	GS	D	M1	M2	H/P
Annualized Total Capital	$1.83	$1.87	$1.87	$1.87	$1.87	$1.87	$1.87	$1.87
Annual O&M	$3.05	$3.50	$3.08	$3.16	$2.98	$3.08	$3.42	$3.30
Electrical	$1.44	$1.66	$1.28	$1.39	$1.20	$1.31	$1.61	$1.42
Membrane Replacement	$0.08	$0.08	$0.08	$0.08	$0.08	$0.08	$0.08	$0.08
Chemicals	$0.93	$0.93	$0.93	$0.93	$0.93	$0.93	$0.93	$0.93
Other	$0.60	$0.83	$0.79	$0.77	$0.77	$0.77	$0.80	$0.87
Total Desal Only Cost (O&M+Cap)	**$4.88**	**$5.37**	**$4.95**	**$5.04**	**$4.85**	**$4.96**	**$5.29**	**$5.17**

The water treatment options are shown schematically in Figure 4-1 along with the potential waste heat recovery options that are discussed later in this study. Each of the options studied required calculations for the capital and O&M costs. Most of the calculations are based on the USBR *Desalting Handbook* (USBR [2003]).

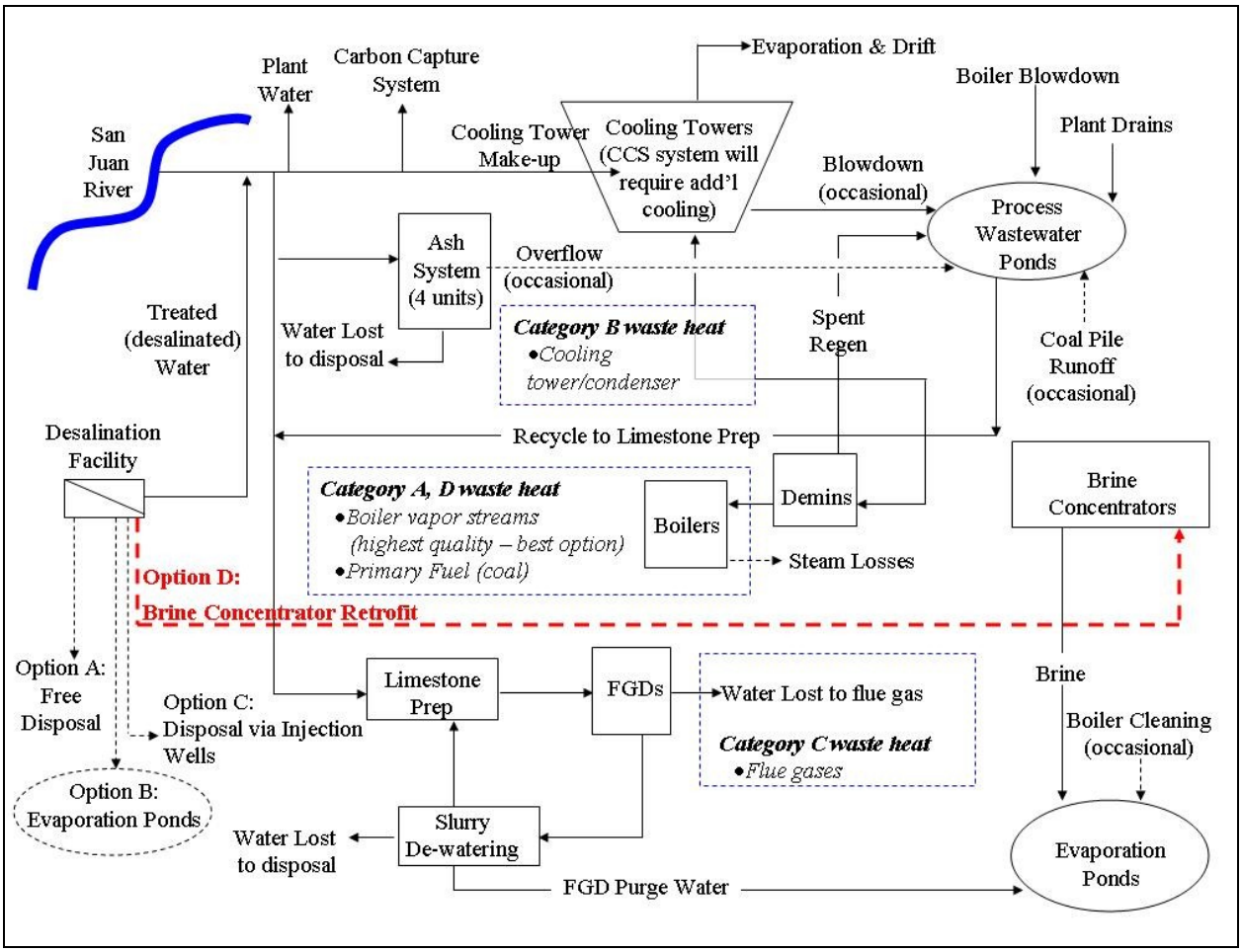

Figure 4-1. Simplified Water Process, San Juan Generating Station. (Adapted from Zammit and DiFilippo, [2004].)

4.1. Water Treatment Calculations

Detailed calculations are shown in Appendix B; however, a summary of the approach is provided here for reference. For each formation, capital and O&M costs were estimated using a series of data, assumptions, and calculations. Table 4-3 summarizes the abbreviations used for the costs.

Table 4-3. Summary of Capital and O&M Cost Abbreviations

Abbreviation	Description
CC_1	Capital Cost: Formation Wellfield Equipment (pumps & materials)
CC_2	Capital Cost: Supply Pipeline equipment
CC_3	Capital Cost: Evaporation Ponds
CC_4	Capital Cost: Desalination Treatment System Equipment
CC_5	Capital Cost: Concentrate Injection Pipeline & Injection Well
OM_1	O&M Cost: Annual Labor
OM_2	O&M Cost: Annual Electrical for RO System
OM_3	O&M Cost: Annual Electrical for BC System
OM_4	O&M Cost: Annual Electrical for Formation Pumping
OM_5	O&M Cost: Annual Electrical for Pipeline Pumping
OM_6	O&M Cost: Annual Membrane Replacement
OM_7	O&M Cost: Annual Chemicals
OM_8	O&M Cost: Other Maintenance
OM_9	O&M Cost: Annual Electrical for Concentrate Injection Pipeline Pumping

4.1.1. Capital Cost Calculation Summary

All capital costs estimated for this model are based on the USBR *Desalting Handbook* (USBR [2003]) figures for brackish water desalination. The handbook provides capital cost estimates based on the desalination capacity (defined as the output, or permeate flow rate) using the units of million gallons per day (MGD). Each figure used for this model was recreated by reading each graph and estimating each of the values (see Appendix B). In most cases, a curve fit was utilized to estimate the capital cost using another metric (e.g., cost per mile of pipeline vs. desalination capacity).

Option D (HERO™ desalination + brine concentrator retrofit) capital costs for CC_3 and CC_4 are calculated slightly different from the other options. The third capital cost (CC_3) component, or the evaporation pond capital cost, is only calculated in the model when the flow to the brine concentrators exceeds their design flow limits as specified in Zammit and DiFilippo (2004).

All options use the same calculation for CC_4, or the desalination treatment system equipment capital cost, which is estimated from the values in Zammit and DiFilippo (2004), Table A-3, for the various equipment pieces associated with that option. **Option A**, **Option B**, and **Option C** include desalination equipment (HERO™) and Receiving, Transfer, and Distribution Piping; **Option D** includes desalination equipment (HERO™) and Receiving, Transfer, and Distribution Piping, and the costs of the brine concentrator retrofits. Since this report is based on lower flow

rates, a ratio of our modeled flow rates to the Zammit and DiFilippo (2004) report flow rates was used to scale the capital costs for CC_4.

4.1.2. Operational & Maintenance (O&M) Calculation Summary

Operation and Maintenance (O&M) costs are somewhat more complicated, and each is summarized here. Most of the O&M calculations assume a capacity factor to allow for time when the desalination plant is not operational. Only the annual labor expense assumes a 100% operational plant. Detailed calculations are described in Appendix B.

- OM_1 (annual labor expense): Based on USBR *Desalting Handbook* (USBR [2003]); desalination capacity in MGD.
- OM_2 (annual HERO™ electricity expense): The energy intensity is estimated from the USBR *Desalting Handbook* in units of kwh/1000 gallons treated water for several water TDS values. A curve fit was used to estimate the electrical consumption for each formation as a function of desalination capacity.
- OM_3 (annual BC electricity expense): This calculation is only performed for **Option D** and is based on the values listed in Zammit and DiFilippo (2004). A ratio of our model's calculated flow rate to the Zammit and DiFilippo report flow rate is used to scale the model's final calculation.
- OM_4, OM_5, OM_9 (various annual pumping electricity expenses): These calculations are based on standard pumping calculations with varying assumptions. They are specific to each formation's depth and distance to the SJGS.
- OM_6 (annual membrane replacement cost): Based on USBR *Desalting Handbook*; desalination capacity in MGD.
- OM_7 (annual chemical cost): Based on the values listed in Zammit and DiFilippo (2004). A ratio of our model's calculated flow rate to the Zammit and DiFilippo report flow rate is used to scale the model's final calculation.
- OM_8 (other maintenance): Assumed to be 1.5% of the total capital cost for equipment. This is similar to the USBR *Desalting Handbook* assumption of 1%.

4.2. Options for Using Power Plant Waste Heat

Thermoelectric power plants often have excess heat that cannot be tapped for additional work due to an unaccommodating design or unfavorable economics. The wasted energy is essentially released into the environment and not reused for other purposes. The most important consideration regarding this waste energy is not necessarily the amount but rather its *value*. Recovery of much of this waste energy could result in other potential benefits such as energy to drive a water cleaning system.

Three possible options exist for waste heat use (listed according to the most to the least economical and effective methods) including (1) **recycle** the heat within the heat system itself, (2) **recover** heat for auxiliary or adjoining systems within the plant, or (3) **convert** the waste heat **to power**.

4.2.1. Waste Heat Recycling and Recovery

Power plants have made substantial advances in recycling waste heat; however, opportunities still exist for advancement in the areas of recovery and power conversion. Advancement in the recovery and power generation areas must evaluate the quality of the waste energy by characterizing the potential attributes, drawbacks, and operating nature of each waste stream. Specific characteristics are summarized in Table 4-4.

Table 4-4. Important Considerations for Waste Heat Recovery[1]

Characteristic	Considerations (operating nature)
Availability	Continuous, cyclic, or intermittent
Temperature	Low or high, constant or variable, predictable or random
Pressure	Positive or negative, high or low, constant or variable
Flow Rate	High or low, constant or variable, predictable or random
Composition	Corrosive, combustible, particulates, condensable, moisture level
Note: 1. Adapted from Thekdi (2007).	

As the temperature of the waste heat goes up so does the efficiency of recovery. As the temperature and reliability of a waste heat stream decrease, the cost to implement and operate may increase. The potential for recovery depends upon the quality of the waste heat, but the options are potentially plentiful. Additionally, combined heat and power systems could be an efficient use of waste heat but also could prove to be very location specific. Table 4-5 summarizes waste heat recovery options.

Table 4-5. Waste Heat Recovery Options[1]

Heat Recovery System	Waste Heat Temperature	Potential Use of Waste Heat	Typical Installed Cost
Steam generation	600°F and higher	Combined heat & power; industrial	$35–60 per 1,000 lb steam generation
Hot water heating	200°F and higher	Plant use	$30,000–50,000 per 1,000 lb steam generation
Plant or building heating	150°F and higher	Plant use	$25,000–50,000 per 1,000 lb steam generation
Absorption cooling systems	300°F and higher	Plant use	$750–1,500 per ton of refrigeration capacity
Cascading to lower temperature heating processes	300°F and higher	Plant use; industrial	$40,000–100,000 per MMBTU transferred
Note: 1. Adapted from Thekdi (2007).			

As described by Shuster (2008 and 2009) and represented in a report by NETL (2007b), the condensers play a vital role in power plant operations because the steam must be condensed for the process. However, the heat is released to the atmosphere. If an industrial process could use this heat beneficially while still providing the condensing necessary for steam plant operations, waste heat recovery implementation opportunities may be found at many existing thermoelectric power plants. Waste energy sources within a power plant system are summarized in Table 4-6.

Table 4-6. Potential Waste Energy Sources

Category	Energy Source	Quality
A	Vapor streams (boiler)	Higher temperature, the greater the value + latent heat also recoverable
B	Cooling water	Low grade–useful gains if heat is exchanged with incoming fresh water, water can be captured
C	Heat and water in flue gases	Higher the temperature the greater the value for heat recovery
D	Moisture in primary fuel (coal)	Drying coal improves overall plant efficiency, water can be captured

In response to projected increases in thermoelectric capacity demand and population growth of 23% and 24%, respectively, from 2005 to 2030, recent efforts have focused on improving process efficiencies within the power plants (Energy Information Administration [2007] and U.S. Census Bureau [2007]). This has resulted in a wide range of projects directed at utilizing waste energy to lower costs and improve efficiency at power plants. A brief summary of current project work in each category utilizing waste energy recovery is summarized here:

Category A–steam to condenser units (highest energy)

- Diffusion Driven Desalination (DDD), University of Florida
- Membrane Distillation (MD), Arrakis/New Jersey Institute of Technology
- Wet Surface Air Cooler (WSAC), Electric Power Research Institute
- Carrier Gas Enhanced Atmospheric Pressure Desalination, Arizona State University
- Low Temperature Evaporation (LTE), Bhabha Atomic Research Centre, India

Category B–cooling tower hot water side (low energy)

- No substantial development in this area with respect to waste heat; however, improvements in cooling tower water quality and capture of evaporating water are being evaluated. The goal of this work is to lower the water consumption of the cooling tower system and/or enable the use of impaired water in recirculating cooling systems. Development in this area may be linked with other category projects.

Category C–flue gas stream/ water recovery

- WETEX (Liquid Desiccant Process), University of North Dakota's Energy & Environmental Research Center, Siemens Power Generation

Category D–coal drying

- Coal Drying, Energy Research Center/Lehigh University concept of coal drying utilizes waste heat from Categories B and C

The majority of the waste heat recovery technologies are not technologically mature enough to provide sufficient economic evaluation at this time. However, a few of the technology developers have conducted preliminary (based on laboratory studies) or theoretical cost analyses. Additionally, the literature addressing projects utilizing waste energy recovery points toward the fact that water is a primary focal point. One study, for example, completed by Levy et al. (2006) provides a detailed and insightful perspective on the role of this technology. This research breaks down all costs, capital and annual, including plant impact costs for anticipated technology operating scenarios.

Additionally, several scenarios were developed for waste heat to be recovered from the condenser stream for coal drying (CCW) and a combined waste heat recovery of the condenser and flue gas streams for coal drying (CCW/FG). The temperature and moisture content of the waste streams drive the costs to implement these types of technologies. A few of the key points of the analysis by Levy et al. (2006) include the fact that as the percentage reduction in moisture increases from just below 10 percent to just over 18 percent for a CCW/FG system, the mean annual millions of dollars in savings across several scenarios may also increase from just over $3 million to over $5 million, whereas the annual costs may reach approximately $5 million to between $5 million and $4 million for these levels, respectively. On the other hand, for a CCW system, as the percentage reduction in moisture increases from below 5% to over 15%, the mean savings may reach from just below $3 million annually to approximately $6 million per year. The corresponding costs for this type of system could reach from between below $6 million per year to over $21 million per year. Thus the cost-benefit analysis may be more attractive for a higher percentage reduction in moisture for the CCW/FG system over the CCW system (Levy et al. [2006]).

4.2.2. Utilization of Power Plant Waste Heat

The energy crisis of the 1970s caused rising electricity and fossil fuel costs resulting in interest in the use of power plant waste heat. In 1976, about two of the 74 quads of energy used–or one million barrels per day of oil equivalent–could have been saved with only 12-percent utilization of available discharge heat (Goss [1978]).

During, and for a short time after, the 1970s energy crisis, numerous nationwide workshops and publications were produced regarding the potential of power plant waste heat; however, the majority of the information was focused on high-level planning. Consequently, the published information is primarily summary/overview in nature.

Some of the potential uses of waste heat identified in the 1970s and 1980s include the following:

1. agricultural uses
    a. greenhouse production
    b. soil warming for crops
    c. frost protection and irrigation
    d. reclamation of livestock waste
    e. wastewater treatment
    f. enhancing crop drying

2. aquaculture uses–primarily to enhance growth of fresh and saltwater species

3. industrial process applications–45 industries were identified ranging from food processing to pulp & paper mills, to foundries

4. residential uses

More recently, production of fresh water has been added to this list as water continues to become more scarce.

Dozens of technology demonstrations related to agricultural uses and aquaculture were field tested during the 1980s, and many more paper studies were conducted on specific applications of waste heat in categories industrial process applications and residential uses.

4.2.3. Challenges and Opportunities

The Tennessee Valley Authority and Northern State Power Company conducted a comprehensive workshop in 1978 to address the status of waste heat utilization technology. In summary, the workshop participants concluded that there were four problem areas constraining commercial adoption of waste heat utilization research as outlined by Goss (1978):

1. the need for meaningful commitments to finance waste heat research and development
2. the lack of site-specific information regarding the potential of waste heat use
3. the questionable reliability of waste heat supply and the seasonal fluctuation of waste heat temperatures
4. the need for information regarding the economics and engineering of waste heat delivery systems

Today the same concerns exist. However, the renewed national focus on the nexus of energy and water systems is an opportunity for review of power plant waste heat.

There exists an opportunity in the power industry to increase the productivity of existing and new power plants by optimizing the usage of waste heat within each facility. The first step toward realizing this opportunity is characterizing the waste heat sources at every facility nationwide. This will require a systematic evaluation of each power plant (or plant type) to identify all potential waste heat sources. The waste sources can be characterized (quantity, quality, site specifics, etc.) and subsequently catalogued. Waste heat delivery and utilization technologies can be screened against this catalogue of waste heat sources. Finally, the

compilation of this data will allow a full scale engineering and economic assessment of the true potential of power plant waste heat. With an effort of this size, it is likely to identify gaps in technology and thereby provide guidance with efficient opportunities to use waste heat in an effort to increase the value of the power plant's overall system.

5. The Integrated Assessment Model

The goal of the integrated assessment model is to illustrate the high-level engineering, scientific, and economic constraints associated with the suite of technologies applied to an existing power plant for both carbon sequestration and the use of brackish water from a saline formation. The assessment model builds on the geochemical, geomodeling, water treatment, and systems analyses to develop an integrated systems model to identify the drivers within the system (e.g., flows of CO_2, costs associated with certain components, etc.).

The analysis first assesses the geologic carbon storage information applied to a representative power generating station, such as the SJGS in New Mexico. The analysis then evaluates CO_2 storage within a saline formation along with a water extraction and treatment system to exploit the potential extracted brackish water to help meet a portion of the power plant's cooling needs. Conceptually, this system may seem straightforward; however, the increasingly complex components of this type of study depend on several key engineering, geological, and economic challenges, as well as interactions to be examined in greater detail in order to assess the system's overall feasibility.

To address these overarching issues, a dynamic simulation model incorporates the flows and stocks associated with this system (e.g., power plant's metrics, electricity production, flows of CO_2, water resource needs and treatment costs, etc.) and the economics associated with the system. This model provides interested parties with the ability to perform *what-if* scenario analyses in real time. For example, the model can address questions such as, What if the level of CO_2 capture increases from 50% to 70%? and What will the electricity costs look like due to this change? Similar scenario questions can be developed for different power plant configurations, geological formations used for CO_2 storage, and brackish water pumping treatment technologies.

5.1. The Power Plant and Carbon Capture and Storage Parameters

Figure 5-1 illustrates the central results page of the Water, Energy, and Carbon Sequestration (WECS) model. The key metrics of interest provided by the model are the input variables for the SJGS, the representative formation characteristics (e.g., size, depth), as well as several high-level results including the potential longevity of the formation to store CO_2, and how much water could be extracted from the formation and, with treatment, supplement the cooling water required for the power plant. The costs associated with the system's components are also represented based on work developed by (NETL [2007c]) and others reported in Appendix C.

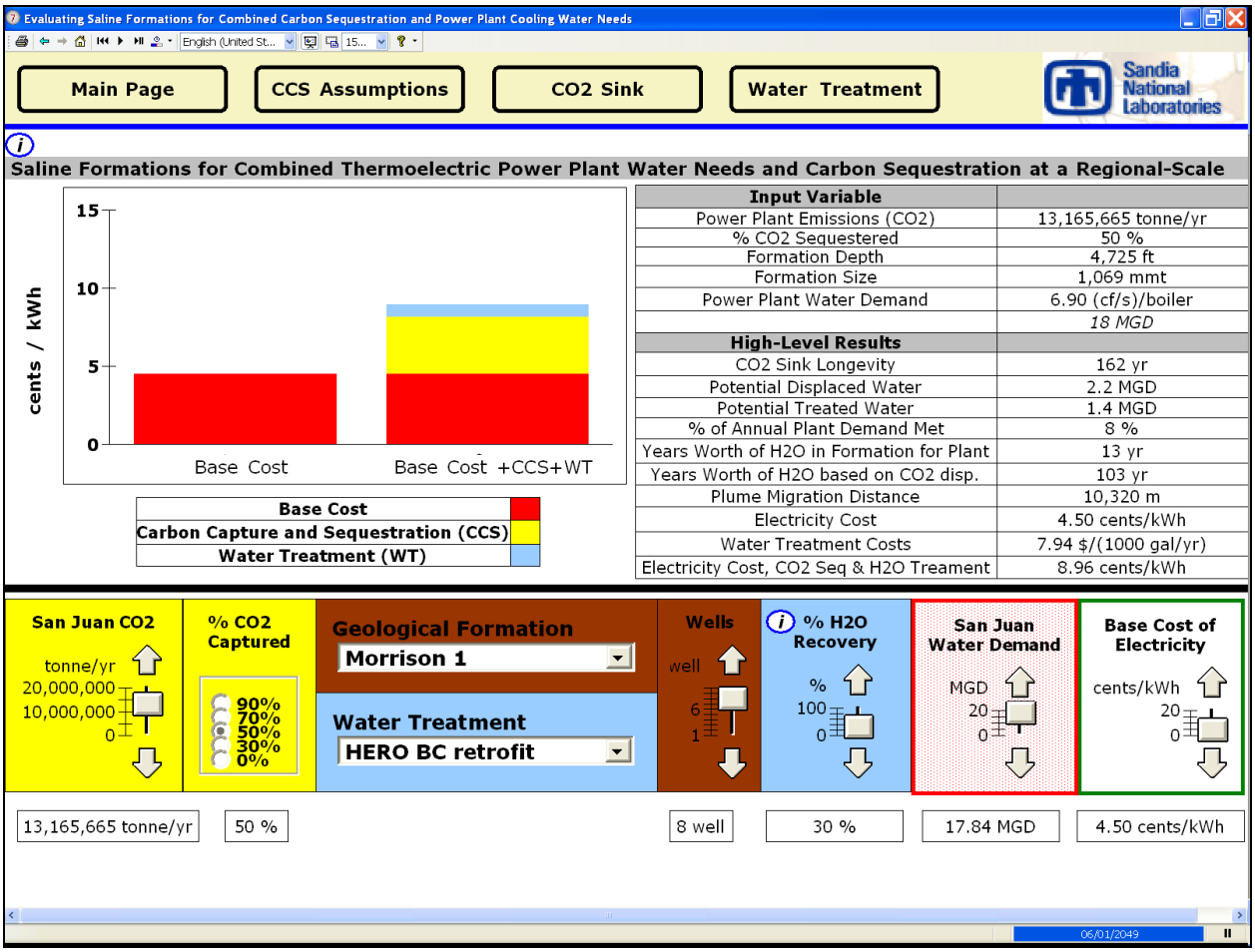

Figure 5-1. The Integrated Assessment Water, Energy, and Carbon Sequestration (WECS) Model

5.2. Hydrological Assumptions

Figure 1-1 (Chapter 1) addresses the high-level geophysical aspects of storing CO_2 in a geological formation and the subsequent (assumed) volume of displaced water. The base case of the analysis uses a shallow location in the Morrison formation to illustrate the scale of the CO_2 storage and potential volumes of displaced water. The Morrison formation, as described and highlighted in the geochemical component of this analysis, may be a candidate to store CO_2 while at the same time serving as a source of non-traditional brackish waters for power plant cooling.

The analysis begins by using the hydrostatic pressure assumption based on the volumes available within the formation to store CO_2.[1] Thus every gram of CO_2 injected underground potentially displaces approximately 1.52 cm^3 of water.

5.3. CO_2 Storage and Brackish Water Volume Analysis

Capturing and storing CO_2 within a saline-bearing formation presents an opportunity to use the potentially displaced saline waters. Using the CO_2 density displacement information outlined in Clark (1966) and Benthan and Kirby (2005), the WECS modeling framework assumes, under the base case scenario, that using the hydrostatic pressure level(s), for every gram of CO_2 injected underground, approximately 1.52 cm^3 of saline water may be displaced. While the pressures involved with this test case framework lie within the supercritical range of the CO_2 density-vapor curve analysis, the dynamic simulation model allows users to adjust the potential density of CO_2 based on attributes of the formation under consideration within the bounds of the geological formation's constraints. The initial depth for the Morrison formation, the first location (Morrison 1) is 4,725 feet.[2] This translates into an approximation where 400 gallons of saline water may be displaced for every tonne of CO_2 stored under these representative conditions. The specific gallons of saline water displaced, along with the tonnes of CO_2 stored in any given formation, will likely be very site-specific. Additionally, the water treatment technologies employed in this analysis further decrease the potential volumes of treated water available from the formations given that there are losses in those processes as well. This assessment framework and subsequent model should be considered a starting point that compiles the key aspects of a combined CO_2 storage and water extraction and treatment system. Field testing may be required to verify the validity and reliability of this assessment framework's metrics and relationships.

Figure 5-2 illustrates the WECS model inputs for the water treatment assessment. The model user has the ability to modify the types of water treatment options one wants to employ as outlined in the water treatment section of this report. The base case analysis uses the High-Efficiency Reverse Osmosis (HERO™) system.

---

[1] NatCarb builds from example conditions of 8,000 feet deep, 140°F, and 3,500 pounds per square inch (psi). With a column of water 33 feet high giving a pressure of around one atmosphere (1 bar), this example indicates NatCarb works from hydrostatic pressure for the well depth: [(8,000 feet / 33 feet) * 14.7 (psi/bar)] = 3,563 psi. The NatCarb example approximates the pressure to 3,500 psi, which corresponds to (3,500 (psi/bar) / 14.7 (psi)) = 238 bars. The density of CO_2 given is 48.55 lbs mass per cubic foot using this assumption. Therefore, the volume displacement relationship of sequestered CO_2 to H_2O is (1,000g/kg * 48.55 lbs / 2.2046 lbs/kg)) / ((2.54^3) * 12^3) cm^3 per ft^3) = 0.777 g (CO_2) / cm^3 (H_2O). The different temperatures and depths associated with this location (Morrison formation) and the subsurface pressures used in the TOUGH2 modeling were approximated to be 170 bar, 1,700–1,750 meters, 30°C/km geothermal gradient, and 0.1 bar/meter hydrostatic gradient, and builds from the works of Clarke (1966) and Bentham and Kirby (2005). The displacement for a CO_2 density of approximately 0.65 equates to ~1.52 cubic centimeters of water per gram of CO_2.

[2] Phase I of the analysis used the *Handbook of Physical Constants* (Clark [1966]). Phase II continues to refine the pressure-volume-temperature relationships using TOUGH2 and other equation-of-state modeling, and the overarching results of the analysis will likely change in subsequent work. This would reflect these changes in the pressure calculations.

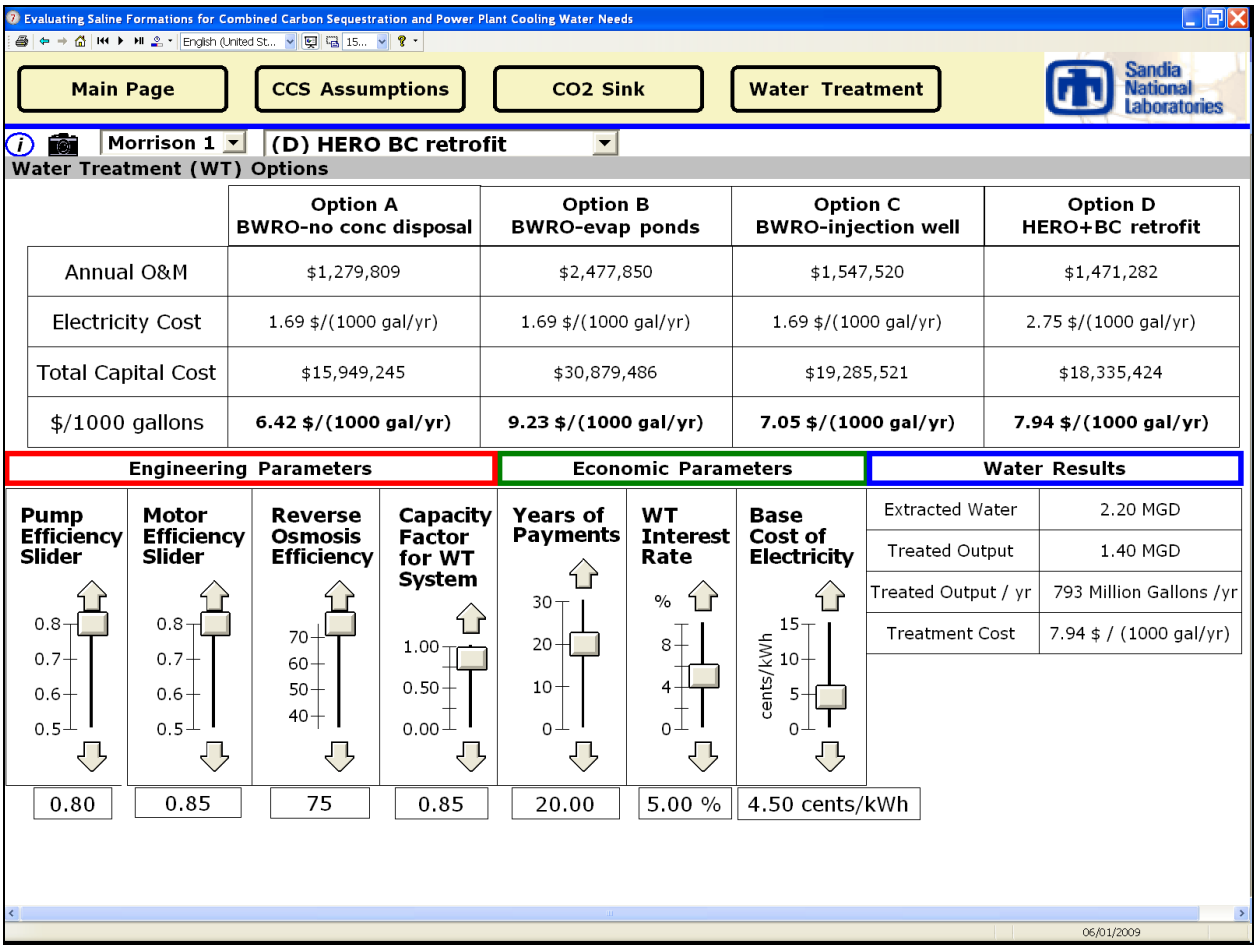

Figure 5-2. The Water Treatment Options of the WECS Model

Figure 5-3 illustrates the initial energy, water, net CO_2 emissions, and costs associated with a base plant with carbon capture and storage and water treatment. Retrofitting the existing plant may increase the energy penalty by approximately 360 megawatts (MW), or a 20% energy penalty under the initial assumptions. Additionally, this will decrease the plant's overall CO_2 emissions profile by 43%, which this includes an initial 50% level of CO_2 capture, plus the associated parasitic power requirements for both the CCS and water treatment systems.

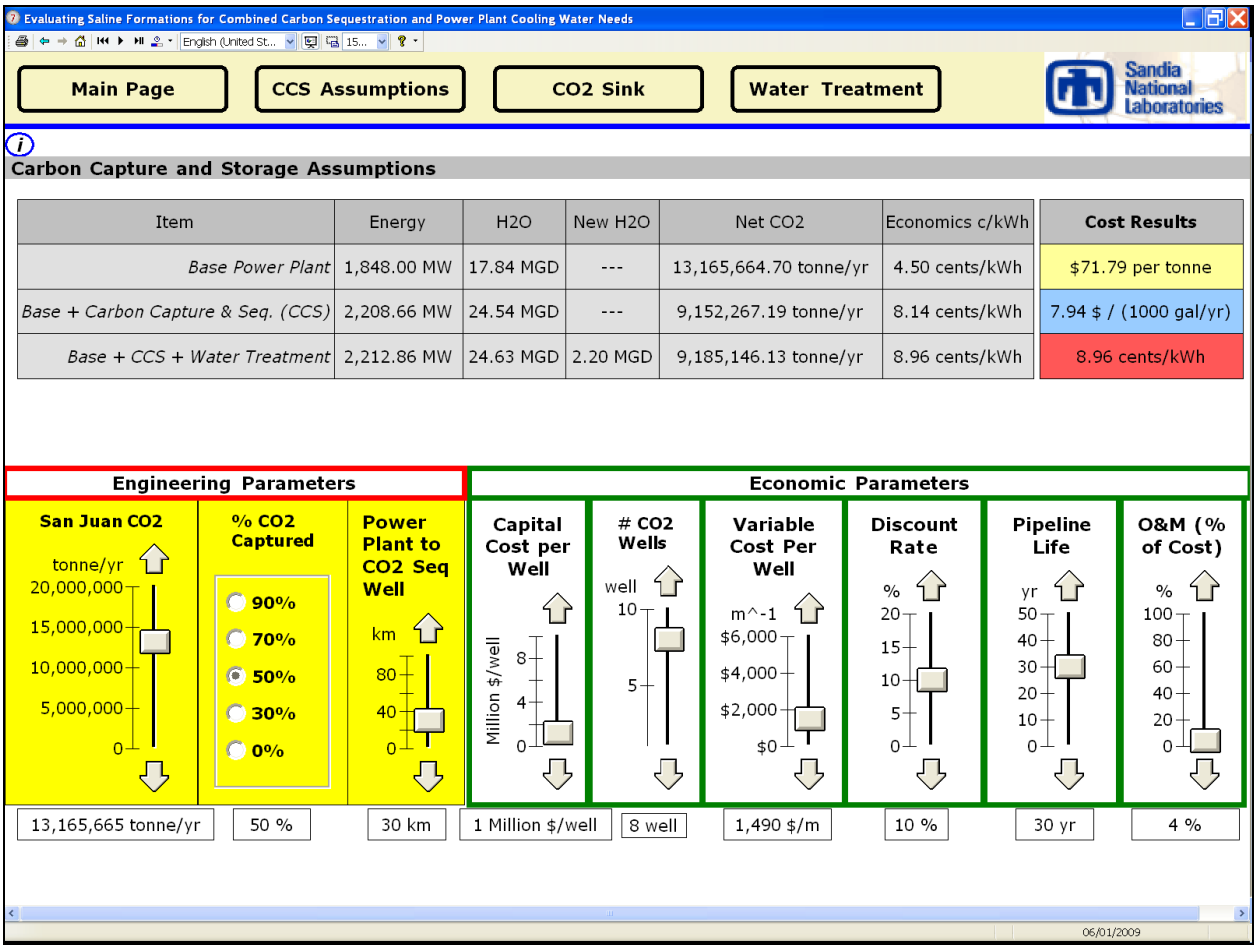

Figure 5-3. The Carbon Capture and Storage Options of the WECS Model

Table 5-1 summarizes the central components of the systems analysis shown in Figure 1-1 (Chapter 1) and those used to populate the working WECS model.[3]

[3] Cost estimates have been updated throughout the analysis to 2009 U.S. dollars (Office of Management and Budget [2009]).

Table 5-1. Integrated Assessment Model Input Parameters and Working Results, Morrison 1 (Shallow) Site, San Juan Power Plant[1]

Section	Description	Assumption	Units	Notes
1	**Power Plant**	1,848	MW	San Juan Generating Station
	Capacity Factor	72	%	U.S. Environmental Protection Agency (EPA) (2006–2007) (eGRID)
	Carbon Dioxide Capture	50	%	Adjustable capture %
	CO_2 Emissions	14,512,417.50	tons/year	EPA (2006–2007) (eGRID)
	CO_2 Sequestered	6,582,722	tonnes/year (2,500 tonnes/day/well)	tonnes sequestered (or 2,500 tonnes/day/well).
2	**Saline Formation**	1,069	mmt	Morrison formation, CO_2 storage volume; calculated using TOUGH2
	Representative Depth	4,725	feet	Calculated using TOUGH2
	Year's worth of CO_2 Storage Resource	160+	years	volume/tonne sequestered
3	**Saline Water Displaced**	170	bar	hydrostatic pressure assumption/approximation, TOUGH2 analysis.
	CO_2 Displacing H_2O	1.52	cubic centimeters of H_2O per gram of CO_2	Based on the density of CO_2 vapor curve and work described in Clark (1966) and Bentham and Kirby (2005).
4	**H2O Displaced and Demand**	793	million gallons/year	Potential water volume assuming 30% recovery
	Annual H_2O Treated	511	million gallons/year	Potential extracted and treated water, 1.4 million gallons/day
	Power Plant Cooling Towers' H_2O demand	6.4	billion gallons/year	27.6 ft3/second, EPA (2006–2007) (eGRID); ~17.8 million gallons/day
	Year's Worth of H_2O Supply	100+	years (based on water displaced)	Based on the water displaced by CO_2.
	Year's Worth of H_2O Supply	10+	years (based on plant demand)	Based on the treated water MGD and demand of the plant
5	**Desalination Costs Base Case**	7.94	$/thousand gallons	**Option D**, HERO+BC option

Note:

1. Adapted and updated from Kobos et al. (2008).

5.3. Sensitivity Analysis: Water Recovery Scenario Framework

The results given in Table 5-2 show that as the percent of CO_2 captured increases, the potential to meet a portion of the power plant's needs also increases. Similarly, the percent of annual water demands met for the representative power plant may also increase as the volumes of CO_2 stored increase. It is paramount to recognize that many key assumptions will require further study and verification through field tests, among other means, to address (or bound) any potential displacement of saline water by the potential CO_2 plume. The CO_2 plume and the brackish water are assumed to not necessarily be in direct communication. Therefore, we initially assume that extracting the brackish water will be driven by pumping rather than any push from a CO_2 plume. This makes the combined system actually two projects in one; both a CO_2 storage system with a conceptually associated saline water extraction and a treatment system in another well with sufficient spacing between the injection and withdrawal wells to ensure no producing of injected CO_2.

Table 5-2. Carbon Capture, Water Treatment, and Electricity Cost Scenarios[1]

Item	Percent of CO_2 Captured				
	0	**30**	**50**	**70**	**90**
CO_2 Sink Longevity	—	271 years	162 years	116 years	90 years
Treated, Displaced Water	—	476 MGY	793 MGY	1,110 MGY	1,427 MGY
Annual Plant Cooling Towers' Demand Met	—	5%	8%	11%	14%
Years Worth of H_2O in Formation (based on the plant's demand)	—	13 years	13 years	13 years	13 years
Water Treatment Costs	—	8.65 $/1,000 gal.	7.94 $/1,000 gal	7.63 $/1,000 gal.	7.94 $/1,000 gal.
Electricity Cost, CO_2 Seq., Pipelines, Injection Wells & H_2O Treatment[2]	—	8 cents/kWh	9 cents/kWh	11 cents/kWh	12 cents/kWh

Notes:

1. Rounded where appropriate for illustration.
2. Preliminary cost calculations assuming a 100 km pipeline.

Lastly, it is important to highlight the number of CO_2 injection wells. During preliminary runs of the TOUGH2 reservoir modeling of the Morrison formation, accepting CO_2 assumes a one well scenario that will likely be developed further. The analysis assumes that each well can inject up to 2,500 tonnes of CO_2 per day. This represents approximately 7% of the SJGS's annual CO_2 emission profile. To sequester 50% of the total annual CO_2 emissions, approximately eight wells may be required. Thus, by implementing this type of system with one initial CO_2 injection well, the potential displaced water would meet approximately 2% of the plant's annual water demands when accounting for sequestering 7% of the plant's total CO_2.

The costs, flow rates, and year's worth of CO_2 capacity and water supply could change dramatically depending on several factors including the geosystem's characteristics, the

engineering of the storage system, and regulatory barriers associated with using a saline formation resource for these purposes.

Table 5-3 shows a base case results scenario that assumes 50% CO_2 capture at ~$72/tonne, with a $0.045/kWh base plant levelized cost of electricity. In the table, the first value given is the cost ($) per 1,000 gallons per year. The value in parentheses is the levelized electricity cost in dollars ($) per kWh. The entries for each option, then, specify

$/1,000 gal/yr ($/kWh)

Table 5-3. Carbon Capture, Water Treatment, and Electricity Cost Scenarios

Formation	Option A BWRO	Option B BWRO-Evaporation Ponds	Option C BWRO-Injection Well	Option D HERO+BC Retrofit
Morrison 1	6.42 (8.80)	9.23 (9.09)	7.05 (8.87)	7.94 (8.96)
Morrison 2	7.42 (8.91)	10.23 (9.20)	8.05 (8.97)	8.94 (9.06)
Fruitland 1	6.68 (8.83)	9.50 (9.12)	7.32 (8.90)	8.21 (8.99)

6. Future Work

In future efforts, the modeling framework will look to include additional formations to offer a multi-formation assessment tool as the project nears completion. The analysis may continue developing and expanding the scale and scope of the user model's input, as well as expand the framework of the integrated assessment model, the WECS model, into a national-scale model.

With a model that includes these additions and enhancements, users will be able to draw from existing saline formation databases such as NatCarb (developed under funding by NETL) and power plant databases such as eGRID (developed by the EPA), as well as build from geochemical and geomechanical studies of CO_2 storage effects and migration rates (developed by the NETL/SNL project team). These capabilities will make it possible to determine optimal locations (throughout the entire U.S.) for power plant systems that use coupled CO_2 storage and extracted, treated water for cooling. This, in turn, will lay the groundwork as a first-order assessment for potential pilot plant-scale studies and provide for assessing the scale-up potential for these combined technologies in the face of water stress throughout the U.S.

References

Allis, R.G., T.C. Chidesy, C. Morgan, J. Moore, and S.P. White. 2003. "CO_2 Sequestration Potential Beneath Large Power Plants in the Colorado Plateau—Southern Rocky Mountain Region, USA." Proceedings of the 2nd Annual Conference on Carbon Sequestration, Alexandria, VA, May 5–8.

Bentham, M., and G. Kirby. 2005. "CO_2 Storage in Saline Aquifers." *Oil and Gas Science and Technology* 60: 559–67.

Bethke, C.M. 1998,. The Geochemist's Workbench: A Users Guide to Rxn, Act2, Tact, React, and Gtplot. Urbana: University of Illinois Hydrology Program.

Bickle, M., A. Chadwick, H. Huppert, M. Hallworth, and S. Lyle. 2007. "Modelling Carbon Dioxide Accumulation at Sleipner: Implications for Underground Carbon Storage." *Earth and Planetary Science Letters* 255: 164–76.

Clark, S.P., Jr. 1966. *Handbook of Physical Constants*. Geological Society of America Memoir 97. New York: GSA Publishers.

Dam, W.L., J.W. Kernodle, G.W. Levings, and S.D. Craigg. 1990a. "Hydrogeology of the Morrison Formation in the San Juan Structural Basin, New Mexico, Colorado, Arizona, and Utah." *U.S. Geological Survey Hydrologic Investigations Atlas HA-720-J*. Reston, VA: U.S. Geological Survey.

Dam, W.L., J.W. Kernodle, C.R. Thorn, G.W. Levings, and S.D. Craigg. 1990b. "Hydrogeology of the Pictured Cliffs Sandstone in the San Juan Structural Basin, New Mexico, Colorado, Arizona, and Utah." *U.S. Geological Survey Hydrologic Investigations Atlas HA-720-D*. Reston, VA: U.S. Geological Survey.

DiPietro, P., Gerdes, K. and C. Nichols, 2008, Water Requirements for Existing and Emerging Thermoelectric Plant Technologies. DOE/NETL-402/080108.

Energy Information Administration. 2007. "Regional Tables." *Annual Energy Outlook 2006*. Washington, DC: U.S. Department of Energy.

Fassett, J.E., and J.S. Hinds. 1971. *Geology and Fuel Resources of the Fruitland Formation and Kirtland Shale of the San Juan Basin, New Mexico and Colorado*. Professional Paper 676. Reston, VA: U. S. Geological Survey.

Frenzel, P.F., and F.P. Lyford. 1982. *Estimates of Vertical Hydraulic Conductivity and Regional Ground-Water Flow Rates in Rocks of Jurassic and Cretaceous Age, San Juan Basin, New Mexico and Colorado*. Report 82-4015. Reston, VA: U.S. Geological Survey, Water Resources Investigations.

Frenzel, P. 1983. *Simulated Changes in Ground-Water Levels Related to Proposed Development of Federal Coal Leases, San Juan Basin, New Mexico*. Open File Report 83-949. Reston, VA: U.S. Geological Survey.

Garrels, R.M., and C.L. Christ. 1965. *Solutions, Minerals and Equilibria*. San Francisco: Freeman, Cooper.

Goss, L.B. 1978. *Factors Affecting Power Plant Waste Heat Utilization*. (1980 ed.) Oxford: Pergamon.

Gozalpour, F., S. Ren, and B. Tohidi, B. 2005. CO_2 EOR and Storage in Oil Reservoirs. *Oil and Gas Science and Technology* IFP 60 537–46.

Heath, J., McPherson, B., Phillips, F., Cooper, S., and Dewers, T. 2009. *Natural helium as a screening tool for assessing caprock imperfections at geologic CO_2 storage sites*, in Gale, J., Herzog, H., and Braitsch, J., eds., Greenhouse Gas Control Technologies 9: Energy Procedia, p. 2903-2910.

Hovorka, S.D., M.L. Romero, A.G. Warne, W.A. Ambrose, T.A. Tremblay, R.H. Treviño, and D. Sasson. 2000. *Sequestration of Greenhouse Gases in Brine Formations*. Austin: Bureau of Economic Geology. <http://www.beg.utexas.edu/environqlty/co2seq/dispslsaln.htm> or: <http://www.beg.utexas.edu/environqlty/co2seq/co2data.htm> (for brine chemistry).

Kernodle, J.M. 1996. *Hydrogeology and Steady-State Simulation of Ground-Water Flow in the San Juan Basin, New Mexico, Colorado, Arizona, and Utah*. Report 95-4187. Reston, VA: U.S. Geological Survey, Water Resources Investigations.

Kernodle, J.M., G.W. Levings, S.D. Craigg, and W.L. Dam. 1989. "Hydrogeology of the Gallup Sandstone in the San Juan Structural Basin, New Mexico, Colorado, Arizona, and Utah." *U.S. Geological Survey Hydrologic Investigations Atlas HA-720-H*. Reston, VA: U.S. Geological Survey.

Kernodle, J.W., C.R. Thorn, G.W. Levings, S.D. Craigg, and W.L. Dam. 1990. "Hydrogeology of the Kirtland Shale and Fruitland Formation in the San Juan Structural Basin, New Mexico, Colorado, Arizona, and Utah." *U.S. Geological Survey Hydrologic Investigations Atlas HA-720-C*. Reston, VA: U.S. Geological Survey.

Kobos, P.H., M.A. Cappelle, ,J.L. Krumhansl, ,T. Dewers, ,D.J. Borns, ,P.V. Brady, and A. McNemar. 2008. "Using Saline Aquifers for Combined Power Plant Water Needs and Carbon Sequestration." 28th USAEE/IAEE North American Conference, New Orleans, December 3–5.

Kobos, P.H., J.L. Krumhansl, T.A. Dewers, J.E. Heath, M.A. Cappelle, D.J. Borns, G.T. Klise, B.P. Dwyer, and A. McNemar. 2009 "Combining Power Plant Water Needs and Carbon Storage using Saline Formations: An Assessment Tool." Eight Annual Conference on Carbon Capture and Sequestration, Pittsburgh, May 4–7.

Krauskopf, K.B. 1967. *Introduction to Geochemistry*. New York: McGraw-Hill.

Levy, E.K., N. Sarunac, H. Billergen, and H. Caram. 2006. *Use of Coal Drying To Reduce Water Consumed in Pulverized Coal Power Plants, Final Report* (March). DOE Award Number DE-FC26-03NT41729. Bethlehem, PA: Lehigh University, Energy Research Center.

Lorentz, J., and S. Cooper. 2003. "Tectonic Setting and Characteristics of Natural Fractures in Mesaverde and Dakota Reservoirs of the San Juan Basin." *New Mexico Geology* 25: 3–15.

McCabe, W., J. Smith, and P. Harriott. 1993. *Unit Operations of Chemical Engineering*. 5th ed. New York: McGraw-Hill.

National Energy Technology Laboratory (NETL). 2007a. Distributed National Carbon Sequestration Database and Geographical Information System (NatCarb). <http://www.Natcarb.org>.

National Energy Technology Laboratory (NETL). 2007b. *Water Supply for Sustainable Thermoelectric Power Production in the Snake/Columbia Basin, Meeting the Energy and Water Needs of the Snake/Columbia River Basin in the 21st Century*. Presentation by A. McNemar. Boise, June 26.

National Energy Technology Laboratory (NETL). 2007c. *Carbon Dioxide Capture from Existing Coal-Fired Power Plants* (December 2006). DOE/NETL-401-110907. Albuquerque: U.S. Department of Energy.

Office of Management and Budget. 2009. "Gross Domestic Product and Deflators Used in the Historical Tables." July 13, 2009. <http://www.whitehouse.gov/omb/budget/fy2010/assets/hist10z1.xls>.

Ogden, J. 2002. "Modeling Infrastructure for a Fossil Hydrogen Energy System with CO_2 Sequestration." Sixth Greenhouse Gas Control Technologies Conference, Kyoto, Japan.

Pruess, K. 2005. *ECO2N: A TOUGH2 Fluid Property Module for Mixtures of Water, NaCl, and CO_2*. LBNL-43134. Berkeley: Lawrence Berkeley National Laboratory.

Pruess, K., C. Oldenburg, and G. Moridis. 1999. *TOUGH2 User's Guide*. Version 2. LBNL-43134. Berkeley: Lawrence Berkeley National Laboratory.

Pruess, K., T.F. Xu, J. Apps, and J. Garcia. 2003. "Numerical Modeling of Aquifer Disposal of CO_2." *SPE Journal* 8.1 (March): 49–60.

Shuster, E. 2008. Personal communication with author.

Shuster, E. 2009. Personal communication with author.

Stone, W., and N. Mizell. 1978. *Basis Subsurface Data Compiled for Hydrogeologic Study of the San Juan Basin, Northwest New Mexico*. Open File Report 89. Socorro, NM: New Mexico Bureau of Mines and Mineral Resources.

Stone, W.J., F.P. Lyfrod, P.F. Frenzel, N.H. Mizell, and E.T. Padgett. 1983. *Hydrogeology and Water Resources of San Juan Basin, New Mexico*. Hydrologic Report 6. Socorro, NM: New Mexico Bureau of Mines and Mineral Resources.

Thekdi, A.C. 2007. *Waste Heat to Power, Economic Tradeoffs and Consideration*. Presentation. 3rd Annual Waste Heat to Power Workshop 2007, September 25, 2007, Houston.

Thomas, B. 1989. *Simulation Analysis of the Ground-Water System in Mesozoic Rocks in the Four Corners Area, Utah, Colorado, Arizona, and New Mexico*. Report 88-4086. Reston, VA: U.S. Geological Survey, Water Resources Investigations.

Thorn, C.R., Levings, G.W., Craigg, S.D., Dam, W.L., and Kernodle, J.M., 1990a, *Hydrogeology of the Ojo Alamo Sandstone in the San Juan structural basin*, New Mexico, Colorado, Arizona, and Utah: U.S. Geological Survey Hydrologic Investigations Atlas HA-720-B, scale 1:1,000,000 and 1:2,000,000, 2 sheets.

U. S. Bureau of Reclamation (USBR). 2003. *Desalting Handbook for Planners*. 3rd ed. Washington, DC: United States Department of the Interior.

U.S. Census Bureau. 2007. *Population Division, Interim State Population Projections*. Washington, DC: Economics and Statistics Administration.

U.S. Department of Energy/National Energy Technology Laboratory. 2007. *Power Plant Water Usage and Loss Study* (May 2007). Albuquerque: U.S. Department of Energy. <http://www.netl.doe.gov/technologies/coalpower/gasification/pubs/pdf/WaterReport_Revised%20May2007.pdf>.

U.S. Environmental Protection Agency (EPA). 2006–2007. Emissions & Generation Resource Integrated Database (eGRID). Version 1.0. <http://www.epa.gov/cleanenergy/energy-resources/egrid/index.html>.

White, S.P., R.G. Allis, J. Moore, T. Chidesy, C. Morgan, W. Gwynn, and M. Adams. 2005. "Simulation of Reactive Transport of Injected CO_2 on the Colorado Plateau, Utah, USA." *Chemical Geology* 217: 387–405.

Xu, T.F., J.A. Apps, and K. Pruess. 2003. "Reactive Geochemical Transport Simulation to Study Mineral Trapping for CO_2 Disposal in Deep Arenaceous Formations." *Journal of Geophysical Research–Solid Earth* 108: 2071.

Xu, T.F., J.A. Apps., and K. Pruess. 2004. "Numerical Simulation of CO_2 Disposal by Mineral Trapping in Deep Aquifers." *Applied Geochemistry* 19: 917–36**.**

Xu, T.F., J.A. Apps, and K. Pruess. 2005. "Mineral Sequestration of Carbon Dioxide in a Sandstone-Shale System." *Chemical Geology* 217: 295–318.

Xu, T.F., J.A. Apps, K. Pruess, and H. Yamamoto. 2007. "Numerical Modeling of Injection and Mineral Trapping of CO_2 with H_2S and SO_2 in a Sandstone Formation." Chemical Geology 242: 319–46.

Zammit, K., and M.N. DiFilippo. 2004. *Use of Produced Water in Recirculating Cooling Systems at Power Generating Facilities, Treatment & Disposal Analysis: Semi-Annual Technical Progress Report, April 12, 2004 to October 22, 2004*. Palo Alto: Electric Power Research Institute.

Appendix A: Geochemical Model Results and Discussion Points for the Morrison and Fruitland Formations

The geochemical modeling results for two additional sites, the Morrison M2 and Fruitland F2 formations are presented as follows:

- Morrison Formation (M2), Table A-1
- Fruitland Formation (F2), Table A-2

See Kobos et al. (2008), Table 1-1, for similar information regarding modeling results for older sites.

Discussion points based on the modeling results follow the tables.

Table A-1. Morrison Formation Geochemical Modeling Results

	Full Equilb.	Full Equilb.	100 years	350 years	Full Equlib
Deep-New Morrison	Fluid plus rk	Fluid + CO2	Fluid + CO2	Fluid + CO2	Fluid & Rock
	rock, no CO2	no rock	plus rock	Plus rock	with CO2
Fluid Chemistry					
Aluminum - ppm	2.199E-02	4.453E-03	3.588E-03	4.332E-03	4.681E-03
Calcium - ppm	35.5	255	1564	1598	516
Carbon - ppm	45.4	3.00E+04	3.07E+04	3.04E+04	2.15E+04
Chlorine - ppm	2589	2303	2304	2309	2404
Iron - ppm	0.031	3.08E-04	25.7	26.2	9.00
Magnesium - ppm	74.3	30.3	151	444	980
Potassium - ppm	8.77	8.91	71.38	170.70	6625
Silicon - ppm	2.83	2.28	23.5	22.7	2.35
Sodium - ppm	5000	4784	4456	3807	221
Sulfate - ppm	7155	7059	3417	3495	869
pH	8.21	3.85	4.92	4.92	5.27
Minerals					
Initially Present Minerals					
Albite - 45 grams initially	39.1	None	44.8	44.4	15.3
Calcite - 45 grams initially	44.1	None	36.6	36.0	13.7
Illite - 45 grams initially	none	None	44.7	44.1	None
K-feldspar - 45 grams initially	50.0	None	44.7	44.4	9.1
Kaolinite - 90 grams initially	102	None	88.0	84.1	133
Ripidolit-14A - 45 grams initially	None	None	44.1	540	None
Quartz - 540 grams initially	514	5.21E-04	540	42.0	638
Smectite-low-Fe - 45 grams initially	148	None	44.4	43.1	None
New Minerals					
Siderite - grams produced	None	None	0.31	1.22	20.7
Goethite - grams produced	None	2.49E-07	0.02	0.07	1.63
Dolomite-dis - grams produced	1.80	None	None	None	56.8
Daswonite - grams produced	None	None	2.50	7.51	59.9
Clinoptil-Ca - grams produced	None	None	2.83	8.80	None
Gypsum - grams produced	None	None	7.45	7.30	None
Magnetite - grams produced	1.80	none	None	None	None
Pyrite - grams produced	0.49	none	None	None	None

Table A-2. Fruitland Formation Geochemical Modeling Results

	Full Equilb.	Full Equilb.	100 years	350 years	Full Equlib
Deep-New Fruitland	Fluid plus rk	Fluid + CO2	Fluid + CO2	Fluid + CO2	Fluid & Rock
	rock, no CO2	no rock	plus rock	Plus rock	with CO2
Fluid Chemistry					
Aluminum - ppm	0.049	0.001	0.001	0.001	0.005
Calcium - ppm	1.11	42.8	738	872	465
Carbon - ppm	256	3.19E+04	3.19E+04	3.16E+04	2.61E+04
Chlorine - ppm	1924	1680	1679	1685	1732
Iron - ppm	0.022	5.31E-06	13.1	15.4	8.35
Magnesium - ppm	1.99	10.7	49.0	143	878
Potassium - ppm	2.88	8.91	88.1	197	6794
Silicon - ppm	3.11	2.32	25.9	24.5	2.32
Sodium - ppm	1747	5165	4709	3789	187
Sulfate - ppm	0.004	6.07	6.06	6.08	6.25
pH	8.61	5.03	5.06	5.01	5.25
Minerals					
Initially Present					
Albite - 50 grams initially	32.7	None	49.8	49.3	None
Calcite - 50 grams initially	50.4	None	47.6	46.4	35.1
Illite - 100 grams initially	None	None	99.4	97.9	None
K-feldspar - 50 grams initially	100.7	None	49.7	49.7	47.0
Kaolinite - 100 grams initially	133.0	None	96.9	90.5	164.8
Quartz - 550 grams initially	586	4.47E-04	550	550	640
Siderite - 50 grams initially	39.1	None	50.0	50.1	54.3
Smectite - 50 grams initially	None	None	49.4	47.9	None
New Minerals					
Dawsonite - grams produced	38.4	2.36E-05	3.41	10.4	66.0
Dolomite-dis - grams produced	None	None	None	None	25.9
Goethite - grams produced	None	8.02E-07	0.02	0.08	1.81
Clinoptil-Ca - grams produced	None	None	3.53	10.9	None
Magnetite - grams produced	2.42	None	None	None	None
Pyrite - grams produced	4.33E-03	None	None	None	None
Ripidolit-14A - grams produced	37.2	None	None	None	None

In the last fifty years, geochemists have made steady progress in applying the principles of chemical thermodynamics to natural systems, and in particular, to predicting what will happen when different kinds of rocks are brought into contact with various types of natural or man-made water resources. The core concept is the principle of chemical equilibrium, which states that for any "system" (e.g., a defined assemblage of rocks, liquids, and gases), there is a single, unique end state where all the constituents in the system are stable with respect to each other. Until this state is reached, however, the minerals, fluids, and gases in a system have the potential for reacting with each other, albeit at rates that may be imperceptible on a human time scale.

A variety of computational tools have been developed to track how minerals, fluids, and gases will interact as a system progresses toward equilibrium. In the early days, relatively simple systems were studied, and results could generally be obtained by performing hand calculations (Garrels and Christ 1965, Krauskopf 1967). However, as more complex systems were investigated, this became impractical because multiple minerals may first appear and then disappear again before the final end state is reached; and all the while, the compositions of the fluids (gases and groundwater) were also continually changing. Hence today, the state of the art involves using relatively elaborate computer codes that are generally obtained from outside sources not directly involved in the research programs of the individual scientist. This report employed a commercially available program called REACT (part of the Geochemist's Workbench® package available through RockWare, Inc.: http://www.rockware.com), but other programs such as PHREEQE and TOUGHREACT (Pruess, Oldenburg, and Moridis 1999) could also have provided similar insights.

The tools that address this class of problems follow a relatively simple hierarchy of increasing complexity. The simplest applications involve just computing the final equilibrium configuration of a system given a specific starting mix of minerals, groundwaters, and gases. This was done to provide the data presented in the far right-hand column of both Table A-1 and A-2 (**Full Equlib Fluid & Rock with CO2**, i.e., *test water equilibrates fully with CO_2 and rock*), which describe the course of rock-water interactions.

The choice of how much rock to mix with how much groundwater and CO_2 is often done at the discretion of the analyst; however, the fact that systems will always contain much more rock than fluid (because the porosity of potential reservoir rocks is typically less than 20%) helps in the analysis. This means that the rock will always completely consume whatever reactive constituents may exist in the fluid phases (i.e., groundwater plus gas). Additionally, the reactions will cease leaving the residual rock; therefore, it remains unchanged. Care must be taken to assure that the model contains enough rock so that the fluid is completely taken care of.

The next level of complexity arises when, instead of asking about the final equilibrium state of a system, the study focuses on what happens along the way as the system progresses to the final equilibrium state. One way of modeling this is to incrementally add small fractional amounts of the total mineral inventory, which will eventually be present in the final system, and in the process, detail what chemical changes have occurred after each addition. These are known as *reaction path* calculations. In the course of such calculations, it is common to see different minerals precipitate and then dissolve as the bulk composition of the system changes with each incremental addition of rock.

However, making realistic reaction path calculations requires adding minerals in proportions that reflect the relative rates at which the different constituents are likely to dissolve. For example, rock salt dissolves almost instantly, quartz can require centuries, and limestone is in between. Thus, rather than adding the same fraction of each mineral in the rock at each step in a reaction path calculation, the tactic taken for this report involved adding the different minerals to the groundwater-CO_2 mix at rates that reflect their relative dissolution rates.

Computationally, this addition process is carried out based on three considerations: (1) a basic rate that reflects fundamental differences in dissolution rates when a mineral is significantly unsaturated in a particular solution (see comparison above), (2) a factor that decreases the dissolution rate as the chemistry of the solution approaches a condition where the mineral in question is saturated, (3) the specific surface area for each mineral along with the mass of the mineral. (The third consideration must be specified so that the program knows how much surface area contributes mass to the solution as each mineral reacts.) These are the kinds of considerations that produced the data in Tables A-1 and A-2 describing the status after 100 years (**100 years Fluid + CO2 plus rock**, i.e., *test water plus CO_2 and rock for 100 years*) and 350 years (**350 years Fluid + CO2 Plus rock**, i.e., *test water plus CO_2 and rock for 350 years*).

Also, it is important to discuss data quality and the subsequent limitations of the dependent calculations. All of these calculations rest on numerous assumptions, so supplemental checks are always warranted. Much effort has gone into developing internally consistent thermodynamic databases that support these programs, but unfortunately, they are still far from perfect. For example, when one has rocks that are millions of years old together with water resources with many thousands of year's worth of residence time, one might expect chemical equilibrium to have been reached. However, when models are constructed using the appropriate formation minerals together with the indigenous water, some changes are almost always predicted.

For the most part, these changes are small enough to be inconsequential for our purposes. However, it is still important to isolate these changes from what happens (computationally) when CO_2 is added to the system This isolation is accomplished with the REACT run script for equilibrium mix as shown in Table A-3, which is specific to the second Morrision site (M2, 6,359 ft). The script shown in the **Equilibrium Mix** column of Table A-3 provides the computational starting point for the M2 formation-plus-groundwater mixes prior to adding any CO_2.

Table A-3. REACT Run Scripts for the Second Morrison Site (M2)

Equilibrium Mix	Kinetic Mix
MORRISON: Equilibrium Box - new 6359' brine Reset React 125 g CO2(g) pH = 7.2 Na+ = 5372 mg/kg Ca++ = 286 mg/kg Mg++ = 34 mg/kg Cl- = 2529 mg/kg SO4-- = 7915 mg/kg HCO3- = 882 mg/kg Li+= 0.3 mg/kg K+ = 10 mg/kg swap Fe+++ for Fe++ Fe+++ = 0.0005 mg/kg Al+++ = .005 mg/kg SiO2(aq) = 6 mg/kg Swap O2(g) for O2(aq) f O2(g) = 1E-10 suppress ALL unsuppress K-feldspar Quartz Kaolinite Smectite-low-Fe-Mg Alunite Analcime Goethite Magnetite Gibbsite Dawsonite Illite Siderite Calcite Dolomite-dis Jarosite-Na Anorthite Albite Anhydrite Gypsum Hydromagnesite Nesquehonite Ripidolit-14A Heulandite Clinoptil-Ca Clinoptil-Na Pyrite go pickup = "system" delxi = .001 react 540 g Quartz react 45 g K-feldspar react 45 g Albite react 45 g Calcite react 90 g Kaolinite react 45 g Illite react 45 g Smectite-low-Fe-Mg react 45 g Ripidolit-14A go	MORRISON: Kinetic Box - new 6359' brine Reset React 125 g CO2(g) pH = 7.2 Na+ = 5372 mg/kg Ca++ = 286 mg/kg Mg++ = 34 mg/kg Cl- = 2529 mg/kg SO4-- = 7915 mg/kg HCO3- = 882 mg/kg Li+= 0.3 mg/kg K+ = 10 mg/kg swap Fe+++ for Fe++ Fe+++ = 0.0005 mg/kg Al+++ = .005 mg/kg SiO2(aq) = 6 mg/kg Swap O2(g) for O2(aq) f O2(g) = 1E-10 suppress ALL unsuppress K-feldspar Quartz Kaolinite Smectite-low-Fe-Mg Alunite Analcime Goethite Magnetite Gibbsite Dawsonite Illite Siderite Calcite Dolomite-dis Jarosite-Na Anorthite Albite Anhydrite Gypsum Hydromagnesite Nesquehonite Ripidolit-14A Heulandite Clinoptil-Ca Clinoptil-Na Pyrite go pickup = "system" go delxi = .001 react 540 g Quartz kinetic Quartz rate_con = **1.26E-18** surf = 37 react 45 g K-feldspar kinetic K-feldspar rate_con = **1.00E-16** surf = 100 react 45 g Albite kinetic Albite rate_con = **1.00E-16** surf = 50 react 45 g Calcite kinetic Calcite rate_con = **1.60E-13** surf = 2E3 react 90 g Kaolinite kinetic Kaolinite rate_con = **1.00E-17** surf = 5E3 react 45 g Illite kinetic Illite rate_con = **1.00E-18** surf = 5E3 react 45 g Smectite-low-Fe-Mg kinetic Smectite-low-Fe-Mg rate_con = **1.00E-18** surf = 1E4 react 45 g Ripidolit-14A kinetic Ripidolit-14A rate_con = **1.00E-17** surf = 1E3 time begin 0 years, end 350 years theta = .5 go

A parallel problem is that just the fluid alone may not be in chemical equilibrium. This problem is exacerbated by the fact that the water resource analyses available for the various formations are, unfortunately, incomplete. Thus several trace constituents (notably silica, iron, aluminum, and potassium) need to be estimated so that the models can mimic the full range of silicate minerals likely to be found in the sediments in question. Making such estimates would seriously limit the utility of such models were these constituents expected in high concentrations in the formation waters, or if the systems were not rock-dominated. Fortunately, neither criterion is met here, so it is expected that the impact of assuming values for these constituents would be small. But to test this presumption, a set of runs was made mixing just the CO_2 and the augmented groundwater chemistry. The results of these runs are provided in the **Kinetic Mix** column in Table A-3, confirming that only trivial amounts of new minerals precipitate prior to adding the rock to the model.

Finally, the thermodynamic database supporting REACT contains far more minerals than appear in the model, so the question arises, "How were the minerals allowed in the model selected in the first place?"

The basic mineralogical makeup of the formations used in the models was based on an examination of the geologic literature. However, not all of the clay minerals found during the field studies actually matched minerals that appeared in the thermodynamic database, so in some cases, close relatives were selected as proxies. Somewhat more subjective was the process of suppressing various minerals. Here, the basic problem is that, at least according to the databases, some of the most computationally stable minerals are simply never found in sedimentary rocks. Whether the problem lies in inaccurate thermodynamic properties for these minerals, or kinetic factors preclude their formation, is unknown.

To deal with these problems, preliminary computations were first made with the full mineralogical database in play. These results were then examined for geologically untenable predictions, and these unreasonable phases were suppressed so that they would no longer enter into the computational process. This process was repeated several times over, and each time the range of minerals allowed into the calculation was further constrained. The run scripts for the models (e.g., Table A-3, for the M2 formation), then, provide a record of what was used in the models.

Table A-3 contains run scripts that illustrate (for the second Morrison selection) how the calculations were set up. The top (purple) entries specify the amount of CO_2 put into the system (125 grams), and the default value in the program is that one liter of ground water is presumed to be present. The composition of the groundwater is represented in black, with the assumed constituents in aqua. Below this (pea green text), the text documents the outcome of the suppression process (i.e., the list of what minerals were actually allowed to potentially form—and dissolve—during the course of the reactions.

The first step in the process reflects the initial groundwater allowed to equilibrate with the CO_2 (i.e., the first "go" statement). In the second step, the minerals in the formation (navy blue) were added to the model. Parenthetically, this two-step process was adopted after some trial-and-error

runs as a procedure that optimized the chances the run would converge on the first try rather than stall out before reaching completion.

The **Equilibrium Mix** column in Table A-3 shows that the rock was titrated into the CO_2-groundwater mix in 0.1% increments (again, to avoid convergence problems) rather than just adding the rock in bulk in a single step. But, in the final analysis, what was used for the report was the state of the system once the titration was completed (see Tables A-1 and A-2, **Full Equlib Fluid & Rock with CO2**, i.e., *test water equilibrates fully with CO_2 and rock*).

The **Kinetic Mix** column in Table A-3 is a run script where reaction rates enter into the process. In this case, in addition to entering the amount of each mineral in the model (blue), the setup also contains information on the reaction rate of a mineral and the specific surface of a mineral—below each mineral is the reaction rate.

Appendix B: Water Treatment Cost Calculations

B.1 Introduction

This appendix provides detailed descriptions of the calculations for water treatment capital cost (CC) items and operational and maintenance (OM) costs. For reference, Table B-1 summarizes water treatment analysis formulae, and Table B-2 provides a list of water treatment analysis symbols and abbreviations.

Subsection B.2 provides details of the calculations for capital cost items 1 through 5 (CC_1 through CC_5). Subsection B.3 provides details of the calculations for operational and maintenance cost items 1 through 9 (OM_1 through OM_9).

Table B-1. Water Treatment Analysis Formulae

Symbol/ Abbreviation	Unit(s)	Description	Equation or Assumption
CF	—	Capacity Factor	% of year plant is operational
$D_{inj.well}$	mi	Injection Well Distance	5 mi
D_{pipe} (mi)	mi	Pipeline Distance	Radial distance from formation sample point to SJGS 30 mi (modeling assumption)
D_{form}	ft	Formation Depth	See Table 2-1.
Eff_{RO}	—	Efficiency of Reverse Osmosis (RO) System	$\frac{Q_{treated}}{Q_{feed}}$, assumed to be 0.75
γ	—	Gravity Equation	$\gamma = \frac{g}{g_c} \cdot \rho$ where ρ (lb/ft^3) and g/g_c (lb/ft^3).
η	—	Efficiency of Pumping System	Efficiency of pump * Efficiency of motor, 0.80*0.85
g	ft/s^2	Gravitational Acceleration Constant	32.174 ft/s^2
g_c	lb_m-ft/s^2/lb_f	Universal Gravitational Constant	32.174 lb_m-ft/s^2/lb_f
H_F	ft	Pressure Caused by Friction	Defined by pipe tables.
H_L	ft	Pressure Caused by Static Head	$H_L = \Delta Z$ Δ = weight difference
H_V	ft	Pressure Caused by Velocity Head	$H_V = \frac{v^2}{2 \cdot g}$

Table B-1. Water Treatment Analysis Formulae, continued

Symbol/ Abbreviation	Unit(s)	Description	Equation or Assumption
$H_{F,inj}$	ft	Injection pipeline Friction Loss (or pressure drop)	Assuming a pipeline design to obtain the following: $\frac{3\text{ ft}}{1{,}000\text{ ft pipe distance}}$
$H_{F,pipe}$	ft	Feed Pipeline Friction Loss (or pressure drop)	Assuming a pipeline design to obtain the following: $\frac{3\text{ ft}}{1{,}000\text{ ft pipe distance}}$
$H_{L,inj}$	ft	Injection Pipeline Static Head, or elevation difference pressure	0 ft (assuming no increase/decrease in elevation)
$H_{L,pipe}$	ft	Feed Pipeline Static Head, or elevation difference pressure	Assuming 100 m increase
hp_{act}	hp	Actual Horsepower Required for Pumping System	$hp_{th} = \frac{Q \cdot \gamma \cdot \frac{H}{ft \cdot lb_f}}{550 \frac{s}{hp}}$
hp_{th}	hp	Theoretical Horsepower Required for Pumping System	$hp_{act} = \frac{hp_{th}}{\eta}$
$Q_{treated}$(gpm)	gpm	Desalination Plant Treated Flow Rate (i.e., *permeate*)	$Q_{feed}(GPM) \cdot Eff_{RO}$
Q_{conc} (gpm)	gpm	Desalination Plant Waste Effluent Flow Rate (i.e., *concentrate*)	$Q_{feed}(GPM) - Q_{treated}(GPM)$ or $Q_{feed}(GPM) \cdot (1 - Eff_{RO})$
Q_{conc} (MGY)	MGY	Desalination Plant Treated Flow Rate (i.e., *permeate*)	$Q_{conc}(MGD) \cdot CF \cdot 365 \frac{days}{year}$
$Q_{treated}$ (MGY)	MGY	Desalination Plant Treated Flow Rate (i.e., *permeate*)	$Q_{treated}(MGD) \cdot CF \cdot 365 \frac{days}{year}$
$S_{e.pond}$	acres	Evaporation Pond Size	$Q_{treated}(MGD) \cdot 35$
TDH	ft	Total Developed Head	$H_F + H_V + H_L$

Table B-2. Water Treatment Analysis Symbols and Abbreviations

Symbol/Abbreviation	Unit(s)	Description
BC	—	Brine Concentrator
BWRO	—	Brackish Water Reverse Osmosis
C_{elect}	$/kwh	Unit Cost of Electricity
Cfs	—	cubic feet per second
Gpm	—	gallons per minute
HERO	—	High-Efficiency Reverse Osmosis
Kwh	—	kilowatt-hours
mg/L	—	milligrams per liter
MGD	——	million gallons per day
MGY	—	million gallons per year
O&M	—	Operational & Maintenance
Q_{conc} (MGD)	MGD	Desalination Plant Waste Effluent Flow Rate (also known as concentrate), MGD
Q_{conc}(CFS)	cfs	Desalination Plant Waste Effluent Flow Rate, cfs
Q_{conc}(gpm)	gpm	Desalination Plant Waste Effluent Flow Rate (i.e., *concentrate*), gpm
Q_{feed} (MGD)	MGD	Desalination Plant Feed Flow Rate, MGD
Q_{feed}(cfs)	cfs	Desalination Plant Feed Flow Rate, cfs
Q_{feed}(gpm)	gpm	Desalination Plant Feed Flow Rate, gpm
$Q_{treated}$ (MGD)	MGD	Desalination Plant Treated Flow Rate (i.e., *permeate*), MGD
$Q_{treated}$(gpm)	gpm	Desalination Plant Treated Flow Rate (i.e.. *permeate*), gpm
ρ	lb_m/ft^3	Density of Water
RO	—	Reverse Osmosis
SJGS	—	San Juan Generating Station
TDS	mg/L	Total Dissolved Solids
UF	—	Ultrafiltration System
CC_1	$	Capital Cost: Formation wellfield equipment (pumps and materials) (Most in U.S. dollars, 2000; updated in WECS to U.S. dollars, 2009)
CC_2	$	Capital Cost: Supply Pipeline Equipment
CC_3	$	Capital Cost: Evaporation Ponds
CC_4	$	Capital Cost: Desalination Treatment System Equipment
CC_5	$	Capital Cost: Concentrate Injection Pipeline and Injection Well
OM_1	$	O&M Cost: Annual Labor
OM_2	$	O&M Cost: Annual Electrical for RO System
OM_3	$	O&M Cost: Annual Electrical for BC System
OM_4	$	O&M Cost: Annual Electrical for Formation Pumping

Table B-2. Water Treatment Analysis Symbols and Abbreviations, continued

Symbol/Abbreviation	Unit(s)	Description
OM_5	$	O&M Cost: Annual Electrical for Pipeline Pumping
OM_6	$	O&M Cost: Annual Membrane Replacement
OM_7	$	O&M Cost: Annual Chemicals
OM_8	$	O&M Cost: Other Maintenance
OM_9	$	O&M Cost: Annual Electrical for Concentrate Injection Pipeline Pumping
F1	—	Fruitland (initial)
F2	—	Fruitland (second or *new*)
PL/MV	—	Point Lookout/Mesa Verde
GS	—	Gallop Sandstone in Mancos
D	—	Dakota
M1	—	Morrison (initial)
M2	—	Morrison (second or *new*)
H/P	—	Hermosa/Paradox

B.2 Capital Cost Calculations

This subsection provides details of the calculations for capital cost items 1 through 5 (CC_1 through CC_5) as follows:

CC_1: Formation Wellfield Equipment (Pumps and Materials)
CC_2: Supply Pipeline Equipment
CC_3: Evaporation Ponds
CC_4: Desalination Treatment System Equipment
CC_5: Concentrate Injection Pipeline and Injection Well

For each calculation, two primary references are used:

- U. S. Bureau of Reclamation (USBR) (2003)
- Zammit and DiFilippo (2004)

Other references are listed as required.

CC_1: Formation Wellfield Equipment (Pumps and Materials)

Using the USBR *Desalting Handbook for Planners* (USBR [2003]), a cost per foot for a well's depth is estimated. Figure 9-18 of USBR (2003) has curves for three well depths (400, 600, and 800 feet) and is based on the flow capacity of the well.

Table B-3 is a re-creation of the data for USBR (2003) Figure 9-18. Figure B-1 shows the cost per foot of depth for various capacities of an 800-ft-deep well; the equation was found by a simple Microsoft® Excel® curve fit. This equation is utilized to calculate the cost of wells that are significantly deeper and is understood that a more accurate number should be utilized. This number does not include any land acquisition or other costs (i.e., it only includes capital equipment). This can be a moving target (slider) so users could adjust to their site needs. The final equation utilized in our model is as follows:

$$CC_1 = \$75.05 \cdot Q_{treated}(MGD) \cdot D_{form}(ft)$$

Table B-3. Wellfield Construction Cost Values Estimated from USBR (2003) Figure 9-18

Capacity (m^3/day)	Cost	Depth (ft)	Cost per Foot
1	$400,000	800	$500
5	$1,500,000	800	$1,875
10	$3,000,000	800	$3,750
50	$15,000,000	800	$18,750
1	$200,000	600	$333
5	$1,100,000	600	$1,833
10	$2,100,000	600	$3,500
50	$12,100,000	600	$20,167

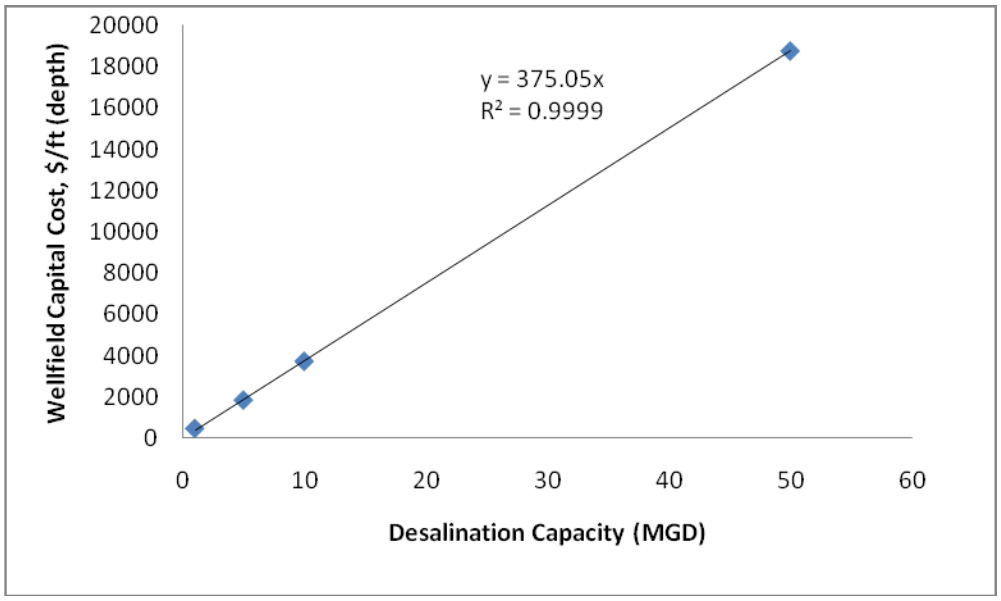

Figure B-1. Estimation of Wellfield Capital Cost

CC_2: Capital Cost: Supply Pipeline Equipment

The USBR *Desalting Handbook* (USBR [2003]), Figure 9-11, describes the cost for three concentrate disposal pipelines for seawater and brackish water applications (1,500, 3,000, and 4,500 feet long). No other pipeline costs are provided in the handbook, and the costs are assumed to be similar. It is understood that a more accurate number could be used. This can be adjusted so users could adjust to their own site needs.

Table B-4 shows the recreation of USBR (2003) Figure 9-11. Figure B-2 shows the estimation of the cost per mile of a pipeline based on the 4,500-ft pipeline. The final equation utilized in our model is as follows:

$$CC_2 = \left[1920 \cdot Q_{treated}(MGD) \cdot 111314 \right] \cdot D_{pipe}(mi)$$

Table B-4. BWRO Concentrate Disposal Pipeline Cost Data Estimated from USBR (2003) Figure 9-11

Length (ft)	Capacity (m^3/day)	Cost	Cost per Mile
1,500	1	$20,000	$70,400
1,500	5	$40,000	$140,800
1,500	10	$70,000	$246,400
1,500	50	$205,000	$721,600
3,000	1	$50,000	$88,000
3,000	5	$100,000	$176,000
3,000	10	$145,000	$255,200
3,000	50	$410,000	$721,600
4,500	1	$90,000	$105,600
4,500	5	$150,000	$176,000
4,500	10	$210,000	$246,400
4,500	50	$600,000	$704,000

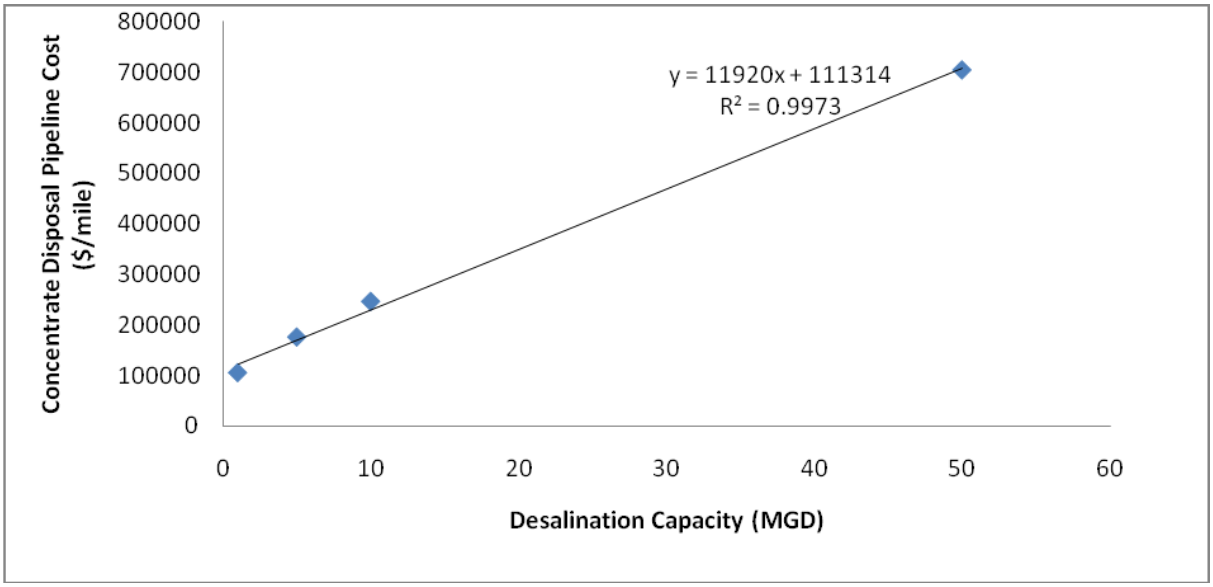

Figure B-2. Estimation of Concentrate Disposal Pipeline Cost

CC_3: Evaporation Ponds

Evaporation ponds are included in Options B and D. In Option B, evaporation ponds are utilized for the entire amount of waste water (i.e., *concentrate*) flow. In Option D, evaporation ponds are only used if the concentrate flow exceeds the maximum design flow rate of the brine concentrators (Zammit and DiFilippo [2004]).

The data from USBR (2003) Figure 9-12, which describes the size and cost of evaporation ponds based on plant capacity (i.e., treated water flow) were interpreted and recreated to determine an equation for the evaporation pond size and cost. Figure B-3 shows the estimation and equation derived for evaporation pond size, and Figure B-4 shows the estimation and equation derived for evaporation cost. The final equation used in our model is as follows:

For Option B,

$$CC_3 = [illegible].0374 \cdot Q_{treated}(MGD) - .8673 \cdot 1000000$$

For Option D,

$$CC_3 = [illegible].0374 \cdot (Q_{treated}(MGD) - Q_{\max}(MGD) - .8673 \cdot 1000000$$

Note that for Option D, $Q_{\max}(MGD)$=5 *MGD*, which is based on the maximum flow rate that the brine concentrators can treat (1,160 gpm).

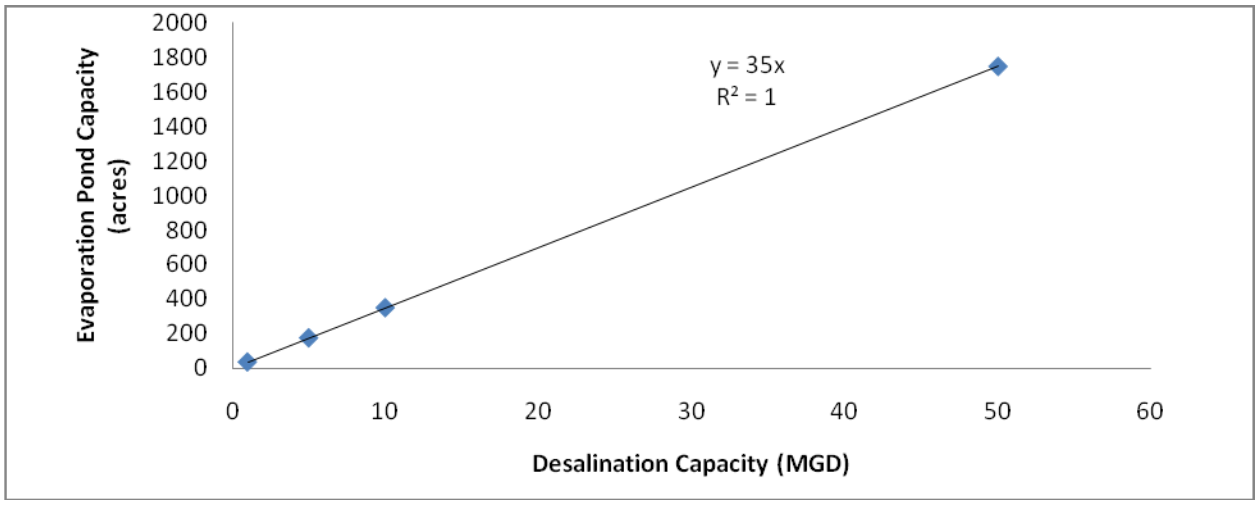

Figure B-3. Capacity Based on Evaporation Pond Size Estimated from USBR (2003) Figure 9-12 Data

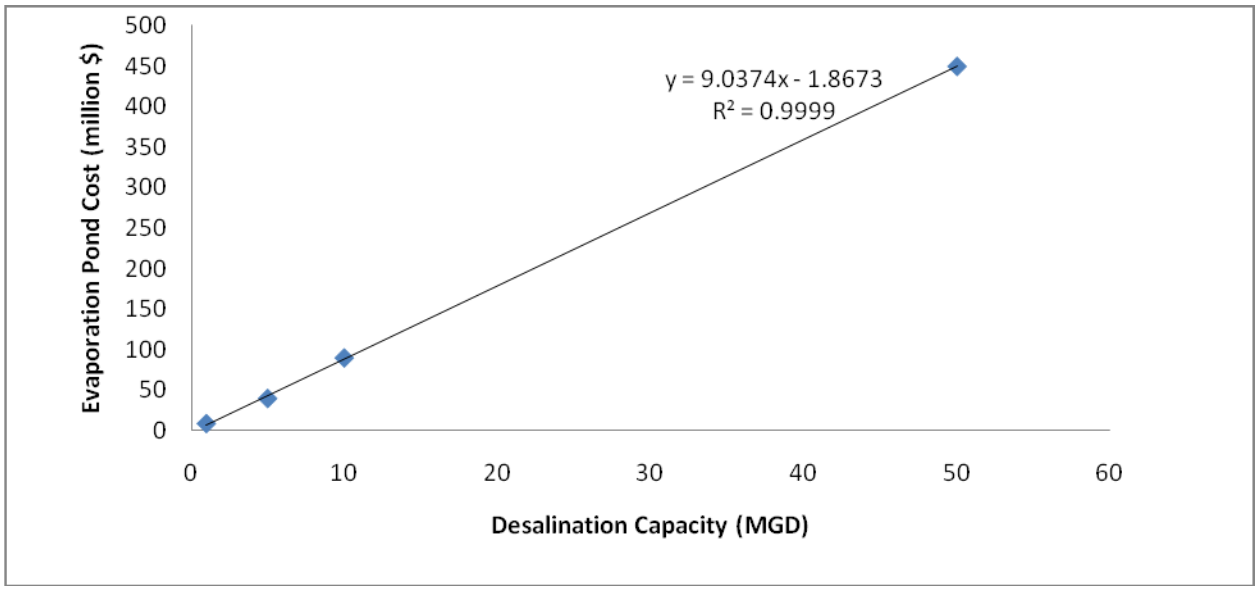

Figure B-4. Estimation of Evaporation Pond Capital Cost

CC_4: Desalination Treatment System Equipment

Using the cost estimations in Zammit and DiFilippo (2004) on produced water desalination by high-efficiency reverse osmosis (HERO™) and brine concentrators (BCs), the information shown in Table B-5 was utilized for capital cost calculations.

Table B-5. Capital Cost Values Utilized for CC_4

Equipment Description	Cost[1]	Design Flow Rate (gpm)
Receiving, Transfer, and Distribution Piping	$1,478,000	1,316
HERO™	$6,700,000	1,316 (feed) (75% efficiency)
Refurbish BC3	$2,970,000	234.5 (580 gpm maximum)
Refurbish BC2	$4,100,000	234.5 (580 gpm maximum)
Note 1. Zammit and DiFilippo (2004), Table A-3).		

Cost estimates for Options A, B, and C only utilize the "Receiving, Transfer, and Distribution Piping" and "HERO™" capital costs shown in Table B-5. Option D uses the capital costs for the BCs (BC2 and BC3, see Table B-5) in a staged fashion. It is assumed that BC3 will be refurbished first because it is less expensive. Further, it is assumed that the full flow rate is achievable (580 gpm) after refurbishment. Desalination equipment capital costs are estimated by using the values in Table B-5 and are multiplied by a ratio of the calculated feed flow rate to the design flow rate used in Zammit and DiFilippo (2004). Equations for each of the options are as follows:

For Options A–C,

$$CC_4 = \left(6700000 + 478000\right) \cdot \frac{Q_{feed}(GPM)}{1316\,gpm}$$

For Option D, a feed flow rate of 2,320 gpm will yield maximum BC3 flow. Above 4,640 gpm, both BC2 and BC3 are fully utilized, and the remaining water will be fed to evaporation ponds. The equations for both of these situations are as follows:

Option D, Q_{feed}(GPM)<2320 gpm:

$$CC_4 = 970000 + \left(6700000 + 478000\right) \cdot \frac{Q_{treated}(GPM)}{1316gpm}$$

Option D, Q_{feed}(GPM)>2320 gpm:

$$CC_4 = 970000 + 100000 + \left(6700000 + 478000\right) \cdot \frac{Q_{treated}(GPM)}{1316gpm}$$

CC_5: Concentrate Injection Pipeline and Injection Well

Similar methodology for the pipeline capital cost is used. The injection well cost is based on the USBR *Desalting Handbook*, Table 18 (Figure 9-13) (USBR [2003]). Table B-6 summarizes our interpretation of the USBR 2003 numbers, and Figure B-5 shows the estimation and equation derived for the injection well capital cost. The final equation used in our model is as follows:

$$CC_5 = \left[1920 \cdot Q_{conc}(MGD) \cdot 111314 \cdot D_{injwell}(mi) + \left(94893 \cdot Q_{treated}(GPM) + 359271\right)\right.$$

Table B-6. Cost Data Estimated from USBR (2003) Figure 9-13

Capacity (MGD)	Injection Well Cost
1	$2,000,000
5	$3,500,000
10	$4,800,000
50	$12,000,000

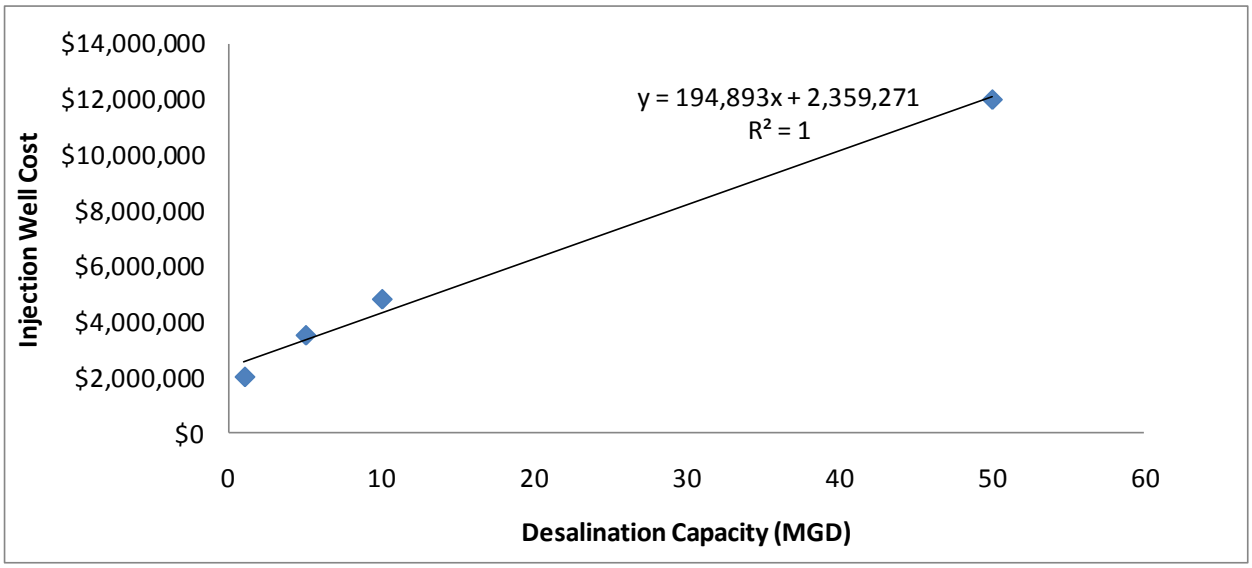

Figure B-5. Estimation of Injection Well Cost

B.3 Operational and Maintenance Cost Calculations

This subsection provides details of the calculations for operational and maintenance cost items 1 through 9 (OM_1 through OM_9) as follows:

OM_1: Annual Labor
OM_2: Annual Electrical for Reverse Osmosos (RO) System
OM_3: Annual Electrical for Brine Concentrator (BC) System (Option D)
OM_4: Annual Electrical for Formation Pumping
OM_5: Annual Electrical for Pipeline Pumping
OM_6: Annual Membrane Replacement
OM_7: Annual Chemicals
OM_8: Other Maintenance
OM_9: Annual Electrical for Concentrate Injection Pipeline Pumping

For each calculation, two primary references are used:

- U. S. Bureau of Reclamation (USBR) (2003)
- Zammit and DiFilippo (2004)

Other references are listed as required.

OM_1: Annual Labor Cost

The annual labor cost (OM_1) was based on the USBR *Desalting Handbook for Planners* (USBR [2003]), Figure 9-37. We recreated the plot and used a curve fit for an equation that would be based on plant capacity. Figure B-6 shows the curve and resulting equation. The final equation used for our model is as follows:

$$OM_1 = 71778 \cdot Q_{treated}(GPM)$$

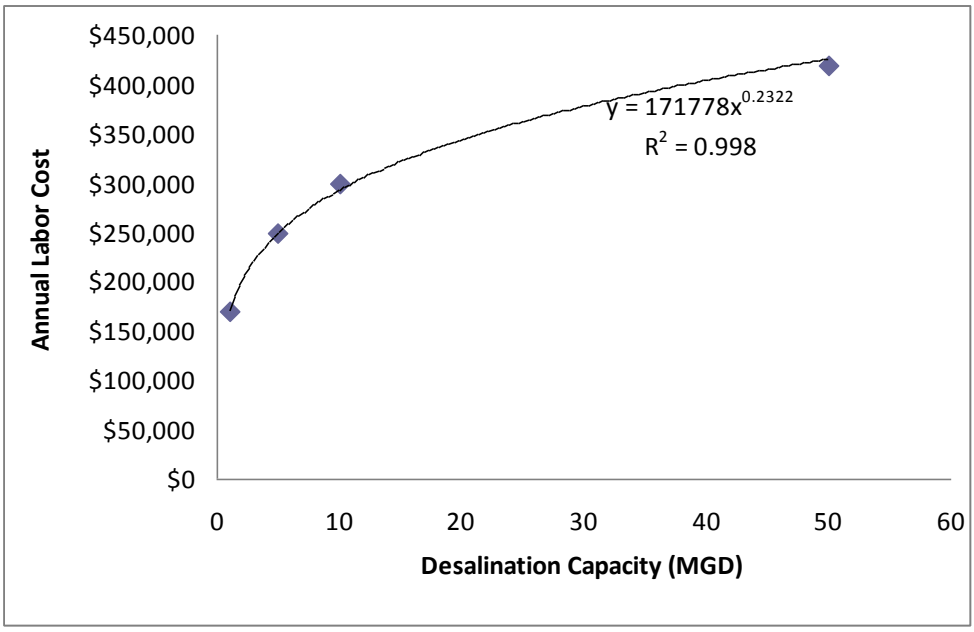

Figure B-6. Data and Estimation of Annual Labor Cost Based on USBR (2003) Figure 9-37

OM_2: Annual Electrical for Reverse Osmosis (RO) System

The USBR *Desalting Handbook* (USBR [2003]), Figure 7-8, describes the energy intensity for several types of desalination: electrodialysis reversal (EDR), low-energy (LE) reverse osmosis, and standard (std) reverse osmosis. We assume that standard reverse osmosis membranes will be utilized in the HERO™ systems to provide a conservative estimate. Table B-7 summarizes the data estimated from USBR (2003) Figure 7-8. ***Bold, italicized*** numbers in Table B-7 indicate where a curve fit was used to estimate other energy intensities for other water total-dissolved-solids (TDS) values not originally included. Figure B-7 shows the data and the equation derived for energy intensity.

Table B-7. Summary of Energy Consumption by TDS

Feed Water TDS (ppm)	Energy Consumption (kWh/m^3 permeate)			Energy Consumption (kWh/1,000 gallons permeate)		
	LE RO	Std RO	EDR	LE RO	Std RO	EDR
1,000	0.6	0.8	0.5	2.27	3.03	1.89
2,000	0.74	0.95	0.73	2.80	3.60	2.76
2,100	—	—	—	***2.86***	***3.67***	—
3,000	0.875	1.12	1	3.31	4.24	3.79
4,000	1.05	1.25	1.3	3.97	4.73	4.92
4,500	—	—	—	***4.30***	***5.11***	—
5,000	1.2	1.4	1.75	4.54	5.30	6.62
6,000	1.4	1.55	—	5.30	5.87	—
7,000	—	1.7	—	***5.80***	6.43	—
8,000	—	1.875	—	***6.40***	7.10	—
9,000	—	2.05	—	***7.00***	7.76	—
10,000	—	2.2	—	***7.60***	8.33	—
11,000	—	—	—	***8.20***	***9.01***	—
12,000	—	—	—	***8.80***	***9.61***	—
13,000	—	—	—	***9.40***	***10.21***	—
13,600	—	—	—	***9.76***	***10.57***	—
14,000	—	—	—	***10.00***	***10.81***	—
15,000	—	—	—	***10.60***	***11.41***	—
17,000	—	—	—	***11.80***	***12.61***	—
19,000	—	—	—	***13.00***	***13.81***	—
35,000	—	—	—	***22.60***	***23.41***	—

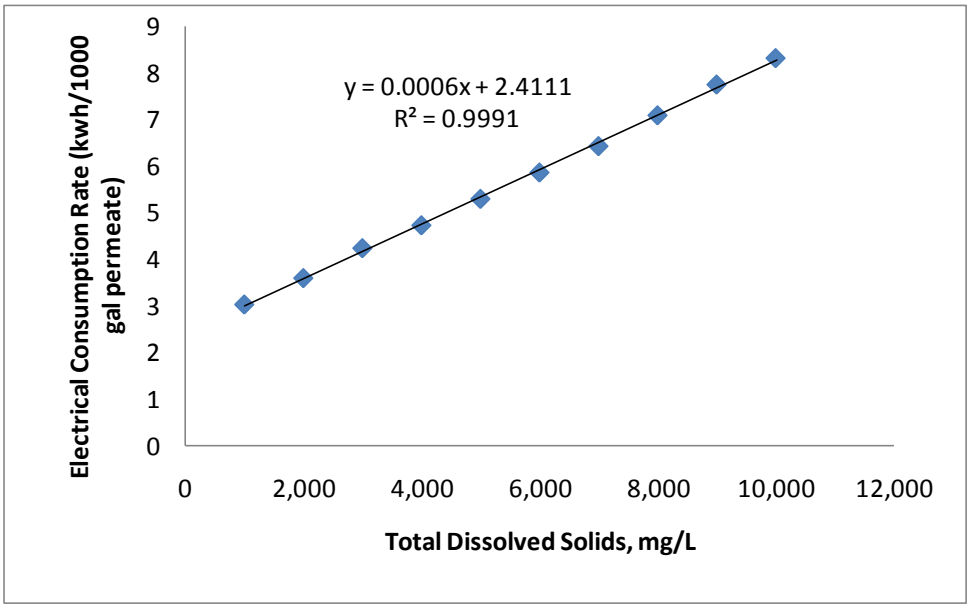

Figure B-7. Estimation of Electrical Consumption by TDS—Standard RO Membranes

The OM_2 calculation requires the following preliminary calculations. First, the energy intensity in kWh/1,000 gallons of treated water (i.e., *permeate*):

$$\frac{kWh}{1{,}000gal\,(permeate)} = 1.0006 \cdot TDS + 1.411$$

Next, the annual energy consumption for each TDS value:

$$Annual\_kWh = \frac{kWh}{1{,}000\,gal\,(permeate)} \cdot Qtreated(MGD) \cdot \frac{1{,}000{,}000}{1{,}000}$$

Figure B-8 shows the graph of the annual electricity consumption (kWh) for each of the formations studied in this analysis. The equations derived for each formation's annual electricity cost as a function of plant capacity are as follows:

$$OM_2(F1) = 3858451 \cdot Q_{treated}(MGD) \cdot CF \cdot C_{elect}$$
$$OM_2(F2) = 5041051 \cdot Q_{treated}(MGD) \cdot CF \cdot C_{elect}$$
$$OM_2(PL/MV) = 1934141 \cdot Q_{treated}(MGD) \cdot CF \cdot C_{elect}$$
$$OM_2(GS) = 2832135 \cdot Q_{treated}(MGD) \cdot CF \cdot C_{elect}$$
$$OM_2(D) = 1312453 \cdot Q_{treated}(MGD) \cdot CF \cdot C_{elect}$$
$$OM_2(M1) = 2141370 \cdot Q_{treated}(MGD) \cdot CF \cdot C_{elect}$$
$$OM_2(M2) = 4603051 \cdot Q_{treated}(MGD) \cdot CF \cdot C_{elect}$$
$$OM_2(H/P) = 3039364 \cdot Q_{treated}(MGD) \cdot CF \cdot C_{elect}$$

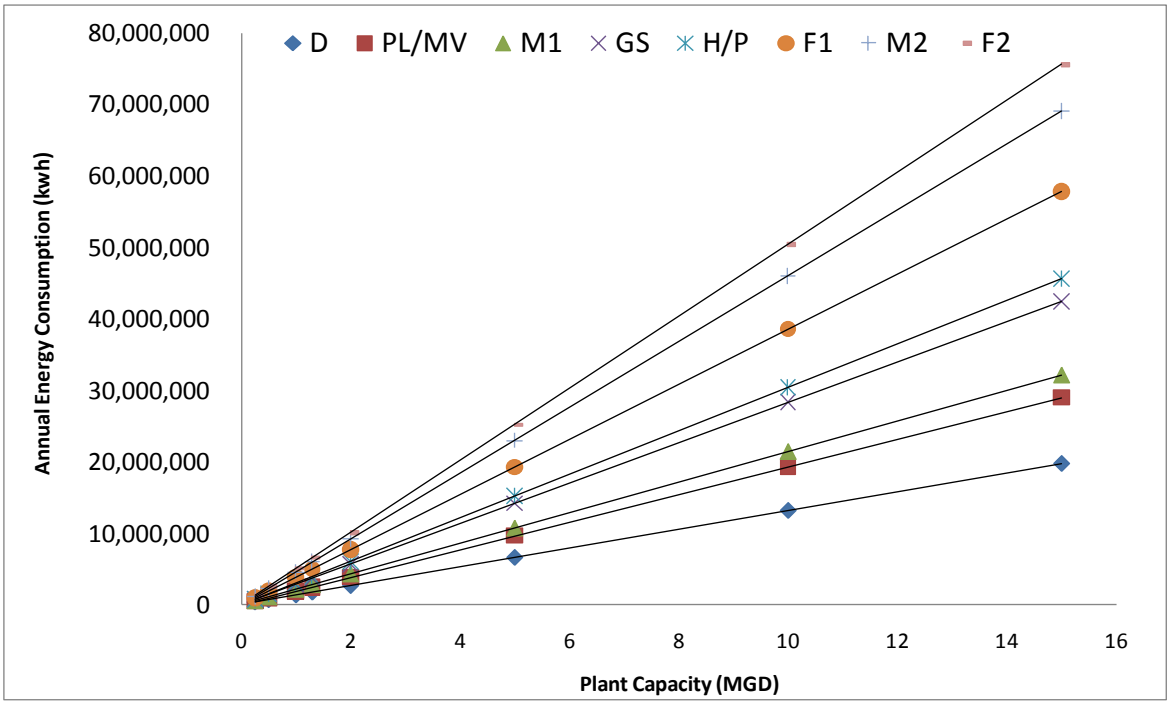

Figure B-8. Estimation of Annual Electrical Consumption by Formation

OM_3: Annual Electrical for Brine Concentrator (BC) System (Option D)

Using the cost information from Zammit and DiFilippo (2004), Table A-3, the annual electrical cost for the BC was estimated. First, the annual electrical cost for their alternative 10 (HERO™ + BC3 retrofit) is $522,000. In their alternative 7 (HERO™ only), the annual electrical cost is $231,000. Subtraciting the two values yields the annual electrical cost for BC3: $291,000. The unit cost for electricity is $0.045/kWh in Zammit and DiFilippo (2004). Using these values, the annual electricity consumption is calculated to be 7,275,000 kWh. Zammit and DiFilippo (2004) indicate that the feed rate to BC3 to be 234.5 gpm.

We assumed a linear relationship for the electricity and derived an equation to scale electrical consumption by our model's calculated flow rate to the BC. Furthermore, we assumed that both BCs (BC2 and BC3) have the same electrical consumptions and scale factors. The final equations used for our model are a staged system in that the BCs will be limited by a maximum feed flow (RO concentrate flow) of 1,160 gpm.

If Q_{conc}(GPM)<1,160, the calculated concentrate flow rate is used to scale the electrical consumption:

$$OM_3 = 7{,}275{,}000 \cdot C_{elect} \cdot \frac{Q_{conc}(GPM)}{234.5 gpm}$$

If Q_{conc}(GPM)>1,160, the maximum brine concentrator electrical consumption is used:

$$OM_3 = \text{'},275{,}000 \cdot C_{elect} \cdot \frac{1{,}160 gpm}{234.5 gpm}$$

OM_4: Annual Electrical for Formation Pumping

Using standard pumping calculations (see below), an estimated annual pumping power was estimated for several temperatures using several flow rates for the Morrison formation. An average was taken for the Morrison formation, and a ratio of the depth of each of the other formations to the Morrison was used to estimate the power consumption for well-water pumping in each formation. All of the following calculations assume a 12-inch pipe diameter.

First, the theoretical pump horsepower (hp) is calculated:

$$hp_{th} = \frac{Q_{feed}(CFS) \cdot \gamma \cdot TDH}{550 \frac{\frac{ft \cdot lb_f}{s}}{hp}}$$

$$TDH = H_L + H_V + H_F$$

$$\gamma = \frac{g}{g_c} \cdot \rho$$

Because the vast majority of the pumping power required for this operation will be power needed to lift water from the deep formations, H_F and H_V are assumed to be negligible. H_L is simply the depth of the formation. An assumed density is also used (62.4 lb_m/ft^3). The equation used to calculate theoretical horsepower in our model is, therefore,

$$hp_{th} = \frac{Q_{feed}(CFS) \cdot 62.4 \cdot D_{form}}{550 \frac{\frac{ft \cdot lb_f}{s}}{hp}}$$

Actual horsepower is found by dividing by the pumping system efficiency:

$$hp_{act} = \frac{hp_{th}}{\eta}$$

Our model assumes a pump efficiency of 0.85*0.80, which allows for the motor and pump efficiencies. The equation used to calculate theoretical horsepower in our model is, therefore,

$$hp_{act} = \frac{hp_{th}}{0.85 \cdot 0.8}$$

A simple unit conversion from hp to kW is used (0.75 kW/hp). Adding this conversion, the cost of electricity, and the capacity factor, the final equation for annual power consumption is as follows:

$$OM_4 = \frac{hp_{th}}{0.85 \cdot 0.80} \cdot 0.75 \frac{kw}{hp} \cdot 24 \frac{hours}{day} \cdot 365 \frac{days}{yr} \cdot CF \cdot C_{elect}$$

OM_5: Annual Electrical for Pipeline Pumping

Starting with the first set of equations used in OM_4, we assume only the velocity head (H_V) to be negligible. Therefore, TDH is the sum of the static head (H_L) and friction loss (H_F). Because the actual pipeline distance and elevation change would need to be calculated for the specific location, we are assuming a 100-m (328-ft) increase in elevation and that a straight pipe is installed. Both of these assmptions could be modified in the model for a more realistic calculation. Using these assumptions, the final equations for our model are as follows:

$$hp_{th}(OM_5) = \frac{Q_{feed}(CFS) \cdot 62.4 \cdot \left(H_{L,pipe} + H_{F,pipe}\right)}{550 \frac{\frac{ft \cdot lb_f}{s}}{hp}}$$

H_F is a function of flow rate and pipe size, and therefore is best calculated by the use of pipe tables. Our model assumes a pipeline design to allow for a friction loss (H_F) of 3 ft per 1,000 ft of pipeline distance. Therefore, the friction loss is calculated as follows:

$$H_F = \frac{3\,ft}{1000\,ft} \cdot D_{pipe}(ft)$$

The final OM_5 equation is as follows:

$$OM_5 = \frac{hp_{th}(OM_5)}{0.85 \cdot 0.80} \cdot 0.75 \frac{kw}{hp} \cdot 24 \frac{hours}{day} \cdot 365 \frac{days}{yr} \cdot CF \cdot C_{elect}$$

OM_6: Annual Membrane Replacement

The USBR *Dealination Handbook* (USBR [2003]) suggests that $0.08 per 1,000 gallons of treated water will cover annual membrane replacement costs. The final equation used in our model is, therefore,

$$OM_6 = \frac{\$0.08}{1{,}000 gal} \cdot Q_{treated}(MGD) \cdot CF \cdot 365 \frac{days}{year} \cdot 1{,}000$$

OM_7: Annual Chemicals

Using Zammit and DiFilippo (2004), Table A-3, Alternative 3 calls out costs for chemicals for both HERO™ operations, as well as for cleaning desalination and BC equipment: chemicals ($392,000), UF/RO cleaning ($10,000), and BC cleaning ($7,000). Similar to other calculations,

we assume that a ratio of the Zammit and DiFilippo (2004) design flow rates to our calculated flow rates is adequate for estimation purposes. Options A, B, and C only have desalination-related costs; Option D has all chemical costs, which includes BC cleaning). The final equations used for our model are as follows:

For Options A–C,

$$OM_7 = \left(392000 + 0000\right) \cdot \frac{Q_{feed}(GPM)}{1316\,gpm}$$

For Option D,

$$OM_7 = \left(392000 + 0000 + 7000\right) \cdot \frac{Q_{feed}(GPM)}{1316\,gpm}$$

OM_8: Other Maintenance

We assume 1.5% of the total capital cost for annual maintenance costs for the desalination and piping systems.

OM_9: Annual Electrical for Concentrate Injection Piping

Starting with the first set of equations used for OM_4, we assume only the velocity head (H_V) to be negligible. Therefore, TDH is the sum of the static head (H_L) and friction loss (H_F). Because the actual pipeline distance and elevation change would need to be calculated for the specific location, we are initially assuming no change in elevation and that a straight 5-mi pipe is installed. Using these assumptions, the final equations for our model are as follows:

$$hp_{th}(OM_9) = \frac{Q_{feed}(CFS) \cdot 62.4 \cdot \left(H_{L,inj} + H_{F,inj}\right)}{550\,\frac{ft \cdot lb_f}{hp}}$$, where $H_{L,inj}$ is assumed to be zero and

$H_{F,inj}$ is calculated as follows:

$$H_F(OM_9) = \frac{3\,ft}{1000\,ft} \cdot D_{inj}(ft)$$

The final OM_9 equation is as follows, which is similar to those for OM_2 and OM_4:

$$OM_9 = \frac{hp_{th}(OM_9)}{0.85 \cdot 0.80} \cdot 0.75\frac{kw}{hp} \cdot 24\frac{hours}{day} \cdot 365\frac{days}{yr} \cdot CF \cdot C_{elect}$$

Appendix C: Water, Energy, and Carbon Sequestration (WECS) Model Equations

The Water, Energy, and Carbon Sequestration (WECS) model was developed using several core model modules. The power plant, carbon storage, geoassessment, water treatment, and economic modules all contributed to the system's overarching results. Table C-1 shows the key assumptions, sources of data, and equations used in the model.

Table C-1. Parameter Descriptions for the WECS Model

Parameter	Unit(s)	Description	Equation, Assumption, and/or Source
MW	megawatts (MW)	Megawatt rating for the San Juan Generating Station	1,848 MW (EPA [2006–2007], eGRID2006, Year 2004 data)
CF	—	Capacity Factor (CF) of operation: % of year plant is operational	77.36% (EPA [2006–2007], eGRID2006_2.1 database)
MWh	megawatt-hours (MWh)	Megawatt-hours	$MWh = MW * CF * 1year \cdot$
CO_2	tonnes/year	Metric tons of CO_2	14,512,417 U.S. tons (converted to metric tonnes in the model) (EPA [2006–2007], eGRID2006_2.1 database)
Net CO_2	tonnes/year	Net metric tons of CO_2 per year base case, including Carbon Capture and Storage (CCS), CCS energy requirement's (CCSEnergy), and water treatment energy requirement's (WTEnergy) subsequent CO_2 emissions	$NetCO_2 = CO_2 - CO_{2,CCS} + CO_{2,CCSEnergy} + CO_{2,WTEnergy}$
$PMD_{Morrison}$	meters/year	Plume Migration Distance per year, Morrison formation	$PMD_{Morrison} = 6.35 meters * (CO_2 / yr)\text{^}0.49 * (years\text{^}0.40)$

Table C-1. Parameter Descriptions for the WECS Model, continued

Parameter	Unit(s)	Description	Equation, Assumption, and/or Source
$PMD_{Fruitland}$	meters/year	Plume Migration Distance per year, Fruitland formation	$PMD_{Fruitland} = 0.019 meters * (CO_2 / yr)^{0.34} * (years^{0.44})$
CO_2Seq	tonnes/year	CO_2 sequestered through the carbon capture and sequestration system	$CO_2Seq = CO_2 * \%CO_2Captured$
H_2Odisp	milliliters/ year	Milliliters of H_2O displaced per year	$H_2Odisp = CO_2Seq * 1.52 cc H_2O / 1 g CO_2$
H_2Orec	millions of gallons/day (MGD)	Million gallons per day of recoverable H_2O	$H_2Orec = H_2O * \%\ recoverable$ [These values enter the design flow rate variable (Q_{feed} (gpm)) within the water treatment module.]
$WT_\$$	\$/thousand gallons	Water treatment cost in 2009 dollars per 1,000 gallons of treated H_2O	$WT_\$ = Annual\ Capital\ Expense\ (5\%\ for\ 20\ years) / Q_{treated} + Total\ O\&M\ Cost / Q_{treated} + Electrical\ (OM_2 + OM_4 + OM_5) / Q_{treated} + Membrane\ Replacement\ (OM_6) / Q_{treated} + Chemicals\ (OM_7) / Q_{treated} + Other$ (Derived through the Water Treatment Module).
$WT_{c/kWh}$	cents/kWh	Water treatment cost in 2009 cents per kilowatt-hour	$WT_{¢/kWh} = WT_\$ * Plant\ Water\ Requirements$ Gallons used per kWh (EPA [2006-2007], eGRID 2005): 6.9 cubic ft/s for each boiler/system (There are 4 systems.) =~ 0.52 gallons/kWh without CCS. With CCS increases water withdrawal by ~99% (DiPietro et al. 2008)
$CCS_{c/kWh}$	cents/kWh	Carbon Capture and Storage (CCS) cost in 2009 cents per kWh	$CCS_{c/kWh,2009} = CCS_{c/kWh,BaseYear} * (Deflator_{2009} / Deflator_{BaseYear})$